NUMERICAL PROCEDURE FOR POTENTIAL FLOW PROBLEMS WITH A FREE SURFACE

By

JOHNSON LAP-KAY CHAN

M.A.Sc. The University of British Columbia, 1984

B.A.Sc. The University of Toronto, 1982

A THESIS SUBMITTED IN PARTIAL FUFILMENT OF

THE REQUIREMENTS FOR THE DEGREE OF

DOCTOR OF PHILOSOPHY

in

THE FACULTY OF GRADUATE STUDIES

(DEPARTMENT OF MECHANICAL ENGINEERING)

We accept this thesis as conforming

to the required standard

THE UNIVERSITY OF BRITISH COLUMBIA

December 1987

In presenting this thesis in partial fulfilment of the requirements for an advanced degree at the University of British Columbia, I agree that the Library shall make it freely available for reference and study. I further agree that permission for extensive copying of this thesis for scholarly purposes may be granted by the head of my department or by his or her representatives. It is understood that copying or publication of this thesis for financial gain shall not be allowed without my written permission.

Department of Mechanical Engineering

The University of British Columbia
1956 Main Mall
Vancouver, Canada
V6T 1Y3

Date 14th April 88.

ABSTRACT

A numerical procedure based upon a boundary integral method for gravity wave making problems is studied in the time domain. The free-surface boundary conditions are combined and expressed in a Lagrangian notation to follow the free-surface particle's motion in time. The corresponding material derivative term is approximated by a finite difference expression, and the velocity terms are extrapolated in time for the completion of the formulations. The fluid-body intersection position at the free surface is predicted by an interpolation function that requires information from both the free surface and the submerged surface conditions. Solutions corresponding to a linear free-surface condition and to a non-linear free-surface condition are obtained at small time increment values. Numerical modelling of surface wave problems is studied in two dimensions and in three dimensions. Comparisons are made to linear analytical solutions as well as to published experimental results. Good agreement between the numerical solutions and measured values is found. For the modelling of a three dimensional wave diffraction problem, results at high wave amplitude are restricted because of the use of quadrilateral elements. The near cylinder region of the free surface is not considered to be well represented because of the coarse element size. Wave forces calculated on the

vertical cylinder are found to be affected by the modelled tank length. When the simulated wave length is comparable to the wave tank's dimension, numerical results are found to be less than the experimental measurements. However, when the wave length is shorter than the tank's length, solutions are obtained with very good precision.

TABLE OF CONTENTS

NOMENCLATURE

Symbol

ϕ	Velocity Potential Function
η	Wave Elevation
ρ	Fluid Density
∇	Differential Operator
$\frac{D}{Dt}$	Material Derivative
δt	Time Increment value or Time Step
ω	Angular Frequency
λ	Wave Length
ϵ	Small Parameter for Dimensional Analysis
α	Half Angle of Wedge Model
A	Wave Amplitude
a	Radius of Vertical Cylinder
Am	Maximum Wave Height Measured Along Ship's Bow
$A\phi=B$	System of Linear Equations
Aw/Am	Wave Amplitude to Wave Paddle Motion Amplitude Ratio
B	Geometric Function for Ship Hull
c	Phase Velocity of Free-Surface Wave
c	Geometric Center of Quadrilateral Elements
d	Mean Water Depth
F	Draft-Froude Number
$\mathcal{F}$	Extrapolation Function in Time

F_x	Longitudinal Force calculated on Vertical Cylinder
F_{max}	Non-dimensional, maximum F_x value in a Wave Cycle
G	Green's Function
g	Gravity Constant
H/λ	Wave Height to Wave Length Ratio
H/d	Wave Height to Water Depth Ratio
k	Wave Number
L_s	Ship Length
$\bar{n}$	$[\ n_x,\ n_y,\ n_z\ ]$ Normal Unit Vector
P	Point of Interest
P	Pressure
Q	Control Point on the Control Surface, **S**
$r,\ r'$	Distance Measured Between Two Points
S	Total Control Surface
S_c	Submerged Surface of Vertical Cylinder
S_f	Control Boundary at the Free Surface
S_h	Control Surface of Ship's Bow
S_m	Control Surface at the Wave Paddle
S_0	Impermeable Control Surface
S_r, S'_r	Vertical Imaginary Boundary at one Wave Length Separation
T	Wave Period
T	Ship's Draft
T_b	Time for High Amplitude Wave to Break
t	Time Variable
U	Model Speed

$\bar{v}$	$[\ v_x,\ v_y,\ v_z\ ]$ Velocity Vector
X_m	Motion Amplitude of Wave Paddle
x_m	Displacement Function of Wave Paddle
Ymax	Non-dimensional Value of Am
a,b,c,d,..	Unknown Constants in Quadratic Functions
$F_2, F_{2b}, F_3,$ and K	Known Functions Defined in the Boundary Integral Equation of associated Problems
I,J,K,L	Element Numbers
P,Q,R,S	Four Corners of Quadrilateral Elements

LIST OF FIGURES

Figure Page

Figure Page

ACKNOWLEDGEMENT

This thesis is written under many unforgettable contributions from many of my best friends, family members, and faculty members. I would like to single out a few persons who have assisted and supported me throughout these years.

Thanks to the Lam's family, for feeding me with their delicious food when I was starving at the end of each month. Their continuous encouragement never run out when I was desperate. I wish them always good luck in their future.

Thanks to Mr. Ken Law, who is one of my best friends in Vancouver. Without his help, the three dimensional graphical plots in this thesis could never have been accomplished. I wish him and his company a very bright future.

Thanks to Annie, my loveable girlfriend, who has been so patient and understanding for these years. I would like to tell her how much I appreciated her encouragement when I was depressed, and I enjoy being her boyfriend for all these years.

Thanks for my eldest brother Lap-Ngai, who partially supported my living for these years, especially on his taking care of our parents independently. I wish him continuous success in his business.

Thanks for Professor Isaacson who gave me the instructions at the final stage of my thesis work when my supervisor was absent on his sabbatical leave. I would like to apologize for my numerous interruptions to him at his work.

Finally, I would like to devote this thesis to my supervisor, Dr. Calisal, for his enormous patience and encouragement to guide me throughout all these years. I am not a good student, and I never was. Thanks for his toleration within the last five years. I wish he has a very bright and successful future in his research career, and good luck to his family.

with love and sincerity

Johnson L.K. Chan

I. INTRODUCTION

In recent years, ocean engineers have become more and more interested in the development of numerical procedures that predict free-surface wave phenomena. This is understandable since today's computer technology is advancing at such a tremendous rate, the need for engineering software to be developed so as to utilize the computer power has become very strong. Moreover, a well developed numerical procedure can reduce the cost of conducting numerous expensive experiments.

Although wave making problems have been studied for almost a century, achievement in this area is still quite limited. The involved numerical solution procedure is considered difficult because of the moving boundaries. Numerical models that simulate this transient, non-linear problem in the time domain seem to be unstable. This numerical instability remained as an obstruction to the progress of ocean engineering technology for years. It was not until 1976 that Longuet-Higgins and Cokelet successfully simulated the deformation of high amplitude waves, and proposed a solution to the instability problem.

Numerical instability associated with free-surface potential flow problems is believed to be initiated by the

formation of local short gravity waves when the long wave crest is compressed in the horizontal direction. In real life, these local short gravity waves are damped by the fluid's viscosity as well as the surface tension effect. However, in the numerical model, the presence of these short gravity waves exaggerates the computation of the free surface, and leads to an unstable solution. In order to suppress the numerical instablity in the solution, Longuet-Higgins and Cokelet have proposed the use of a smoothing function to correct the result every few time step intervals. Solutions obtained with such a smoothing procedure then become very stable.

Another existing problem that causes difficulties in the numerical model is the determination of the position where the free-surface intersects an impermeable body's surface, such as the wave paddle. This point was indentifed by Lin (1984) as a singularity, and an analytic solution could not be obtained. However, it can be accommodated by applying both the velocity potential and the streamline function as prescribed conditions to reinforce a solution numerically. Results obtained by following this approach are very promising. Unfortunately, formulations are accomplished by using complex variables which are applicable for two dimensional problems only. Since it is more desirable to establish a three dimensional numerical procedure for real

life applications, a free-surface formulation that contains only real variables is, therefore, introduced and investigated.

In the following chapters, a solution method based upon the Boundary Integral Equation is studied. The presented method differs from Longuet-Higgins' approach by coupling a finite difference formulation onto the free-surface boundary conditions. Additional assumptions are made to obtain a more appropriate form to march the solution in time. The singularity problem at the fluid-body intersection point is handled by a simple interpolation function. Four different kinds of wave making problems are examined, and comparisons are made between numerical solutions and published experimental results.

The solution procedure is first applied to simulate a two dimensional wave tank. A piston type wave maker is modelled for the wave generating process, and numerical solutions are compared with linear wave theory. The next application is on the modelling of a two dimensional, spatially periodic wave problem. Deformation of high amplitude waves at a finite water depth is considered. Results similar to those by Longuet-Higgins and Cokelet (1976) are obtained. Then, ship's bow waves which are generated by a wedge-shaped model at different drafts are

investigated. Predictions using a *slender ship* assumption are compared with measurements by Ogilvie (1972). Finally, the three dimensional applicability of the free-surface formulations is illustrated by modelling a simple wave diffraction problem. Forces experienced by a surface-piercing cylinder located in a wave tank are calculated and compared to published experimental works.

Numerical results obtained in the following chapters do not require any smoothing procedure. The free-surface formations with a small time step assumption are considered to be adequate to yield a numerically stable solution. It is believed that the presented procedure provides a subsequent way to model wave making problems other than the Longuet-Higgins' approach. Moreover, the introduced free-surface formulations enable practical problems to be solved in three dimensions.

II. BASIC THEORY

When an object is moving at or near the water surface, the air-water interface is disturbed from its equilibrium, and the free surface is set into motion. However, since a gravitational force is acting on the fluid, there is a tendency for the air-water interface to return to its equilibrium position. As a result, gravity waves are formed at the free surface as a balance of the kinetic and the potential energy. These waves which are commonly known as gravity waves, propagate away from the source of disturbances in the radial direction. In general, certain parameters such as water depth, and velocity of disturbance are considered important for wave formation, while some other fluid properties like surface tension, viscosity, and compressibility of the fluid medium are considered less important for the study of gravity waves. In the following chapters, wave making problems are formulated by assuming the fluid as incompressible and inviscid. Surface tension effect is considered as negligible compared to gravity effect and fluid inertial forces. These assumptions are generally accepted when there is no flow separation. For gravity wave problems, flow separation will occur when the characteristic dimension of the structure is not large relative to the orbital path length of fluid particles. That is, the inviscid assumption is acceptable when the dimension of the structure

to the wave length ratio is at about the order of unity.

With these assumptions, the problem can be treated as a potential flow problem. A velocity potential function, ϕ, is defined within the flow field. This potential function, whose gradients are the fluid velocity components, satisfies the Laplace Equation :

$$\nabla^2 \phi = 0$$

or

$$\phi_{,xx} + \phi_{,yy} + \phi_{,zz} = 0 \qquad (1).$$

In the following chapters, a right-hand Cartesian coordinate system with y pointing up as the positive direction is used (Figure 1). The origin of the coordinate axis is located at the undisturbed free-surface, and the wave elevation is designated by the symbol η.

Equation (1), which is the governing equation for the flow field, can be solved by many well established numerical or analytical methods. Although the Boundary Integral Method is used in the following studies, there is no reason that other numerical methods cannot be used to solve the problem. In the next chapter, the Boundary Integral Method for solving

potential flow problems will be discussed. However, boundary conditions must first be arranged in an appropiate form for the use of the selected numerical method.

II.1 Boundary Conditions

Although the Laplace Equation is a linear, second order differential equation, the associated problem can be a non-linear one, depending on the kind of boundary conditions involved. In fact, there exist different kinds of boundary conditions for free-surface wave problems. In order to derive the boundary conditions in forms suitable for the different applications investigated in later chapters, they are discussed under two main categories :

i. The Wetted Surface Condition

ii. The Free-surface Condition

The following formulations are arranged specifically for the use with the Boundary Integral Method. For some other numerical methods, certain rearrangements should be considered.

II.1.i. The Wetted Surface Conditions

The wetted surface is defined as the submerged impermeable surface of solid bodies that is either moving or

stationary. In wave making problems, the wave maker, the tank wall, and the submerged surfaces of any floating or standing structures belong to this category. This type of boundary condition can be formulated as follows :

$$\phi_{,n} = v_n = \bar{V} \circ \bar{n} \qquad (2).$$

$\phi_{,n}$ is the fluid velocity component in the normal direction to the considered surface, and is equal to the dot product of $\bar{V}$ and $\bar{n}$. $\bar{V}$ is the velocity vector at any point on the moving surface, and $\bar{n}$ is the normal unit vector pointing outward from the considered domain (Figure 1).

In equation (2), fluid particles at the wetted surface are forced to have a velocity component, normal to the surface, equal to the normal velocity component of the surface because of the impermeable boundary requirement. As for the tangential velocity component of fluid particles on this surface, there is no restriction because of the inviscid fluid assumption. The *no-slip* boundary condition for viscous fluids does not apply here.

When equation (2) is applied to the submerged surface of stationary objects, such as the wall of a wave tank, $\bar{v}$ is identically equal to zero. Therefore, $\phi_{,n}$ is also equal to zero, which means fluid particles on this surface have a zero

normal velocity component, and penetration of fluid particles into the surface is not allowed. If the surface under consideration is on the wave piston, then $\bar{v}$ is a known function of time. Fluid particles on any point of this surface are moving at a velocity equal to that of the surface in the normal direction. However, if the submerged surface is on a floating object and the object's motion ($\bar{v}$) is the unknown to be solved as part of the solution, the boundary condition, $\phi_{,n}$, cannot be defined by following the form as in equation (2). Additional arrangements or assumptions have to be made to avoid solving for $\bar{V}$ directly. This can be done by a predictor-corrector kind of procedure for the value of $\bar{V}$ in the time domain. Since floating objects are not included in the following studies, the formulation of this kind of boundary condition is, therefore, excluded from the discussions.

In Figure 1, a physical wave tank problem is illustrated by a schematic diagram. A piston type wave maker is located on the left-hand side of the tank. A displacement function, x_m, which is periodic in time, is assigned to this piston for wave generation. Further down the other end, the considered domain is completed by a vertical wall. In frequency domain problems, an artifical boundary that simulates a radiation condition is necessary. However, the radiation boundary condition is not required for a time stepping solution

scheme. Although a non-reflecting boundary condition can be used to reduce the computational effort, no such attempt was made in this study. Instead of using a non-reflecting boundary, a standard wave tank was considered as a physical model. In order to ensure that the solution is free from the interference of reflected waves, a reasonable tank size is necessary, and the simulation time is limited. A discussion of the radiation boundary condition can be found in Sarpkaya and Isaacson (1981) as well as in Newman (1977).

II.1.ii. The Free-Surface Condition

The free surface is identified as the air-fluid interface which is free to move under any disturbance. One of the difficulties involved in solving the problem is to predict the position of the free surface before the solution is obtained. At the free surface, the flow has to satisfy two conditions, namely the kinematic and the dynamic boundary conditions. Kinematically, fluid particles on the free surface must remain there. That is, at the free surface, fluid particles are moving with a velocity component equal to the normal velocity component of the free surface in a direction normal to the free surface. Dynamically, the flow condition must obey the Bernoulli Equation. These two conditions are defined as in equations (3) and (6) respectively in Lagrangian notation.

$$\frac{Dx}{Dt} = \phi_{,x}$$

$$\frac{Dy}{Dt} = \phi_{,y} \qquad \text{on } y=\eta \qquad (3),$$

$$\frac{Dz}{Dt} = \phi_{,z}$$

and

$$\phi_{,t} + \frac{1}{2}\left(\phi_{,x}^{2} + \phi_{,y}^{2} + \phi_{,z}^{2} \right) + \frac{P}{\rho} + gy = 0 \quad \text{at } y=\eta \qquad (4),$$

where $\frac{D}{Dt}$ is the material derivative given as :

$$\frac{D}{Dt} = \frac{\partial}{\partial t} + \phi_{,x}\frac{\partial}{\partial x} + \phi_{,y}\frac{\partial}{\partial y} + \phi_{,z}\frac{\partial}{\partial z} \qquad (5).$$

$\phi_{,x}$, $\phi_{,y}$, and $\phi_{,z}$ are the fluid velocity components in the **x**,**y**, and **z** directions. η is the free-surface elevation measured in the **y** direction, P is the pressure taken as zero at η, ρ is the fluid density, and g is the gravitational constant.

In order to trace the motion of fluid particles at the free surface, equation (4) is rearranged as :

$$\frac{D\phi}{Dt} - \frac{1}{2}\left(\phi_{,x}^{2} + \phi_{,y}^{2} + \phi_{,z}^{2} \right) + gy = 0 \qquad \text{at } y=\eta \quad .$$

When this above equation is combined with equation (3), the

following equation can be obtained :

$$\frac{D^2\phi}{Dt^2} - \frac{1}{2}\frac{D}{Dt}(\phi_{,x}^2 + \phi_{,y}^2 + \phi_{,z}^2) + g\phi_{,y} = 0 \quad \text{at } y=\eta \qquad (6).$$

Equation (6) which is a combined form of the kinematic and dynamic free-surface conditions, has to be satisfied at $y=\eta$. A detailed discussion of the free-surface boundary conditions is given in Newman (1977).

Although, the kinematic and dynamic conditions are combined as in equation (6), most of the terms are not known before the problem is solved. In order to proceed and rearrange equation (6) into a useable form, two additional assumptions must be made. A finite difference expression is coupled into the equation to approximate the material derivative term, and a second order extrapolation function is used in time to predict unknown velocity terms. They are discussed in sections II.2 and III.2 respectively.

II.2 Time Stepping Formulation

Upon applying the Boundary Integral Method, either ϕ , $\phi_{,n}$, or their combinations must be defined at the control surface as boundary conditions. Therefore, the following rearrangements of equation (6) are made.

On $y=\eta$, $\phi_{,n}$ is defined by the dot product of $\nabla\phi$ and $\bar{n}$. If n_x, n_y, n_z are the components of the normal unit vector, $\bar{n}$, located at the free-surface, then,

$$\phi_{,n} = \phi_{,x}n_x + \phi_{,y}n_y + \phi_{,z}n_z \qquad (7),$$

where $\phi_{,y}$ can be obtained from equation (6). Upon the substitution of $\phi_{,y}$ from equation (6) into (7), the following form is obtained.

$$\phi_{,n} = \phi_{,x}n_x + \phi_{,z}n_z + \frac{1}{g}\left\{ \frac{1}{2}\frac{D}{Dt}\left(\phi_{,x}^{2} + \phi_{,y}^{2} + \phi_{,z}^{2} \right) - \frac{D^2\phi}{Dt^2} \right\} n_y \quad \text{at } y=\eta \qquad (8).$$

Two additional assumptions are made here to approximate the unknown values for computing the time stepping solution. These assumptions are considered as follows :

i. In time stepping solution problems, a time increment value (time step), δt, must be chosen. This time increment value has to be small for the solution to be accurate. If δt is small enough, unknown velocity terms on the right-hand-side of equation (8) can be extrapolated in time (from their previous known values) without introducing large errors into the solution. In general, the smaller the time step, the more precise the extrapolated values will be. The order of this extrapolation function can be chosen arbitrarily. In the

following studies, a second order extrapolation function is used. The dicussion of the extrapolation procedure can be found in section III.2. A prime notation is used to identify the extrapolated terms in equation (10).

ii. A finite difference form is used to approximate the second material derivative term in equation (8). A four points function with constant time interval , δt , is written as :

$$\frac{D^2\phi}{Dt^2} = \frac{2\phi^0 - 5\phi^{-1} + 4\phi^{-2} - \phi^{-3}}{(\delta t)^2} \qquad (9),$$

where the potential functions with a negative superscipt represent solutions from previous time steps, and ϕ^0 is the unknown value to be solved at the current time step. There is no restriction on the number of terms used in the expression.

With these two assumptions, equation (8) can be rewritten as :

$$\phi_{,n} = -\frac{2\,n_y}{g(\delta t)^2}\,\phi^0 + \frac{n_y}{g}\,\frac{5\phi^{-1} - 4\phi^{-2} + \phi^{-3}}{(\delta t)^2}$$

$$+ \phi'_{,x}n_x + \phi'_{,z}n_z + \frac{n_y}{2g}\,\frac{D}{Dt}(\phi_{,x}^2 + \phi_{,y}^2 + \phi_{,z}^2)' \quad \text{.... at } y=\eta \qquad (10),$$

where ϕ^0 is now the only unknown variable on the right-hand side of equation (10).

The linearized form of equation (6) applied at the undisturbed free surface and used to obtain the linear numerical solution (see Newman, 1977), is given as :

$$\phi_{,tt} + g\phi_{,y} = 0 \qquad \text{at } y=0 \quad (11),$$

where all the non-linear terms are dropped. Moreover, since the linearity assumption is made, the following expressions can be accepted when formulating the linear free-surface boundary condition :

$$n_y \simeq 1 \qquad (n_x \simeq 0 \ , \ n_z \simeq 0)$$

$$(\phi_{,x}^{\ 2} + \phi_{,y}^{\ 2} + \phi_{,z}^{\ 2}) \ll \phi_{,tt}$$

$$\phi_{,tt} \simeq \frac{D^2\phi}{Dt^2} \qquad .$$

Therefore, equation (11) can be rearranged in a form similar to equation (10) as :

$$\phi_{,n} = - \frac{2}{g\ (\delta t)^2}\phi^0 + \frac{1}{g}\ \frac{5\phi^{-1} - 4\phi^{-2} + \phi^{-3}}{(\delta t)^2} \qquad \text{at } y=0 \ (12).$$

Finally, it must be emphasized that the non-linear free-surface boundary condition is applied at η, while the linearized condition is satisfied at y=0. Equation (10) and

(12), which are now arranged in an suitable form, can be included in the Boundary Integral Equation for different applications.

III. NUMERICAL METHOD

In this chapter, the Boundary Integral Method is briefly introduced. This particular numerical method is chosen because it is considered to be an effective solution method for modelling potential flow problems with a moving boundary. The grid generation procedure involved with this method is not as complicated as it is in the other numerical methods. When applying the Boundary Integral Method, the numerical model is constructed by representing the control surface using small facets (elements). Only values at the control surface are stored and calculated, whereas in other methods such as the Finite Element Method, discretization of the entire control volume is necessary, and all the unknowns inside the control volume must be calculated.

This surface grid generation requirement of the Boundary Integral Method offers a relatively easy management of the results for the moving boundary in comparison with other numerical methods especially in three dimensional applications. With a boundary integral equation derived from Green's Theorem, a system of linear equations can be written with the potential function and their derivatives at discrete points on the control surface as unknowns. Upon solving this set of equations, the potential distribution on the control surface is obtained, and values at any point inside the

control volume can be calculated.

Although the Boundary Integral Method may not be the most efficient numerical method, it is considered to be a very effective numerical approach for moving boundary problems. One of the disadvantages associated with the Boundary Integral Method, criticized by most Finite Element Method users, is on its generated matrix. This matrix, which is neither 'band' nor 'sparse', must be solved by the very time consuming Gaussian Elimination Method.Therefore, not only more computer storage will be required, but the computational efficiency will be poor. However, since problems solved in this thesis are used as an illustration of the formulation's validity, the comparison between different numerical methods is of no concern here and is left to someone with the interest and adequate knowledge in numerical analysis.

III.1 Boundary Integral Method

The Boundary Integral Method was first introduced by Fredholm (1903) who proved the uniqueness of a solution by using a finite number of elements on the boundary of the considered domain. It was not until 1963 when Jawson and Ponter confirmed the use of Green's function in the Boundary Integral Equation that the method became popular. With the

continuous developments of the computer's capacity and performance in the last two decades, the method has become an effective numerical tool, and is now broadly applied on a great variety of engineering problems (see Banerjee and Butterfield, 1981).

The Boundary Integral Equation which can be derived through the Weighted Residual Method for solving the Laplace Equation has a general form given as :

$$\phi(P) + \int_S \phi(Q)\, G_{,n}\, dS = \int_S \phi(Q)_{,n}\, G\, dS \qquad (13),$$

where G is the Green's function defined between two points, P and Q. Point P is the point of interest inside the flow field, and Q is a control point on S (Figure 2).

The above Green's function has a different form for two dimensional and three dimensional problems. It is given as :

$$\begin{aligned} G &= \frac{1}{2\pi} \ln\left(\frac{1}{r} \right) && (\ 2D\ ) \\ &= \frac{1}{4\pi r} && (\ 3D\ ) \qquad (14), \end{aligned}$$

where r is the distance measured between P and Q.

$$r = \sqrt{(x_Q - x_P)^2 + (y_Q - y_P)^2} \qquad \text{(2D)}$$

$$= \sqrt{(x_Q - x_P)^2 + (y_Q - y_P)^2 + (z_Q - z_P)^2} \qquad \text{(3D)} \quad .$$

The term $G_{,n}$ can be calculated by taking the dot product of ∇G and $\bar{n}$, where $\bar{n}$ is the normal unit vector defined according to the location of Q.

In some conditions, when the problem involves a flat impermeable surface (such as the bottom of the wave tank), the Green's function can have an additional image term to represent the image of the source point. This permits a reduction on the number of elements or unknowns involved in the problem (Figure 2). The Green's function then has the following form :

$$G = \frac{1}{2\pi} \{ \ln(\frac{1}{r}) + \ln(\frac{1}{r'}) \} \qquad \text{(2D)}$$

$$= \frac{1}{4\pi r} + \frac{1}{4\pi r'}, \qquad \text{(3D)} \qquad (15),$$

where r remains the same as in equation (14), and

$$r' = \sqrt{(x_Q - x_P)^2 + (y_Q + y_P + 2d)^2} \qquad \text{(2D)}$$

$$= \sqrt{(x_Q - x_P)^2 + (y_Q + y_P + 2d)^2 + (z_Q - z_P)^2} \qquad \text{(3D)} .$$

d is the mean water depth measured from the undisturbed free-surface (y=0).

A physical interpretation of equation (13) is that, if the velocity potential and its normal derivative (ie. normal velocity component) are known on the control boundary, **S**, the potential value at any point, **P**, inside the control domain can be evaluated. Therefore, if **S** is represented by N elements, where on each of these elements, either the potential value or its normal derivative is known, a single equation of N unknowns can be written with point **P** on one of the elements. Since there are N elements, N equations of N unknowns can be written, and the unknown potential values on each element can then be solved.

It must be emphasized that in such a case, **P** is a point on **S**, a special consideration should be made in the calculation of the integral when **P** is at **Q**. A detailed discussion on the derivation of equation (13) and its applications can be found in Brebbia (1978).

There is also a choice on the order of the boundary element being used. When zeroth order elements are adopted, the potential value as well as its normal derivative are assumed as constant along each element. Solutions are calculated at elements' mid points. For first order elements, potential values are assumed to vary linearly within each element. Results are computed at the node points between adjacent elements. In general, it is true that the higher the

order of the elements, the better the resolution and accuracy of the results will be, and more complicated numerical integration procedures will be involved. Therefore, zeroth order elements are used here to simplify the programming procedure of the studied problems. The calculations of matrix entries based on zeroth order elements by equation (13) is briefly discussed in Appendix I. A detailed discussion on the choice of element orders as well as the involved numerical integrations can be found in Banerjee and Butterfield (1981). In the following chapters, most of the two dimensional applications are based on a Gaussian 5th order numerical integration procedure. Whereas the three dimensional problem is solved by considering the Green's function at the geometric node point of the quadrilateral elements rather than a complicated numerical integration procedure.

III.2 Extrapolation in Time

As mentioned in section II.2, extrapolation of velocity terms in equation (10) is required to establish the time stepping solution scheme. These velocity terms are approximated by a second order function of time. It must be emphasized that this order is arbitrarily chosen, and solutions should not be affected by using higher order functions provided the time increment value is reasonably small. The extrapolation function being used here is

$$\mathcal{F} = at^2 + bt + c \tag{17}$$

where $\mathcal{F}$ is the function of interest, **t** is the time variable, and **a**, **b**, and **c** are unknowns different at each element.

If the value of $\mathcal{F}$ is known at time $t-\delta t$, $t-2\delta t$, and $t-3\delta t$, **a**, **b**, and **c** can be obtained from the solution of a 3x3 matrix. $\mathcal{F}$ can then be approximated at time **t**, and $\frac{D\mathcal{F}}{Dt}$ is given as 2at+b. Equation (17) is used in the following chapters to approximate the velocity of fluid particles on free-surface elements before the solution is achieved at each time step. These extrapolated values are found to be good approximations to the computed solutions except at the zero start up stage. However, once the solution proceeds for some time steps, the extrapolated values follow the trend of the solutions and predict the numerical results quite accurately. Extrapolation using a higer order function than equation (17) has never been used, and whether it can result in a better solution cannot be told.

IV. APPLICATIONS

In this chapter, the non-linear free-surface formulations and the solution procedure defined in previous chapters are tested by modelling four different problems. They are :

i) Wave Tank Modelling

ii) Deformation of High Amplitude Wave

iii) Prediction of Ship's Bow Wave

iv) Wave Diffraction by Circular Cylinder

Comparisons are made to available experimental and analytical results in each case to evaluate the solution procedure. The developed solution procedure is first applied to simulate a two dimensional wave tank of finite water depth. A piston type wave paddle is assigned a sinusoidal motion for wave generation. The numerical result is compared to linear wave theory to calibrate the procedure. Then, the deformation of high amplitude waves is studied by a two dimensional, spatially periodic wave model. Different breaking waves are obtained as solutions to confirm the introduced free-surface formulations as well as the assumptions. Although the same study was reported by Longuet-Higgins in 1976, modelling of such high amplitude waves is believed to be a good test to establish the effectiveness of the free-surface formulations.

After the solution scheme is confirmed, it is applied to predict a ship's bow wave. A wedge-shaped model of constant

draft is used for studies. Numerical results are obtained at different *draft-Froude* numbers, and are proved to be within the acceptable limits when compared to experimental measurements. Finally, the three dimensional applicability of the solution procedure is illustrated by a wave diffraction model. A surface piercing circular cylinder is considered in a wave tank. Forces experienced by the cylinder are obtained at different wave frequencies. Comparisons are made to some published experimental results.

Each of these problems is reported individually in a separate section. Solutions obtained in each case are numerically stable. Smoothing of the result is never applied and is considered as unnecessary.

IV.1 Wave Tank Simulation

The wave tank (or towing tank) is probably the most common facility for ocean engineers and naval architects to test the performance of their designs. Although the main purpose of the tank is to tow ship models in calm water and measure the resistance, it also has facilities to generate waves to simulate a regular sea state or a random sea state during the experiment. This wave making process is usually operated by a wave maker located at one end of the tank. Electronic signals are usually input to the wave maker to

govern its motion at a desired frequency and amplitude. Waves are then generated and travel down the tank.

IV.1.1 Formulation

In this section, the motion of the wave maker is governed by the following equation :

$$x_m = X_m (1 - e^{-ct}) \sin \omega t \qquad (18),$$

where X_m is the piston's motion amplitude, and ω is the angular frequency. The term ($1 - e^{-ct}$) is a ramp function and is used to ensure that the wave maker starts its motion smoothly at time (t) equal to zero. c is chosen as 2.303 to recover 99% of the piston's motion within 2.00 seconds.

The velocity of the wave piston is, therefore, simply given by taking the derivative of equation (18) as :

$$v_x = X_m \{ (1 - e^{-ct}) \omega \cos \omega t + c\, e^{-ct} \sin \omega t \} \qquad (19).$$

At time t=0, the wave maker starts at zero velocity.

In Figure 3, the considered problem is illustrated by a diagram. The wetted surface of the wave piston is designated by a symbol S_m . The free-surface is denoted by S_f , and the

vertical wall on the right as S_0 . Since a mirror image assumption is used as illustrated, the tank bottom is not included in the numerical model.

With the control surface, **S**, given as :

$$\mathbf{S} = S_m + S_f + S_0 \quad ,$$

equation (13) can be rewritten as :

$$\phi(P) + \int_{S_0} \phi\, G_{,n}\, dS + \int_{S_f} \phi\, G_{,n}\, dS + \int_{S_m} \phi\, G_{,n}\, dS$$
$$= \int_{S_0} \phi_{,n}\, G\, dS + \int_{S_f} \phi_{,n}\, G\, dS + \int_{S_m} \phi_{,n}\, G\, dS \quad ,$$

where the Green's function, G, is given in equation (15). Then, by substituting the corresponding boundary conditions into the above equation, the following form is obtained :

$$\phi(P) + \int_{S_0} \phi\, G_{,n}\, dS + \int_{S_f} \phi \left(G_{,n} + \frac{2\, n_y}{g\, (\delta t)^2} G \right) dS + \int_{S_m} \phi\, G_{,n}\, dS$$
$$= \int_{S_f} F_2\, G\, dS + \int_{S_m} v_x n_x\, G\, dS \qquad (20),$$

where

$$F_2 = \frac{n_y}{g} \frac{5\phi^{-1} - 4\phi^{-2} + \phi^{-3}}{(\delta t)^2}$$

$$+ \phi_{,x}' n_x + \frac{n_y}{2g} \frac{D}{Dt}(\phi_{,x}^2 + \phi_{,y}^2)' \qquad (21).$$

F_2 is obtained by dropping the z derivative terms from equation (10), and moving $[\frac{2 n_y}{g (\delta t)^2} G \phi]$ from the right-hand-side to the left-hand-side of equation (20). $\phi_{,n}$ on the wave maker, S_m , is given by $v_x n_x$.

For linear applications, equation (12) is used instead of equation (10) in equation (13). The corresponding integral equation becomes :

$$\phi(P) + \int_{S_0} \phi G_{,n} \, dS + \int_{S_f} \phi (G_{,n} + \frac{2}{g (\delta t)^2} G) \, dS + \int_{S_m} \phi G_{,n} \, dS$$

$$= \int_{S_f} K G \, dS + \int_{S_m} v_x n_x G \, dS \qquad (22),$$

where

$$K = \frac{1}{g} \frac{5\phi^{-1} - 4\phi^{-2} + \phi^{-3}}{(\delta t)^2} \qquad (23).$$

An essential difference between equation (20) and equation (22) is on the definition of the control surface. In equation (20), S_m and S_f are considered to be the instantaneous locations of the wave maker and the free

surface. However, in equation (22), S_m and S_f only designate the mean position of the wave piston and the undisturbed free-surface. Boundary conditions are not satisfied at the exact boundary position. The control surface is considered moving in time for the non-linear cases but remains stationary in the linear numerical model.

When these two equations are applied for wave tank simulations, the physical problem is represented by a numerical model of N elements as in Figure 3 . Then, depending on whether the non-linear or the linear free-surface boundary condition is used, a set of equations obtained by these two equations is considered with point P on each element. The procedure is very similar to the discussion in Appendix I. Upon solving the resulting set of equations, the potential value on each individual element is obtained, and the velocity components can be calculated. In non-linear problems, the free-surface is redefined by considering the motion of fluid particles with the resolved velocity components. As for linear problems, the free-surface elevation is computed by the linearized Bernoulli Equation which has the following form :

$$\phi_{,t} + g\eta = 0 \qquad \text{at } y=0 \quad .$$

A similar procedure is used to proceed the solution at the

specified time increment except that the corresponding integral equation using a linear free-surface condition has fewer terms.

IV.1.2 Interpolation

In this example, the considered problem is in two dimensions, and the control boundary is defined by line segments as shown in Figure 3. Although the element size can be chosen very small to increase the resolution of the potential value along the control surface, potential values can only be obtained at discrete points along the boundary. In order to define the free-surface position at the next time step, interpolations and extrapolations of the potential values between elements are usually required in the calculations.

In chapter III, it was mentioned that zeroth order elements are applied here to model the problems for simplicity. Therefore, an interpolation function is used to determine the velocity of fluid particles at the free surface. It must be emphasized that when the free surface is considered moving in time, its motion is simulated by a *time-step* displacement of the free-surface elements. This *time-step* displacement of a surface element is the resultant motion by considering the motions of its two ends and not its

mid point movement. That is, the element's length is not a constant but changes through each time increment.

Before velocity values are interpolated between elements, the normal and tangential velocity components at the mid point of each element are determined. The normal velocity component at the free-surface element's mid point is calculated by equation (10) without the **z** associated terms. As for the tangential component, it is evaluated by the change of ϕ value along the free surface. Since these two velocity components are obtained in directions normal and tangential to the free-surface, its **x-y** components can be resolved by a vector transformation procedure.

After the velocity components on each element are known, their values between adjacent elements are interpolated by the following function :

$$\begin{aligned} v_x &= \mathbf{ax} + \mathbf{by} + \mathbf{c} \\ v_y &= \mathbf{dx} + \mathbf{ey} + \mathbf{f} \end{aligned} \qquad (24),$$

where v_x and v_y are velocity components between elements, **x** and **y** are the coordinates of elements, and **a**, **b**, **c**,...etc are unknown constants (different from those in equation (17)).

With equation (24), values on three successive elements are required for the interpolations (see Appendix II for

details). The unknown constants, **a**, **b**, **c**,...etc, are found in each case so as to establish the interpolation functions, and the velocity components between two elements can then be evaluated (Figure 4).

At the fluid-body intersection point, the same criterion is applied. Three elements are chosen with two of them at the free-surface and one located on the wave piston. In this case, (Figure 4) the intersection point has a v_x value equal to the velocity of the piston, and v_y is the only quantity to be determined. When v_y of the intersection point is known, its location at the next time step can be predicted.

Although it is very crucial to evaluate this intersection point for a proper representation of the free surface near the moving body, it is observed from the numerical studies that the approximation of the intersection point by equation (24) is quite realistic. A numerical problem related to this singularity as reported in Lin (1984) was never encountered. It is also believed that improvements can be achieved by a higher order function than equation (24). However, the effect of using a higher order function as well as the limitations of such an interpolation scheme are not studied here. As long as the element size is small enough, predictions of the fluid-body intersection point by

equation (24) seem to be a good approximation for the use of the zeroth order element.

IV.1.3 Results and Discussions

First order solutions are calculated by using the linearized free-surface condition :

$$\phi_{,t} + g\eta = 0 \qquad \text{at } y=0 \qquad (25)$$

where

$$\phi_{,t} \simeq \frac{D\phi}{Dt} = \frac{3\phi^{0} - 4\phi^{-1} + \phi^{-2}}{2\ \delta t} \quad .$$

The calculation of $\phi_{,t}$ is expressed in a finite difference form since ϕ is calculated at a constant time increment, δt. Solutions obtained by equation (22) are labelled as linear solutions while computations through equation (20) are defined as non-linear solutions. In this example, comparisons are mainly between numerical solutions and the first order analytical theory.

The first set of results which are presented in Figure 5 is on wave generations by a numerical wave tank. Linear free-surface conditions are used, and motion of the wave maker is at 0.50 Hz. A motion amplitude of 0.3 m is

considered. The tank is chosen arbitrarily to be 40.00 m in length, and 4.00 m in depth. Time domain solutions are obtained at a δt increment of 0.05 second. Results are illustrated in Figure 5. Quantities like wave amplitude, phase velocity, and wave length can then be obtained directly or indirectly from the plots.

Computations are repeated at different frequencies and the corresponding wave lengths are measured. In Figure 6, the calculated wave lengths are plotted against the *dispersion* relationship at different frequencies. Agreements between the linear numerical solutions and the dispersion relationship are very good over a wide range of frequency. This dispersion relationship obtained from linear theory is defined by the following expressions :

$$\frac{\omega^2}{g} = k \tanh kd$$

$$c^2 = \frac{\omega^2}{k^2} = \frac{g}{k} \tanh kd \qquad (26),$$

where

$$k = \frac{2\pi}{\lambda} \qquad (27).$$

ω is the angular frequency, k being the wave number, d is the water depth, and λ is the wave length. When ω and d are chosen, the value of k can be solved by iteration of equation (26), and the wave length, λ, can be obtained through

equation (27).

Comparisons of the phase velocity, c, are also made with equation (26). In Figure 7, the computed value is denoted by symbols at different frequencies. Similar to the case in Figure 6, the numerical predictions (which are linear) agree well with equation (26).

In addition to the wavelength and phase velocity computations, wave amplitudes are also calculated and compared to the wave maker theory by Dean and Dalrymple (1984). A deep water situation ($kd = 4.0$) is considered in Figure 8, and results are expressed in wave amplitude to piston's motion amplitude ratios (A_w/A_m). Small discrepancies (less than 5%) are found between the numerical solutions and the theory, which is probably explained by a numerical truncation error. (Situation is considered as deep water when $kd > \pi$).

With the above comparisons, results obtained by the introduced solution scheme with a linear free-surface condition are considered to be satisfactory. However, it was observed that numerical results are partially affected by the number of elements per wave length. In Figure 9, a sinusoidal curve is represented by different numbers of line segments. In order to maintain a smooth profile, it is found that at

least 24 elements per wave length should be used. This observation, unfortunately, can only give some indications to the relationship between the resolution of a curve and the number of elements per wave length. When the simulated wave amplitude to length ratio becomes very high, more elements should be used. Although it is true that the smaller the element size, the better the free-surface definition will be, there is always a limitation on how small an element can be used. If the size of elements is too small, not only does the computation become very inefficient, but numerical problems can possibly arise in the solutions when adjacent elements are too close to one another. This can be realized if the velocity is changing rapidly between adjacent free-surface elements. Any improper choice of the time step (too large) can result in elements crossing each other and causing the numerical model to fail.

Solutions of wave generation with linear and non-linear free-surface condition are found in Figure 10. The tank's dimensions used in this case are 80.00 m in length, and 4.00 m in depth. A wave piston with motion amplitude of 0.15 m is moving at 0.25 Hz. Solutions are computed at a 0.05 second increment for 20.00 seconds. Free-surface elevations are calculated for both solutions, and presented in graphical form.

The non-linear solution which is plotted on the right half of Figure 10 is very similar to the linear solution. Non-linearity effect is insignificant in the solution since the simulated wave amplitude is small. However the calculated wave profiles in the linear solution are not very smooth after computations have been carried on for some period of time. The same problem is not observed in the non-linear solution. A possible explanation for their behaving differently is believed to be in the linearization assumption that the linear boundary condition is satisfied at the undisturbed free surface. This error that is tolerated in the linear model accumulates as the solution proceeds in time. As for the non-linear solution, though some uncertainties exist in the free-surface predictions, results are generally smooth and remain numerically stable in time. Since it is known that the difference between linear and non-linear solution is significant when wave amplitude is high, and that the non-linear wave will break when the wave slope is steep, the comparison can only be carried out in a very narrow range of wave height to length ratio. However, the main purpose of Figure 10 is to show the reader that the non-linear solution is calibrated and better than the linear solution. A vigorous comparison of the two solutions is beyond the scope of this study

There exists a relationship between the wave's breaking

mode and the initial wave height to wave length ratio. When the wave amplitude is very high, it is observed in nature that the wave will deform and eventually fail at different breaking modes. This is the next topic to be discussed in the following section.

Finally, the drift motion of fluid particles at the free surface is studied. Figure 11 is the plot of the non-linear free surface at time t equal to 5.00 and 6.00 seconds. The simulated wave tank's dimensions are 10.00 m in length and 6.00 m in depth. The motion amplitude of the wave maker is at 0.10 m, and waves are generated at a frequency of 0.5 Hz. 50 elements are used at the free surface, and the time step is chosen as 0.05 second. Solutions exhibit a wave length of approximately 6.00 m, and a wave height at about 0.36 m. The equivalent wave height to length ratio (H/λ) is 0.06, which is still within the *1/7 limit* (theoretical limit before breaking). A sharper crest and shallower trough are observed in the solution.

Fluid particles at the free surface are also traced in time, and their loci are recorded in Figure 12. Particles at three locations inside the tank are chosen at 0.20 m, 2.00 m, and 6.00 m from the wave maker. It can be observed in Figure 12 that these particles all experience a non-linear drift motion. At 0.2 m from the wave maker, fluid particles, though

mainly following the piston's motion, are slowly drifting to the right. Whereas at 2.00 m from the piston, fluid particles are drifting down the tank at a mean drift velocity of 0.1 m/s. According to the prediction by Newman (1977), a fluid particle's second order motion is given as :

$$\frac{dx_0}{dt} = \omega A\ e^{ky} \cos\ (\ kx-\omega t\ ) + \omega k A^2\ e^{2ky} + O(\ A^3) \quad ,$$

where A is the wave amplitude, k is the wave number, and ω is the frequency. x_0 is given in the Lagrangian notation, and y is taken at the undisturbed free-surface. In this equation, the only term that is responsible for the non-linear drift motion is the second order term ($\omega k A^2\ e^{2ky}$). This second order mean drift velocity is calculated as 0.1066 m/s, which indicates that the numerical prediction has an difference of about 7% .

At 6.00 m down the tank, fluid particles do not experience any drift motion until a well developed wave crest arrives. The motion due to the first wave cycle drifts the particles at a greater distance than their migration in later wave cycles. Since these particles are close to the tank wall, their motions in later cycles are believed to be affected by the reflected waves.

With the above observations in the numerical solutions,

it is believed that the natural drift phenomenon is obtained by the proposed free-surface formulations. However, although the numerical solutions are stable within the considered simulation time, failure of the numerical model is expected for a longer simulation time. This failure is related to the improper sizing of free-surface elements near the wave maker, and to the use of the interpolation function (equation (24)) at the fluid-body intersection point. Moreover, as the size of the elements near the wave maker is growing in time (a consequence of elements drifting downstream), resolution of the computed wave profile near the piston will become so poor that the solution down stream will be affected and become imprecise. Improvement to the solution is possible by breaking an element which becomes too long into two elements during the computation. However, this involves not only a reconstruction of the matrix, but the initial condition and the position history of the newly created elements must be defined. This is considered very difficult and is not being carried out in this study.

IV.2 Deformation of High Amplitude Waves

The solution procedure outlined above is applied to the same problem investigated by Longuet-Higgins and Cokelet in 1976. This study on the deformation of high amplitude waves is considered a straight-forward way to test how well the

introduced free-surface formulations can model a highly non-linear situation. A two dimensional, spatially periodic wave model is used to simulate a high amplitude wave until it becomes unstable. Initial conditions are obtained from linear wave theory to start the computation with a well developed wave profile. Although this numerical model by Longuet-Higgins seems artificial, it is still considered as an effective way to study breaking wave phenomenon.

In real life, wave breaking is expected to occur when the velocity of fluid particles exceeds the phase velocity at the free surface. In other cases, it can also happen when the particles' acceleration is larger than the gravitational acceleration. It can be observed later in Chapter IV.2.2 that particles at the wave crest are moving at a relatively higher velocity than those at the trough. As a result, the crest travels faster and eventually forms a jet. This wave form cannot be described with linear theories as the function that defined the wave profile is multi-valued. The numerical computation stops when particle paths defining the free surface intersect each other. This condition is taken to represent numerical wave breaking.

IV.2.1 Formulation

In Figure 13, numerical models for linear and non-linear

applications are illustrated. These numerical models are at exactly one wave length so as to take advantage of the spatially periodic assumption. Finite water depth is considered, and a mirror image is assumed about the bottom surface in order to reduce the number of unknowns involved in the problem. The modified Green's function (equation (15)) is used in the Boundary Integral Equation.

The control surface is divided into S_f , S_r , and S_r' . S_f represents the free-surface, while S_r and S_r' denote two artificial, vertical boundaries for the completion of the control domain. According to the spatially periodic assumption, S_r and S_r' are one wave length apart, and the potential distribution as well as velocity values should also be identical at corresponding points (Figure 13). Therefore, if N elements are used on the total boundary and element i is on S_r , the following conditions should be true:

$$\phi_i = \phi_{N+1-i}$$
$$v_x \big|_i = v_x \big|_{N+1-i} \qquad (28),$$

where the subscripts are element numbers. These additional conditions provide an extra set of equations to solve the problem.

With

$$S = S_r + S_f + S_r' \quad ,$$

the corresponding integral equation can be written as :

$$\phi(P) + \int_{S_r + S_r'} \phi\, G_{,n}\, dS + \int_{S_f} \phi \left(G_{,n} + \frac{2n_y}{g(\delta t)^2} G \right) dS$$

$$= \int_{S_f} {}_2\, G\, dS + \int_{S_r + S_r'} (v_x\, n_x)\, G\, dS \qquad (29),$$

where F_2 is as given in equation (21). However, since v_x on S_r and S_r' is still not known, its associated integral terms could be moved to the left-hand-side of the equation to give the following form :

$$\phi(P) + \int_{S_r + S_r'} \phi\, G_{,n}\, dS + \int_{S_f} \phi \left(G_{,n} + \frac{2n_y}{g(\delta t)^2} G \right) dS + \int_{S_r + S_r'} v_x n_x\, G\, dS$$

$$= \int_{S_f} F_2\, G\, dS \qquad (30).$$

Now, with the v_x associated terms as extra unknowns, it is evident that there are more than N unknowns to be solved though only N equations can be written by equation (30). Fortunately, equation (28) provides an additional set of conditions to complete the matrix with the right number of equations. Thus, the velocity on both S_r and S_r' are solved simultaneously with the potential values. A complete form of the established matrix can be found in Calisal and Chan

(1987).

For linear results, the linearized free-surface conditions are applied, and equation (30) is rewritten as :

$$\phi(P) + \int_{S_r + S_r'} \phi\, G_{,n}\, dS + \int_{S_f} \phi \left(G_{,n} + \frac{2}{g(\delta t)^2} G \right) dS + \int_{S_r + S_r'} v_x n_x\, G\, dS$$

$$= \int_{S_f} K\, G\, dS \qquad (31),$$

where K is as given in equation (23). This equation, because of linearization, has a different definition for the control surface. Boundary conditions are applied at the undisturbed free surface, while S_r and S_r' are considered as not moving in time.

In the non-linear model, S_f , S_r , and S_r' are moving freely in time. Since the two vertical boundaries are at the same velocity, the single wave length restriction can always be maintained.

In this problem, since there exists no external driving mechanism (such as the wave maker) to govern the change of the free surface in time, function F_2 and K in equation (30) and (31) are considered as the only driving functions for the solutions to proceed in time. In fact, during the moment of start up, these two functions only contain information of a

well developed free-surface wave, and wave theory of any order can be used to calculate F_2 and K at time t=0 . For simplicity, the linear wave theory is chosen here.

The analytic potential function from linear theory is given in Newman (1977) as :

$$\phi = \frac{Ag}{\omega} \frac{\cosh k(y+d)}{\cosh kd} \sin (kx-\omega t) \qquad (32),$$

where A is the wave amplitude, ω is the angular wave frequency, d is the mean water depth, and k is the wave number defined as in equation (27).

At time t = 0, wave elevation η is calculated by equation (25) as :

$$\eta = \frac{-1}{g} \phi_{,t}$$
$$= A \cos kx \qquad \text{at } y=0,\ t=0 \quad (33).$$

The free-surface boundary for non-linear simulation is then defined by this expression. As for the functions F_2 and K, they can be evaluated by substituting equation (32) into equations (21) and (23).

IV.2.2 Results and Discussions

The numerical solution with a linear free-surface

boundary condition is obtained and illustrated in Figure 14. The considered wave length is 10.00 m with a depth at 4.00 m. Initial wave amplitude is assigned as 0.50 m, and 50 elements are used at the free surface. The corresponding wave height over length ratio (H/λ) is 0.10, and the height to depth ratio (H/d) is 0.25 . The solution is allowed to proceed for 20.00 seconds at a time increment of 0.05 second. Wave profiles calculated by equation (25) are illustrated at 19.00, 19.50, and 20.00 second. Results are observed to be smooth and propagate at constant speed. At 20.00 seconds, the wave amplitude has lost 2% of its original magnitude, which is believed to be a consequence of numerical truncation errors. These numerical results obtained with a linear free-surface condition are, therefore, considered as numerically stable and compatible to linear theory within 2% error.

As for non-linear solutions, the change of wave shape is so dramatic that it eventually fails at different breaking modes. In the following results (Figures 15, 16, 17), wave length is chosen at 10.00 m, and 1.00 m of water depth is considered. 50 elements are used to represent the free surface, and solutions proceed at 0.01 second increments until breaking waves are obtained.

In Figure 15, the H/λ ratio is selected at 0.10 . The

corresponding H/d ratio is 1.00 . Wave profiles are calculated until a spilling breaker is obtained which stops the computation at 1.25 second. The breaking time to wave period ratio (T_b/T) is therefore calculated as 0.3686 . The numerical model is found unstable at the wave crest where the fluid flow condition changed rapidly. Elements in this region become so close to each other that eventually, they cross each other and fail to represent the free-surface anymore.

At higher H/λ ratio, the wave possesses more energy per wave length, and formation of a plunging breaker at a much shorter time is expected. This is illustrated in Figures 16 and 17 . In these two cases, the initial H/λ ratios are at 0.125 and 0.150 , and the respective H/d ratios are 1.25 and 1.50. Plunging breakers are formed at 0.87 and 0.75 second, equivalent to T_b/T ratios of 0.2565 and 0.2212 respectively.

Although a careful study of the results in Figures 15, 16, and 17 shows that the wave crests are not as smooth as those reported by Longuet-Higgins and Cokelet (1976), they behave very similarly, and fail at similar breaking modes. This imperfection is not surprising, since smoothing is never applied to the crest region where the flow condition is changing so rapidly.

With the provided results, there is enough evidence to

believe that the introduced free-surface formulations are adequate for modelling the free-surface behavior, and the solution procedure provides an alternative to the method by Longuet-Higgins (1976).

IV.3 Predictions of Ship's Bow Wave

In this section, a more practical problem will be used to demonstrate the solution procedure, as well as to test the body free-surface interpolation function. The prediction of ship's bow waves has been considered as one of the important topics for Naval Architects. The understanding of such a phenomenon is considered important because it greatly affects a ship's performance. A major portion of the ship's wave resistance is believed to be contributed by the flow conditions near the bow. This problem, which is a high Froude number problem (as indicated by Ogilvie (1972)), is formulated within a *slender ship* assumption. Such an assumption not only means a small parameter, ϵ, is found characterizing the beam/length or draft/length ratio, it also implies that the size and shape of the cross-sectional hull form changes gradually in the longitudinal direction.

In this section, a wedge-shaped model is used to simulate the ship's bow. A wide range of the *draft-Froude* number is considered in the calculations. Solutions are

obtained with linear and non-linear free-surface conditions, and comparisons are made to the experimental and analytical work by Ogilvie (1972).

IV.3.1 Formulation

When a ship is moving at a constant speed, U , a steady wave pattern moving with the ship is formed at the bow. This pattern, which is three dimensional, is affected by the ship's speed as well as the form of the ship's bow. In order to simplify the problem, a wedge-shaped bow of constant draft is considered. A right hand cartesian coordinate system is used with its origin located at the bow. The **x** axis is pointing in the longitudinal direction of the ship, and **y** is chosen positive in the upward direction. In Figure 18, the model is moving at a constant speed, U , in the -**x** direction. Water depth is considered to be large compared to the model's draft.

With the *slender ship* assumption, the three dimensional wave pattern can be treated as a two dimensional problem and solved along the ship length at constant **x** increments. The same argument was made by Ogilvie (1972), that if the ship's hull form is defined by a function $z = \pm B(x,y)$, the slope of the waterlines in the **x** direction can be assumed small since the change in the longitudinal direction is gradual.

Therefore,

$$B_{,x} = O(\epsilon) \qquad 0 < x < L_s \quad ,$$

where B is a geometric function that described the hull form, L_s is the ship's length, and ϵ is any small parameter such as the beam/length ratio.

Whereas in the bow near field, since the rate of change of flow condition in the longitudinal direction is higher than that in the far field, the order of x should be smaller than the usual thin ship assumption (ie. O(x) = 1), but remain less than ϵ. Therefore,

$$x = O(\epsilon^{1/2}) \quad ,$$

and

$$R = (y^2 + z^2)^{1/2} = O(\epsilon) \quad .$$

The order of differential operators is, therefore, given as :

$$\frac{\partial}{\partial x} = O(\epsilon^{-1/2})$$
$$\frac{\partial}{\partial y}, \frac{\partial}{\partial z} = O(\epsilon^{-1}) \quad .$$

The associated order of terms for equation (1), then becomes:

$$\phi_{,xx} + \phi_{,yy} + \phi_{,zz} = 0$$

$$[\ \tfrac{1}{\epsilon}\ ] \quad [\ \tfrac{1}{\epsilon^2}\ ] \quad [\ \tfrac{1}{\epsilon^2}\ ]$$

This indicates that the **x** associated terms are much smaller than the other terms, and solutions can be obtained by treating the problem as in the **y-z** plane. The above order of magnitude analysis follows the arguments given by Ogilvie (1972). As a consequence, the governing equation becomes :

$$\phi_{,yy} + \phi_{,zz} = 0 \qquad (34).$$

Now, since the model is moving at constant speed, U, the total velocity potential, Φ , can be assumed to have the following form :

$$\Phi = \mathbf{U}\mathbf{x} + \phi(y,z) \qquad (35),$$

where ϕ is a function of **y** and **z** only.

When equation (35) is substituted into equation (4), and the pressure P , is taken as zero at atmospheric pressure, the Bernoulli Equation can be rewritten as :

$$U\,\phi_{,x} + \frac{1}{2}\left(\phi_{,y}^{\,2} + \phi_{,z}^{\,2}\right) + gy = 0 \quad \text{at } y=\eta \quad (36).$$

It must be clear that, the term $\Phi_{,t}$ is equal to zero since the wave pattern is steady at the ship's reference. However, it is also true that at a fixed reference, the ship is moving in the -**x** direction at velocity -**U**. Tracing the ship's motion in time at a reference fixed in space is given by :

$$\mathbf{x} = \mathbf{U}t \qquad (37),$$

and the change along the ship at the fixed reference can be written as :

$$\delta x = U\,\delta t \qquad ,$$

$$\Rightarrow \qquad U\frac{\partial}{\partial x} = \frac{\partial}{\partial t} \qquad (38).$$

Equation (36) is therefore re-expressed at a fixed reference as :

$$\phi_{,t} + \frac{1}{2}\left(\phi_{,y}^{2} + \phi_{,z}^{2}\right) + gy = 0 \quad \text{at } y=\eta \quad (39),$$

where the change of ϕ in the **x** direction at the ship's reference is expressed as a change in time.

Following the approach in chapter II, equation (39) is combined with equation (3) to yield the combined free-surface boundary condition at $y=\eta$. This is given as :

$$\phi_{,n} = -\frac{2n_y}{g(\delta t)^2}\phi^0 + \frac{n_y}{g}\frac{5\phi^{-1} - 4\phi^{-2} + \phi^{-3}}{(\delta t)^2}$$

$$+ \phi'_{,z}n_z + \frac{n_y}{2g}\frac{D}{Dt}(\phi_{,y}^2 + \phi_{,z}^2)' \qquad \text{at } y=\eta \qquad (40),$$

where $\bar{n}$ is defined on the y-z plane.

As for the impermeable boundary that represents the ship hull,

$$\phi_{,n} = U\left(\frac{\partial y}{\partial x}n_y + \frac{\partial z}{\partial x}n_z\right) \qquad \text{on } z = B(x,y) \quad .$$

However, since a wedge-shaped model of constant draft is considered, $\frac{\partial y}{\partial x}$ is taken as zero on the ship hull. Moreover, if the wedge half angle is α , the above condition can be written as :

$$\phi_{,n} = U\,B_{,x}\,n_z$$

$$= U \tan\alpha\, n_z \qquad \text{on } z = B(x,y) \qquad (41).$$

A schematic drawing for the y-z plane is shown in Figure 19.

In Figure 19, the illustration is very similar to a wave tank problem. The only difference between Figure 19 and Figure 3 is that the wave maker is now being replaced by the cross section of the ship hull. This cross section of the ship hull is moving in the z direction at constant velocity instead of oscillating back and forth. A more precise way to

explain Figure 19 is to consider the illustrated **y-z** plane moving along the ship length, so that the ship's section appears on the figure as if a vertical partition is moving to the right at constant speed. Therefore, a similar approach to the modelling of a wave tank can be applied in this problem, except that the time variable, **t** , is used instead of **x** to proceed the solution in the **y-z** plane along the ship's length direction.

Finally, the boundary condition on the vertical wall at the right end of the considered domain is simply defined as zero. As illustrated in Figure 19, only the right half of the considered problem is modelled because of symmetry about the ship's mid plane. The vertical wall is located very far away from the ship to reduce any possible interference on the result by reflected waves. Water depth is also taken to be deep enough to avoid any shallow water effect in the solution.

It must be clear that, because of the *slender ship* assumption, wave elevation ahead of the bow is not formulated in the solution. Since it is assumed not affecting the solution by a significant amount, the flow condition at the bow is considered as undisturbed to start the computation.

With the control surface S, divided into S_0 , S_f , and

S_h , as illustrated in Figure 19, the associated Boundary Integral Equation can be written as :

$$\phi(P) + \int_{S_0} \phi\, G_{,n}\, dS + \int_{S_f} \phi \left(G_{,n} + \frac{2n_y}{g(\delta t)^2} G \right) dS + \int_{S_h} \phi\, G_{,n}\, dS$$

$$= \int_{S_f} F_{2b}\, G\, dS + \int_{S_h} U \tan\alpha\, n_z\, G\, dS \qquad (42),$$

where

$$F_{2b} = \frac{n_y}{g} \frac{5\phi^{-1} - 4\phi^{-2} + \phi^{-3}}{(\delta t)^2}$$

$$+ \phi'_{,z} n_z + \frac{n_y}{2g} \frac{D}{Dt}\left(\phi_{,y}^{2} + \phi_{,z}^{2} \right)' \qquad (43).$$

As for linear applications, the integral equation is, of course, very similar except simpler. The linearized boundary conditions are applied at the undisturbed free surface, and the ship's thickness is ignored. This integral equation is written as :

$$\phi(P) + \int_{S_0} \phi\, G_{,n}\, dS + \int_{S_f} \phi \left(G_{,n} + \frac{2}{g(\delta t)^2} G \right) dS + \int_{S_h} \phi\, G_{,n}\, dS$$

$$= \int_{S_f} K\, G\, dS + \int_{S_h} U \tan\alpha\, n_z\, G\, dS \qquad ,$$

where K is defined as in equation (23).

IV.3.2 Results and Discussions

The following results are obtained by considering wedge models of 15° and 30°. The model is at different drafts and moving at a wide range of velocities. The chosen tank width is taken as 10.00 feet to reduce the possible interference on the results by reflected waves. Water depth is also taken at 5.00 feet to avoid any shallow water effect for the considered velocity range. Linear and non-linear results are obtained and compared to the measurements by Ogilvie (1972).

An example of the wave elevation calculated along the model is shown in Figure 20. The wedge's half angle (α) is 7.5°, and the wedge is moving at 8.00 ft/sec. The draft is considered to be 8.00 inches. Solutions are calculated at increments of 0.05 feet in the longitudinal direction of a 5.00 feet model. The obtained non-linear wave crest is observed to be higher than the linear result, and it is located closer to the bow. A secondary crest, which is absent in the linear solution, is observed to show a different characteristic in the non-linear solution.

The peak of the bow wave (Am) and the longitudinal position of its occurrence are calculated at different drafts and velocities. Both linear solutions and non-linear

solutions are plotted against the experimental results by Ogilvie (1972), as shown in Figure 21. In order to avoid confusion, Am is plotted against velocity U, and presented separately according to their drafts (T). In Figure 21, comparisons are made in dimensional units to give some indication of the scale range being used. The linear predictions of the wave peak obtained on the wedge model behave linearly with the model speed. The slope of this straight line increases as model draft increases.

In Figure 21, at T = 4 inches, the non-linear solution though over predicting Ogilvie's measurements, agrees with the experimental results much better than the linear solutions. Moreover, the trend of the non-linear predictions are similar to that of the experimental values. However, the hump-hollow behavior of the experimental results is absent in the non-linear predictions. This is probably due to an inadequacy of the slender body assumption that is made in the formulations. The hump-hollow behavior of the bow wave amplitude at increasing speed is known to be a contribution of the transverse wave. As the problem is modelled and simplified to be solved in two dimensions, it is expected that this hump-hollow behavior will be absent in the solution.

As the model draft increases, the over-prediction of the

non-linear solution becomes more and more serious. At T = 16 inches, the non-linear solution can no longer predict the measured values precisely. In order to study the difference between the experimental results and the numerical solutions, the same figure is reproduced based on a non-dimensional scale.

In Figure 22, the same results from Figure 21 are reproduced in non-dimensional units. Y_{max} is used instead of Am, and a *draft-Froude* number, **F**, is used instead of U. Their relationships are given by the following equations :

$$\mathbf{F} = \frac{U}{\sqrt{gT}} \qquad (44),$$

and

$$Y_{max} = \frac{\pi}{2\alpha U}\sqrt{g/T}\ Am \qquad (45),$$

From Figure 22, the linear prediction of Y_{max} is found to be at a constant value, independent of the *draft-Froude* number, **F**. This constant Y_{max} value from linear solutions appears to be quite insensitive to the model draft, T. It varies slightly from 1.5 at T = 4.00 inches to 1.7 at T = 16.00 inches. The analytic Y_{max} value obtained by Ogilvie has a constant value at 1.65, and is shown as a horizontal straight line.

The non-linear solutions of Y_{max} in Figure 22 agree better in the shallow draft case than in the deep model draft situation. Although the case where T = 16 inches is compared at a lower draft-Froude number, it is obvious that the linear solutions predict the experimental results more accurately than the non-linear solutions. As one can see in Figure 22, because of the over-prediction in the non-linear solutions, the non-linear solution can no longer be claimed as a better prediction than the linear solution. However, irrespective of its inaccuracy, the non-linear solution still exhibits a trend that is followed by the experimental data. Such a trend on Y_{max} is never shown in the linear solution.

This discrepancy between the non-linear solutions and the experimental results is believed to arise by different factors. Firstly, although the slender body assumption simplifies the problem to be solved in two dimensions, it has induced some error into the solution . In Figure 22, it is observed that the hump-hollow behavior does not appear in the solutions, which means that the transverse wave is not included in the solution. This transverse wave which contributes to ship resistance is expected to counteract and affect the overall wave pattern of a ship moving in a calm sea. As a result, the failure of the non-linear solution at deep model draft is believed to be partially affected by an

inadequacy of the slender body assumption.

Anothor reason for the inaccuracy appearing in the non-linear solution is believed to be in the inviscid assumption. For wave generation by moving objects, the potential flow solution is known as an adequate solution for the outer flow region. The inner solution (ie. very near the fluid-body intersection) requires a more rigorous approach. Although an interpolation scheme used to take care of the singularity at the fluid-body intersection point is derived in chapter IV.1.2, a rigorous verification of this scheme has never been carried out. However, it is believed especially in the bow wave problem, that the bow wave amplitude is damped by the viscosity of fluid. Since an inviscid assumption is made in the formulation, over-prediction is expected in the solution.

Finally, the numerical model has a different initial condition than in the real life phenomenon. In the real life situation, there is a free surface elevation ahead of the ship's bow, which is not a small magnitude. However, in the numerical model, because of simplicity, a zero initial condition is used at the wedge's leading edge. Therefore, with a different initial condition, a difference in the prediction of the bow wave amplitude is expected. Perhaps it is more suitable to declare that the assumptions, the

formulations, and the slender body approach have restricted the applicability of the solution to a shallow draft problem. When model draft is deep, some corrections or remedies must be made.

At low *draft-Froude* numbers, both solutions fail to predict the measured Y_{max} values. In fact, this is not surprising since upon the acceptance of the *draft-Froude* number as an independent parameter, it is realized that the problem under investigation is essentially a high Froude number problem, and the low Froude number solutions may not be valid. Therefore, as the *draft-Froude* number approaches zero, predictions will become more and more unreliable. Moreover, the *slender ship* assumption is also being contradicted at the bow, which was explained by Ogilvie (1972) in detail.

From a general point of view, although the non-linear solutions always over predict the measurements, the corrections (to the linear results) with a non-linear free-surface condition are in the right direction. Since surface tension and viscous effects are not included in the formulations, over predictions in the solution can be expected.

In Figure 23, the same comparisons are made with a 30°

wedge model. The numerical predictions are observed to be less accurate than the results for the 15° wedge. A possible explanation for this is the considered wedge angle being too large, making the *slender ship* assumption no longer valid.

The longitudinal positions (X_{max}) where wave peaks occurred are also calculated in Figure 24. From most of the calculations, the first peak measured along the wedge model is higher than its successive one. It is again observed that the linear predictions of X_{max} exhibit a linear relationship with the model's velocity. The slope of the straight lines drawn through the computed X_{max} values increases at deeper draft. Although the non-linear solutions over predict the measured values, they have corrected the linear results in the right direction. At T = 16.00 inches, the non-linear predictions tend to agree with Ogilvie's measurements quite well in the high Froude number range.

In order to visualize the computed solutions, some of these results are presented in graphical form. In Figure 25, a model at 12.00 inches draft and with a half wedge angle of 7.5^{0} is moving at 5.00 ft/sec. Linear and non-linear result are computed for graphical illustrations. The model thickness is ignored in the linear numerical solution, and no significant differences are found between the two solutions since the velocity is considered low.

At a shallower draft (8.00 inches) and higher model speed (8.00 ft/sec), the differences observed in the two solutions become quite obvious. As in Figure 26, the non-linear wave generated by the wedge exhibits a higher crest and travels at a higher speed in the transverse direction. As a consequence, the bow wave angle observed in the non-linear solution is larger than that in the linear solution.

In order to show the formation of a secondary bow wave, the computation is repeated for a model with a larger wedge angle. In Figure 27, a 30° wedge at 12.00 inches draft is moving at 4.00 ft/sec . A secondary bow wave is easily observed in the solution. It can be seen that in this case, the first wave decays very fast in the longitudinal direction. At approximately 2.50 feet down the wedge's leading edge, it becomes almost insignificant. Whereas the secondary wave picks up its amplitude at about 3.00 feet down the wedge's leading edge.

Finally, a 15° model at 12.00 inches draft is considered at 14.00 ft/sec. As the model speed is very high, spray formation along the model may be expected. It is remarkable that this natural phenomenon is obtained in the solution without any numerical problem. In Figure 28, the spray

formation can be seen clearly along the model. Although this is not reported by Ogilvie, such a natural phenomenon is not unexpected when the model speed is high enough.

Before entering the next section, it is worth while to mention the weakness involved in the use of the *slender ship* assumption. When a ship is assumed to be slender, not only are its beam and draft considered as small compared to its length, it also carries the meaning that the ship's geometry is changing gradually in the length direction. Moreover, the rate of change of fluid flow conditions is assumed to be very large in the transverse direction in comparison with the longitudinal direction. However, near the bow, because of the very sudden change of flow around the bow, the assumption of the inertia force is comparable to the gravity force can be locally invalid. Upon the acceptance of the *draft-Froude* number, it is already realized that the bow wave problem is a high Froude number problem, and the low Froude number solution cannot be expected to be very accurate.

It is also true that, at some distance along the wedge, the wave peak occurs at a region where model thickness can no longer be assumed small. There is always a question on how thin the model should be so as to validate the *slender ship* assumption . From the solutions, the wave height predictions in Figure 23 are obviously worse than the predictions in

Figure 22, simply because the wedge angle is larger. Therefore, when one considers the factors that cause the discrepancies between the calculations and the measurements, it is more appropriate to include the possibility of the *slender ship* assumption being violated by using a model too thick.

Another possibility for the discrepancies can be due to an inadequacy in the introduced interpolation function (Equation (24)) which over predicts the fluid-body intersection position. This function, which is linear in order, probably requires higher order terms to improve the solution. However, from a general point of view, the proposed procedure as well as the free-surface formulations are considered as acceptable for the applications in bow wave modelling. The corrections to linear numerical solutions by including the non-linear terms in the free-surface formulations, predict the trend of the bow wave amplitude at increasing *draft-Froude number* more accurately than the analytic solution provided by Ogilvie. Moreover, the formation of water spray along the model at high speed found in the solution is very encouraging. It is believed that with some minor adjustments, this solution approach originated by Ogilvie can become a very efficient modelling technique for studying the performance of a ship.

IV.4 Wave Diffraction of a Circular Cylinder (3D)

In this final example, the three dimensional applicability of the introduced free-surface formulations is tested by modelling a wave diffraction problem. A surface-piercing cylinder is located in a wave tank of constant water depth. Waves are generated by assigning sinusoidal motions to the wave maker. The diffraction of incident waves by the cylinder is calculated in the time domain and presented in graphical form. Both linear and non-linear results are obtained and plotted at constant time intervals. Forces experienced by the cylinder are compared to published experimental results by Hogben and Standing (1974) as well as Mogridge and Jamieson (1975).

IV.4.1 Formulation

A basic difference between solving a two dimensional problem and a three dimensional problem is purely in the definition of the control surface. In equation (13), which is the basic form of the Boundary Integral Equation, the control boundary, S, can no longer be represented by line elements in the following application. It is probably one of the most painful procedures to define S by using surface patches when applying equation (13) in three dimensions. As one can see in the following derivation of the specific form of equation

(13), the procedure is very similar to those in previous applications except an additional mesh generation procedure is required. It is therefore considered to be more appropriate to discuss the discretization of three dimensional surfaces under a separate topic heading. In this section, discussions are concentrated on the problem's formulation.

An illustration of the problem is given in Figure 29 . A surface piercing circular cylinder is considered numerically in a small wave tank. The coordinate axis is located as shown in the diagram with **y** pointing up. In order to cut down the number of unknowns involved in the problem, Green's function (G) defined as in equation (15) is applied to simulate a mirror image effect about the bottom of the numerical tank. Moreover, because of symmetry about $z = 0$, modelling of either half of the tank is considered adequate.

As in previous studies, the control surface that encloses the considered domain is divided into S_0 , S_f , and S_m . S_0 is used to represent impermeable surfaces such as the tank wall, and the cylinder's submerged surface. The free-surface is designated by S_f , and the wave piston by S_m. Therefore, equation (13) can be rewritten as :

$$\phi(P) + \int_{S_0} \phi\, G_{,n}\, dS + \int_{S_f} \phi\, G_{,n}\, dS + \int_{S_m} \phi\, G_{,n}\, dS$$

$$= \int_{S_0} \phi_{,n}\, G\, dS + \int_{S_f} \phi_{,n}\, G\, dS + \int_{S_m} \phi_{,n}\, G\, dS \qquad (46),$$

where G is defined in equation (15).

Since the impermeable surface is not moving, fluid particles on this surface have a zero normal velocity, that is,

$$\phi_{,n} = 0 \qquad \text{on } S_0 \qquad (47).$$

As for the free surface, equation (10) is considered as appropriate.

$$\phi_{,n} = -\frac{2n_y}{g(\delta t)^2}\phi^0 + \frac{n_y}{g}\frac{5\phi^{-1} - 4\phi^{-2} + \phi^{-3}}{(\delta t)^2}$$

$$+ \phi'_{,x}n_x + \phi'_{,z}n_z + \frac{n_y}{2g}\frac{D}{Dt}(\phi_{,x}^2 + \phi_{,y}^2 + \phi_{,z}^2)'$$

$$\ldots\ldots \text{at } y=\eta \qquad (10).$$

For convenience, a function F_3 is used to represent the known terms in the above expression, and it is rewritten as :

$$\phi_{,n} = -\frac{2n_y}{g(\delta t)^2}\phi + F_3 \qquad \text{at } y=\eta \qquad (48),$$

where

$$F_3 = \frac{n_y}{g} \frac{5\phi^{-1} - 4\phi^{-2} + \phi^{-3}}{(\delta t)^2} + \phi'_{,x} n_x + \phi'_{,z} n_z$$

$$+ \frac{n_y}{g} \frac{D}{Dt}(\phi_{,x}^2 + \phi_{,y}^2 + \phi_{,z}^2)' \qquad (49).$$

It can be recalled from Chapter II.2 that the prime notation is used to identify the terms that are approximated by an extrapolation function in time.

As for the linearized free-surface condition,

$$\phi_{,n} = - \frac{2}{g(\delta t)^2} + K \qquad \text{at } y=0 \qquad (50),$$

where K is given in equation (23).

Finally, for completion of the problem, a displacement function should be assigned to the wave maker. Although this can be arbitrar*ily* chosen, it is very desirable to have a function that starts the piston smoothly at time equal to zero. For this reason, the following function is used.

$$x_m = X_m (1 - \cos \omega t) \qquad \text{on } S_m \qquad (51),$$

where X_m is the motion amplitude, and ω is the angular frequency. The corresponding velocity function is, therefore, given as :

$$v_x = X_m \omega \sin \omega t \qquad \text{on } S_m \qquad (52).$$

With equations (47), (48), and (52) substituted into equation (46), the corresponding form of the integral equation is obtained as follows :

$$\phi(P) + \int_{S_0} \phi\, G_{,n}\, dS + \int_{S_f} \phi \left(G_{,n} + \frac{2n_y}{g(\delta t)^2} G \right) dS + \int_{S_m} \phi\, G_{,n}\, dS$$

$$= \int_{S_f} F_3\, G\, dS + \int_{S_m} (v_x n_x)\, G\, dS \qquad (53).$$

This equation is then used to establish a system of equations and yield solutions at designated time intervals. If linear solutions are desired, equation (50) should be used instead of equation (48) upon the substitution, and results are calculated at the undisturbed free surface. Since there is nothing special about the linearized form of the integral equation, its derivation is not included here.

IV.4.2 Mesh Generation

Before the system of equations can be constructed, the control surface must be defined. For three dimensional applications, the boundary surface is discretized and divided into small elements. These small patches with their size,

position, and orientation known, enclose the considered domain. Certain numeric codes are then developed to keep track of the potential and velocity values on particular elements during the computations. The choice on the shape of elements is arbitrary. Under normal conditions, triangular patches are the most popular to use. However, in the case of insufficient computer memory, quadrilateral elements can be used provided that the leakage problem found between elements is treated carefully. Unfortunately, there is no general rule or guideline for the choice of what kind of elements should be used. Therefore, it is up to the programmer to figure out the most efficient way to represent the problem numerically.

At the University of British Columbia (UBC), the best current computer facility available is the Michigan Terminal System (MTS). It is linked to a FPS-164/MAX array processor located in the computer center. With the main processor rated at 11 MFLOPs (Million FLOating point OPerations per second), and the MAX boards rated at 55 MFLOPs, solutions of large matrices can be calculated at high speed. However, the size of the computed matrix is restricted by its accessible memory. Its 1 Mwords of main memory with two 135 Mbyte drives, can only handle a system of equations up to approximately 900 unknowns. For this reason, the following problem can only be solved in the present system with poor resolution. In order to maintain solutions at reasonable

resolution with small enough element numbers, quadrilateral elements are reluctantly used.

A discussion on the advantages of using triangular patches over quadrilateral elements can be found in Webster (1975). In his paper, he pointed out that there is a danger of source leakage and discontinuity found between elements when a three dimensional surface is represented by quadrilateral elements. Since larger memory computers are currently inaccessible, quadrilateral elements are used under the following assumptions :

i. Wave amplitude is assumed to be small compared to wave length, such that the slope of the free surface is small in all directions, and all changes are gradual in time.

ii. In order to ensure that there is no source leakage between elements, each quadrilateral element is considered to be composed of 4 triangular planes. In Figure 30, the 4 corners of an element are labelled as P, Q, R, and S. Its geometric center, c, is calculated by :

$$x_c = \frac{x_P + x_Q + x_R + x_S}{4}$$
$$y_c = \frac{y_P + y_Q + y_R + y_S}{4} \qquad (54).$$
$$z_c = \frac{z_P + z_Q + z_R + z_S}{4}$$

There is no necessity for these 4 corners to lie on the same plane. In other words, each quadrilateral element can twist in space. Its area is given by the sum of the 4 triangular facets' area, and its normal unit vector is considered by taking the average of the normal unit vectors on these triangles.

When computing the solution, the respective potential value and velocity on an element are calculated at c . Therefore, source leakage and discontinuity problems found between elements are considered to be reduced. Provided the small amplitude wave assumption is not violated, the above assumption for the quadrilateral element can be accepted.

Although these two assumptions have greatly simplified the programming work, there is no intention to insist on the use of quadrilateral elements. In fact, the reason why they are used here is clearly explained. When bigger memory computers are accessible, triangular patches should be used. Therefore, this example serves mainly as a numerical experiment for the three dimensional applicability of the

free-surface formulations.

After the quadrilateral element is chosen, the dimensions of the considered domain have to be determined. In most of the following computations, the wave tank is chosen to be 5 times the cylinder's diameter in length and 2.5 times in half width. As a radiation condition is not involved in the formulations, this chosen tank length is only good enough for studying the first two waves without suffering from the disturbance of reflected waves. The simulation time is calculated by linear wave theory for the first wave to travel back and forth along the tank. Computations should be terminated before the flow near the cylinder is disturbed by reflected waves.

It is also important to maintain a fine enough size of elements on the free-surface in order to provide good results. In most of the following calculations, the free surface is represented by 450 elements. A minimum of 12 elements are used to define the submerged surface of the half cylinder. They are arranged in layers of six, depending on water depth (see Figure 31). The generated mesh of the free surface is illustrated in Figure 32. The wave maker is on the left-hand side, while on the other end, a rigid wall is placed.

IV.4.3. Interpolation (3D)

The material discussed in this section serves mainly as an extension of section IV.1.2 . In the three dimensional numerical model, after the potential distribution is known on the free surface, velocity components can be resolved since the free-surface's gradient is known. These velocity components are then used to predict the free-surface motion within the next time increment, so as to advance the solution in time. The motion of an element is calculated by considering the resultant motions at its 4 corners. Its geometric center, **c**, is always given by equation (54). In order to define the velocity at an element's corner, a simple interpolation function (equation (55)) is used.

In Figure 33a, point **P** is considered as the common point surrounded by element **I**, **J**, **K**, and **L** . Since the velocity is known at the center of these element, the following function is used for the interpolations of velocity at **P**.

$$\left.\begin{matrix} v_x \\ v_y \\ v_z \end{matrix}\right\} = \mathbf{ax} + \mathbf{by} + \mathbf{cz} + \mathbf{d} \qquad (55),$$

where **a**, **b**, **c**, and **d** are constants different from element to element.

When this equation is applied at the centers of 4 adjacent elements I, J, K, and L , 4 equations with 4 unknowns can be written. The velocity component,for example v_y , on the four elements contributes to the column vector on the right-hand-side of the matrix equation, and the constants (a, b, c, and d) are the unknowns to be solved. When these unknowns are found, v_y at point P can be calculated. The procedure is very similar to the discussion in Appendix II.

It is found that equation (55) can be applied to a point which is located at the fluid-body intersection boundary. In Figure 33b, element I and J are on the free-surface, while K and L are on the cylinder wall. The normal velocity component on the cylinder wall is taken as zero to prevent fluid particles from penetrating into the surface. Other components are computed as discussed in Appendix II.

Although there was a hesitation in applying equation (55) to the fluid-body intersection boundary as its limitation is not quite clear, reasonable results are obtained in most of the studies. It only happens to fail in modelling a high amplitude wave case, where the wave run-up on the cylinder is improperly represented by coarse elements. This computer deficiency situation can be improved by using more free-surface elements near the cylinder. It is, of course, possible to use a second order function for better

interpolations, except such an idea is not very practical for the following studies. Computer cost is a prime factor to be considered upon the acceptance of a second order interpolation function.

IV.4.4 Results and Discussion

In the following results, the diameter of the vertical cylinder is chosen to be 50.00 m. The wave tank is determined to be 250.00 m in length, and its half width is taken as 125.00 m. 450 elements are used at the free surface. Water depth is at 10.00 m, and 12 elements, arranged in two layers, are used to represent the cylinder. Motion amplitude (X_m) of the wave maker is assigned at 1.00 m. Results are obtained at two frequencies.

The first set of solutions is calculated by moving the wave maker at 0.061 Hz. The corresponding ka value is equal to 1.0 , where k is the wave number and a is the radius of the vertical cylinder. Computations proceeded in time at 0.2 second real time increments for 36.00 seconds. Results are plotted at every 4.00 second interval. In Figure 34, both linear and non-linear solutions are illustrated in their graphical form. Results obtained by a linear free-surface condition are on the left-hand-side of the diagram. The vertical plotting scale is enlarged 50 times for better

illustration.

At t=0, the piston located at the left end of the tank starts its motion. Waves are generated and propagate down the tank at constant speed. Since the simulated wave amplitude is small, the difference between the two solutions is not very obvious. The second wave crest is calculated at 0.20 m by the linear formulation, while it is at 0.21 m from the non-linear solution. Wave length is observed at about 157 m which corresponds to a height over length ratio (H/λ) of 0.00255 (linear) and 0.00268 (non-linear) respectively.

The non-linear waves are observed to travel slightly faster than the linear waves. At 36.00 seconds, the non-linear solution exhibits a crest high enough to differ from the linear result. It is believed that the solutions at this moment are disturbed by reflected waves from the end wall. Although at t=36 seconds, these reflected waves are almost insignificant, the force calculated on the cylinder is thought to be influenced and become unreliable.

Figure 35 is a horizontal projection of the free-surface elements distribution at t=0 and t=36 seconds. Basically, there is no major difference between the two, except at the near cylinder region, elements seem to suffer from very great distortions. It is believed that, at the forward and after

stagnation points of the cylinder, more elements should be used to define the wave run-up situation. Moreover, it is desirable to model the tank length as long as possible, so as to delay the disturbance from reflection until later cycles. In order to illustrate how the results are affected by the chosen tank length, a shorter length is used to repeat the computations.

In Figure 36, a tank length of three times the cylinder diameter is considered (ie. 150.00 m). Other parameters remain the same as in Figure 34 . The free surface now consists of 270 elements (see Figure 37), and the simulation continues for 32.00 seconds. Results are basically similar to Figure 34 , except that the generated waves are slightly higher than in the previous case. However, when the free-surface elements in Figure 37 are examined at time t=32, it shows that some of these elements have partially penetrated into the cylinder. This observation indicates that the tank length has a very strong influence on the solutions, and probably there exists a numerical weakness in the constructed model. If the chosen tank dimension is too short, numerical solutions will be exaggerated and consequently a failure within a very short period of time. This is observed by comparing the calculated wave amplitude in Figure 34 and Figure 36. As the same plotting scale is used, the wave amplitude obtained in the shorter tank is obviously higher in

magnitude.Therefore, a tank with a length 5 times the cylinder diameter is taken to be the minimum acceptable limit in this study.

The motion frequency of the wave maker is doubled to 0.122 Hz in Figure 38 in order to model a shorter wave length. In this case, the vertical dimension is scaled up only 25 times for plotting. Wave length is 1.5 times the cylinder diameter. Computation is designed to terminate at 36.00 seconds. Linear solutions are shown on the left-hand side and non-linear solutions are shown on the right-hand side of Figure 38. No major difference is observed between the two. The non-linear wave crest is slightly higher and travels slightly faster.

In order to test the limitations on the constructed model, the piston's motion amplitude is increased to 2.5 m to simulate a high amplitude wave situation. The frequency remains at 0.061 Hz. With a vertical plotting scale 25 times the calculated dimension, results are shown in Figure 39. The first wave, which is highly transient in nature, has an amplitude of about 1.00 m before it reaches the cylinder. Although the H/λ is equal to 0.0127 (which is considered as acceptably small), computations of the non-linear solutions failed at 16.00 seconds. This is explained by an improper modelling of the wave run-up situation on the cylinder with

the coarse size elements. In Figure 39, the free surface exhibits a depression at the forward stagnation point of the cylinder. Similar failure is not found in the linear solution. It is believed that the failure is caused by an improper modelling of the wave run-up at the cylinder by quadrilateral elements. A finer grid is probably required to represent this region where flow changes rapidly. Moreover, as the H/λ ratio is higher, the quadrilateral element will be twisted badly at the near cylinder region.

However, irrespective of this imperfection, the constructed numerical model behaves very well at low amplitude wave simulations. There is enough evidence to support that the introduced free-surface formulation and solution procedure are sufficiently accurate for modelling transient, non-linear, three dimensional wave making problems in the time domain.

Finally, the wave force exerted on the cylinder is computed and plotted in Figure 40. The continuous line appears in the diagram is the frequency domain solution based on Chan (1984). The non-linear time domain calculations are compared to measurements made by Hogben and Standing (1974) as well as Mogridge and Jamieson (1975). Since the non-linear solutions are calculated in a time domain wave tank, forces due to the first wave cycle are ignored. The presented

results are considered to be the maximum force calculated after the first wave has passed by the cylinder. The non-dimensional form was suggested by Sarpkaya and Isaacson (1981) as :

$$F_{max} = \frac{| F_x |}{\rho g H d a \, [\tanh kd / kd]} \qquad (56),$$

and

$$F_x = \int_{S_c} P \, dS \qquad (57).$$

S_c is the submerged surface of the cylinder. P is the pressure calculated in equation (4). ρ is the fluid density, H is the incident wave height, d is the water depth, and **a** is the radius of the cylinder.

F_{max} calculated at different ka values is shown in Figure 40. At a ka value greater than 1.00, the agreement between the time domain solutions (non-linear) and the experimental results is excellent. Not only the forces are accurately predicted, and the trend of the non-linear solution is observed very similar to the measurements by Hogben (1974). As for the frequency domain solution, which is linear, the prediction is not as good as the non-linear solution. In fact, the trend of the experimental results cannot be observed in the linear solution when ka is greater

than 1.00.

However, at a *ka* value less than 1.00, the experimental results follow the frequency domain solution while the time domain solution diverge from the measured values. The smaller the *ka* value is, the bigger the discrepancy is found. Since the error is behaving systematically, there must be an explanation for it.

These discrepancies are believed to be associated with the chosen tank dimension. At *ka* equal to 1.00, the wave length is calculated to be 157 m, which is about 0.628 times the chosen tank length. Below this value, the wave length becomes very long and eventually exceeds the tank's dimension. When this happens, since F_{max} is the force calculated after the first wave cycle, it is very possible that the first wave being reflected from the end wall interferes with the second wave before it reaches the cylinder. Although, the time domain prediction is very poor at low *ka* values, the fact that this result (which is non-linear) at *ka* values greater than 1.0 is much better than the linear solution that this argument is strongly supported. As for the frequency domain solution, the same problem does not exist since a radiation boundary is used (see Chan 1984). It only happens at *ka* value greater than 1.00 that the linear solution becomes not as reliable as the

non-linear solution.

If the modelled tank length can be increased to about 10 times the cylinder's diameter, the time domain solution of F_{max} can possibly be calculated more precisely without being disturbed by reflected waves.

From the experience gained in this study, the free-surface representation is very critical to the numerical model's stability. More elements should be used at the near cylinder region. A longer tank is thought to be helpful to eliminate the interference from reflected waves in the time doamin solution. Moreover, if it is possible, triangular patches should be used to obtain a much better definition of the wave run-up situation on the cylinder. Results obtained in this section are regarded as encouraging, and the three dimensional applicability of the proposed free-surface formulations is shown with some restrictions. These restrictions seem to depend on the free-surface element definition rather than the methodology.

V. DISCUSSIONS AND CONCLUSIONS

In this chapter, discussions are made from a general point of view. Although, some of the discussions seem to overlap the ideas from previous chapters, conclusions cannot be established without an overview of all the accomplishments. The following discussions are mainly on three kinds of topics. They are on the formulation of problems, numerical results, and recommendations. Since there is certain unavoidable overlapping between the ideas, they are discussed simultaneously in the following section.

V.1 General Discussions

The proposed solution procedure is, in fact, parallel to Longuet-Higgins' approach, except that the free-surface boundary conditions are expressed in real variables only. The time or material derivative term is replaced by a finite difference form based on known values at previous time steps. A predictor method is used to extrapolate future values for velocity terms and used to calculate the free-surface boundary condition to advance the computations in time. As a consequence, a very systematic procedure is established to solve gravity wave problems in the time domain.

The first two problems presented in chapter IV actually serve as test cases for the study of the non-linear free-surface boundary conditions. The free-surface condition is emphasized here because it has remained as the source of problems for many years. As mentioned in the introduction, this moving boundary causes difficulties, not because of the uncertainty involved in the free-surface definition, but because of the numerical instability found in the time domain solution.

One of the contributions achieved by Longuet-Higgins was his introduction of a smoothing procedure during computations to inhibit the growth of instability in the time stepping solution. From then on, many transient free-surface problems were modelled numerically.

It must be admitted by the author that the rearrangement of the free-surface boundary conditions presented in this thesis is finalized through a series of numerical trial and error studies. The idea of extrapolating the unknown velocity terms and maintaining them in an unexpanded form are believed to be the crucial assumption made in these studies. The wave tank study and the modelling of breaking waves enabled the author to study the different algebraic forms of the free-surface boundary conditions to result in a numerically stable solution without any smoothing requirement.

The choice of this unexpanded form given in equation (10) is based purely on numerical test experience gained by the author. Other possible arrangements, all based on various expansions of the non-linear terms in equation (10), have been tried without any success. One possible explanation for this chosen form to yield a numerically stable solution is probably related to the nature of the Bernoulli Equation. In equation (4), the velocity square terms can be considered associated with the kinetic energy of the fluid particle. Its material derivative (as in equation (6)) is thought to be related to the change of kinetic energy of the same particle being traced in time. It is possible that fluid particles' kinetic energy, which is a scalar quantity, changes gradually in time and can be approximated momentarily by a second order function of time.

As for an expanded form of the material derivative of the velocity square terms, numerical error tolerated in the approximation of the change of kinetic energy could be exagerated by increasing the number of unknown terms in the representation. Instead of treating the associated kinetic energy terms as a single quantity, each velocity component as well as its material derivative have to be approximated by a time extrapolation scheme. As a result, the error involved in the free-surface formulation could become intolerable, and

the solution could become unstable.

It is also remarkable how the interpolation function works at the fluid-body intersection point. As studied by Lin (1984), this point requires special treatment. It can be proved that, when this intersection point is extrapolated by values at the free-surface only, it behaves reasonably for low amplitude wave cases. The idea of including information on the wave piston to interpolate the velocity at this intersection point is believed to be an acceptable approach. In fact, the wave splashing phenomenon obtained in the bow wave simulation at high model speed has proven to a certain extent that the idea is correct. However it is also a disadvantage that this interpolation skill only works on the zeroth order elements. For higher order boundary elements, since end points are node points and defined the intersection point, another interpolation criterion must be developed.

The drift of free-surface elements, though bringing some excitement since the natural phenomenon is modelled, is a bad indication on the stability of the numerical model. If all the elements at the free surface are drifting down the tank, it is only a matter of time for the numerical model to fail because of the improper sized elements representing the free surface. Although, there are many remedies to this problem, such as breaking an element which is too long into two, it is

considered to be more appropriate to leave this study to the future. Fortunately, it takes many wave cycles to worsen the problem, and it can be ignored for the first few cycles.

From the studied problems, certain limitations are found. Theoretically, better solutions can always be obtained by using a finer grid, increasing the tank length, adopting triangular patch elements, or even reducing the size of the time step. Most of these recommendations require more computer memory. Since in real life, there is always a hardware limitation on computers, it is very unwise to rely on expanding computer memory for better solutions. Some actions should be taken to reduce the chances of having a bad solution. For time stepping solution problems of this kind, it would be very helpful to formulate some sort of beach condition. As it was shown in the three dimensional modelling problem, a great obstruction found in programming the problem is the limited accessible computer memory. If such a boundary condition can be formulated for time domain problems, at least the solution can be free from the disturbance of reflected waves. However, at this present moment, such a boundary condition is not ready, so upon constructing a numerical model, special care must be taken on the decision of the dimensions of the control domain, the size of elements, as well as the problem's computer simulation time.

Prior to considering the conclusions, the efficiency of the time stepping solution procedure is worth some discussion. Although solutions are obtained for various problems, the computer cost is very high. In two dimensional problems, solutions can be obtained at quite a low cost since the number of unknowns is usually small. However, for three dimensional problems, it is extremely easy to come up with a numerical model with a few thousand unknowns. Access to very huge and super computers seems to become a necessity. It is very unfortunate that the established matrix is unsuitable for iterations. Since this huge matrix must be solved by a direct method (such as the Gaussian Elimination Method), a major portion of the computer time is consumed in solving the matrix.

Moreover, starting the simulations at the zero initial stage consumes a large amount of computer time. It would be ideal if the initial conditions were given at a time just prior to the moment of interest, and the transient behavior were studied from that point on. If this can be done, free-surface problems can be studied very efficiently. However, at this present moment, such an idea is not very practical. For example, many of the steady state solutions are calculated for an infinite domain or with a radiation condition. In order to apply these analytic solutions as initial conditions, the boundary conditions between the time

domain model and the frequency domain model must be compatible within some degree.

V.2 Conclusions

The presented numerical procedure is considered as a reliable approach for solving potential flow problems with a free surface. The time domain solutions obtained for two and three dimensional problems are numerically stable and do not require any smoothing procedure. The free-surface boundary condition is rearranged to yield non-linear solutions under a small time step assumption. The fluid-body intersection singularity problem is handled by an interpolation function that requires information from both surfaces. Numerical results are comparable to linear theory as well as published experimental work. Limitations are found in modelling a three dimensional diffraction problem. Solutions for high amplitude waves are restricted by the use of quadrilateral elements and coarse grid size. Wave forces calculated on the surface-piercing cylinder are influenced by the chosen tank length. As the simulated wave length becomes comparable to the tank length, the calculated force experienced by the cylinder diverges from the experimental result. When the wave length is short compared to the tank, good results are obtained.

REFERENCES

Banerjee, P.K. and Butterfield R. 1981. *Boundary Element Methods in Engineering Science*, London : McGraw Hill.

Brebbia, C.A. 1978. *The Boundary Element Method for Engineers,* London : Pentech Press.

Calisal, S.M. and Chan, J.L.K. 1987. Breaking Waves Simulation. *Second International Workshop on Water Waves and Floating Bodies,* Dept. of Math., U. of Bristol, U.K., Report no. AM-87-06, pp. 9-12.

Calisal, S.M. and Chan, J.L.K. 1986. *Stability of Low L/B Vessels*. Unpublished Report, Dept. of Mech. Engineering, U. of British Columbia, Vancouver, B.C.

Chan, J.L.K. 1984. *Hydrodynamic Coefficients of Axisymmetric Bodies at Finite Water Depth*. Master Thesis, Dept. of Mech. Engineering, U. of British Columbia, Vancouver, B.C.

Dean, R.G. and Dalrymple, R.A. 1984. *Water Wave Mechanics for Engineers and Scientists,* New Jersey : Prentice Hall.

Fredholm, I. 1903. *Sur une class d'equations fonctionelles,* Acta. Math., Vol 27, pp 365-390.

Hogben, N. and Stanging, R.G. 1974. Wave Loads on Large Bodies. *Proc. Int. Symp. on the Dynamics of Marine Vehicles and Structures in Waves,* Univ. College, London, pp 258-277.

Hunt, B. 1980. The Mathematical Basis and Numerical Principles of the Boundary Integral Method for Incompressible Potntial Flow over 3-D Aerodynamic Configurations. *Numerical*

Methods in Applied Fluid Dynamics, London : Academic Press, pp. 49-136.

Jawson, M.A. 1963. *Integral Equation Method in Potential Theory*, I. Proc., R. Soc. Lond., Series A 275, pp 23-32.

Lin, W. 1984. Non-linear Motion of the Free Surface Near a Moving Body. *Ph D Thesis*, Dept. of Ocean Engineering, MIT, Cambridge, Mass.

Longuet-Higgins, M.S. and Cokelet, E.D. 1976. The Deformation of Steep Surface Waves on Water, I.A Numerical Method of Computation. *Proc. R. Soc. Lond.*, Series A, 350, pp. 1-26.

Mogridge, G.R. and Jamieson, W.W. 1975. Wave Forces on Circular Caissons : Theory and Experiment. *Can. J. Civil Eng.*, Vol 2, pp 540-548.

Newman, J.N. 1977. *Marine Hydrodynamics*. Cambridge, Mass., MIT Press.

Ogilvie, T.F. 1972. *The Wave Generated by a Fine Ship Bow*. Dept. of Naval Architecture and Marine Engineering, U. of Michigan, Report no. 127.

Sarpkaya, T. and Isaacson, M. 1981. *Mechanics of Wave Forces on Offshore Structures*. New York : Van Nostrand Reinhold.

Vinje, T. and Brevig P. 1980. *Non-linear, Two Dimensional Ship Motion*. SIS Report, Norwegian Hydrodynamic Laboratory Trondheim.

Webster, W.C. 1975. The Flow About Arbitrary, Three Dimensional Smooth Bodies. *Journal of Ship Research*, Vol. 19,

no. 4, pp 206-218.

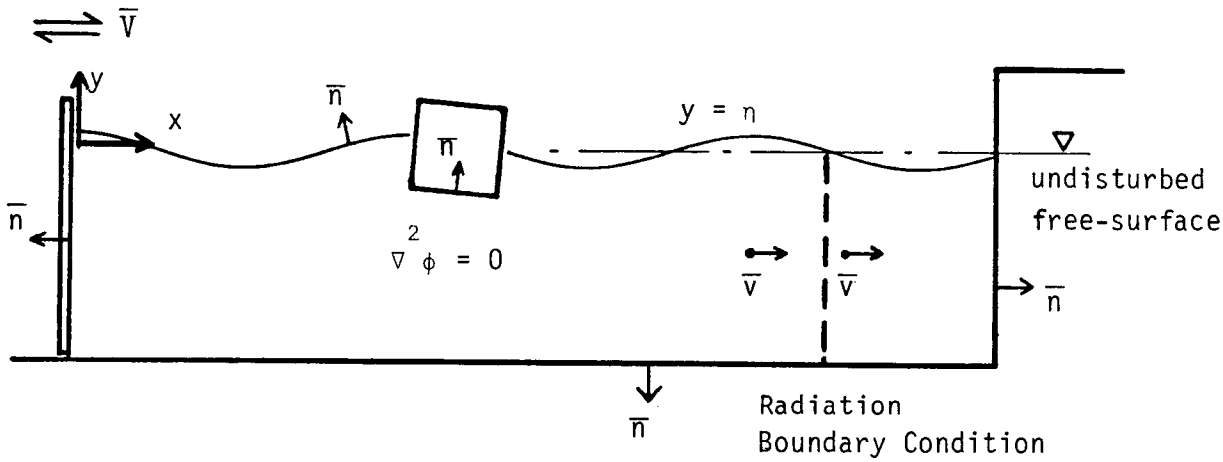

Figure 1. A Typical Wave Making Problem

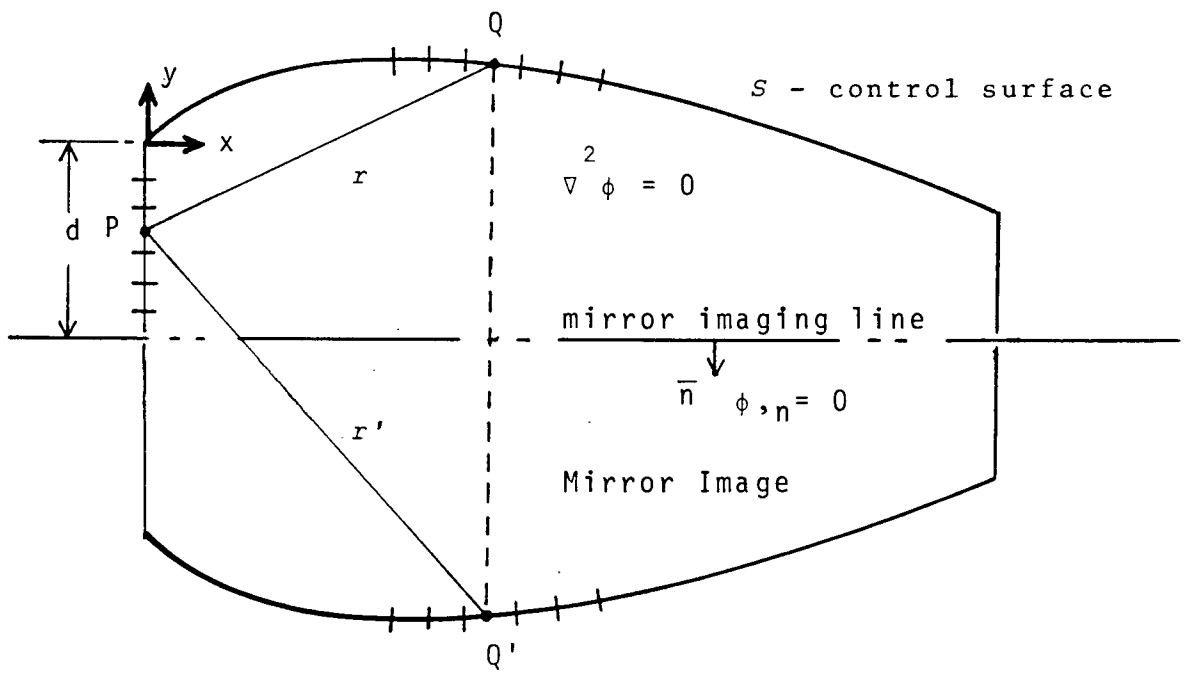

Figure 2. Numerical Model with Mirror Image at y=-d

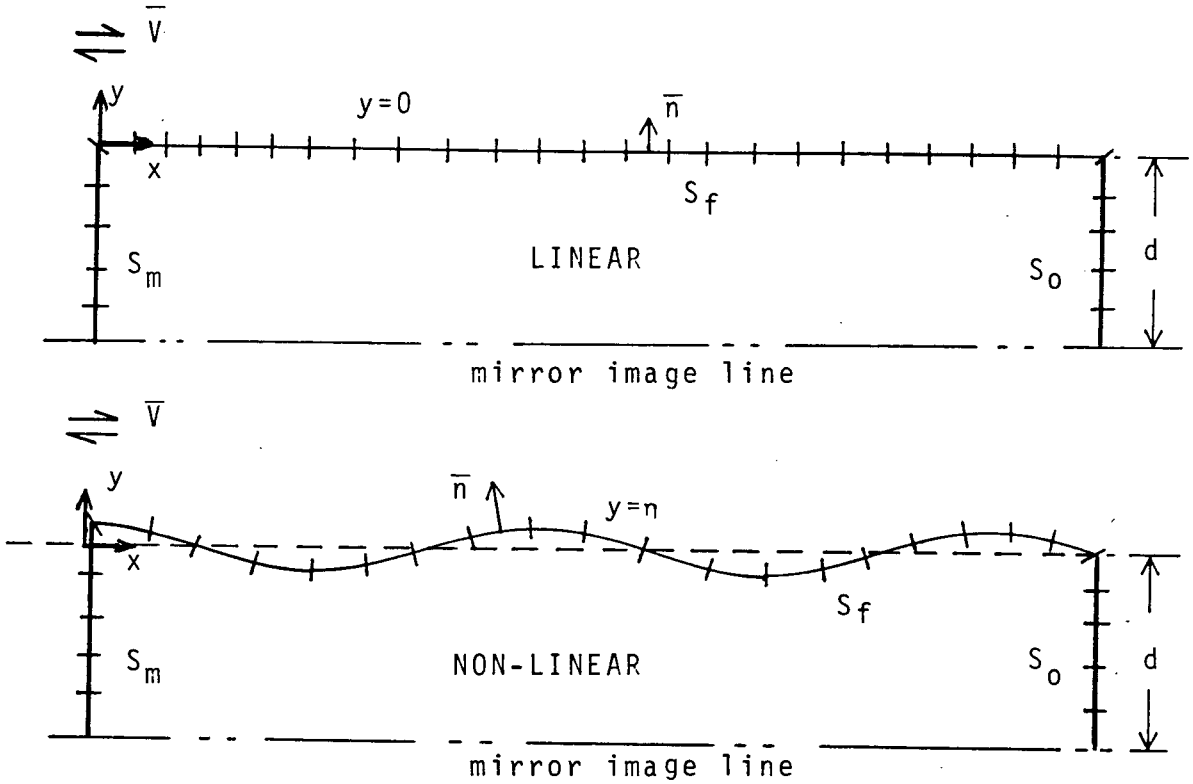

Figure 3. Linear and Non-linear Wave Tank Models

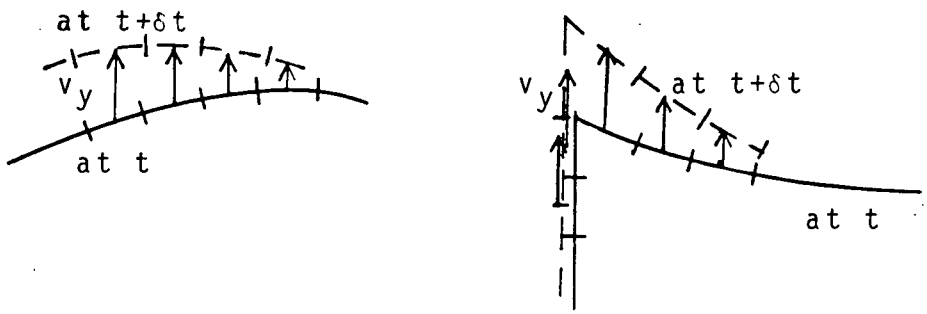

at Free-Surface

at Fluid-Body Intersection

Figure 4. Interpolation of Velocity Between Elements

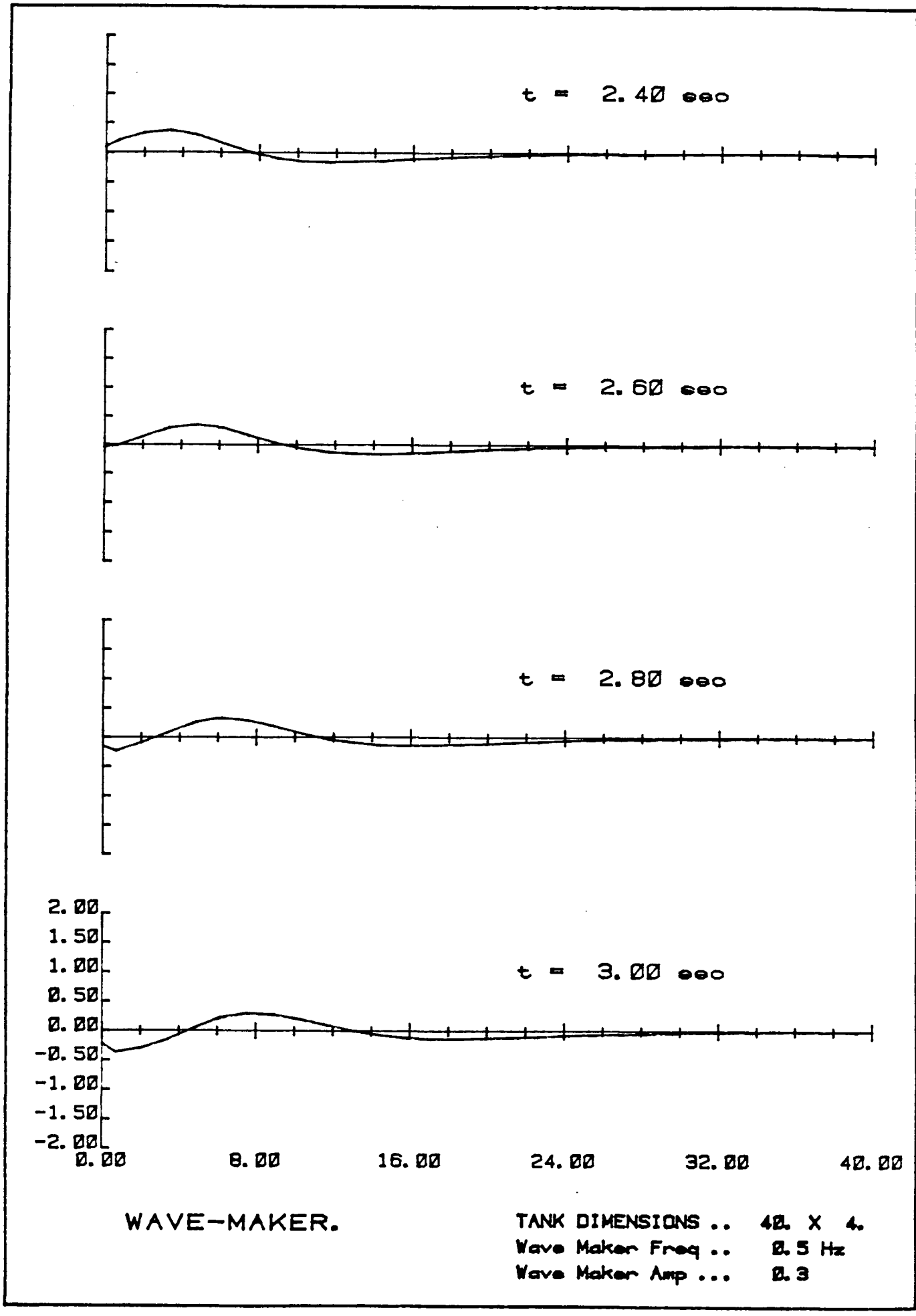

Figure 5. Wave Generation by a Numerical Wave Tank Model (dt = 0.05 sec.)

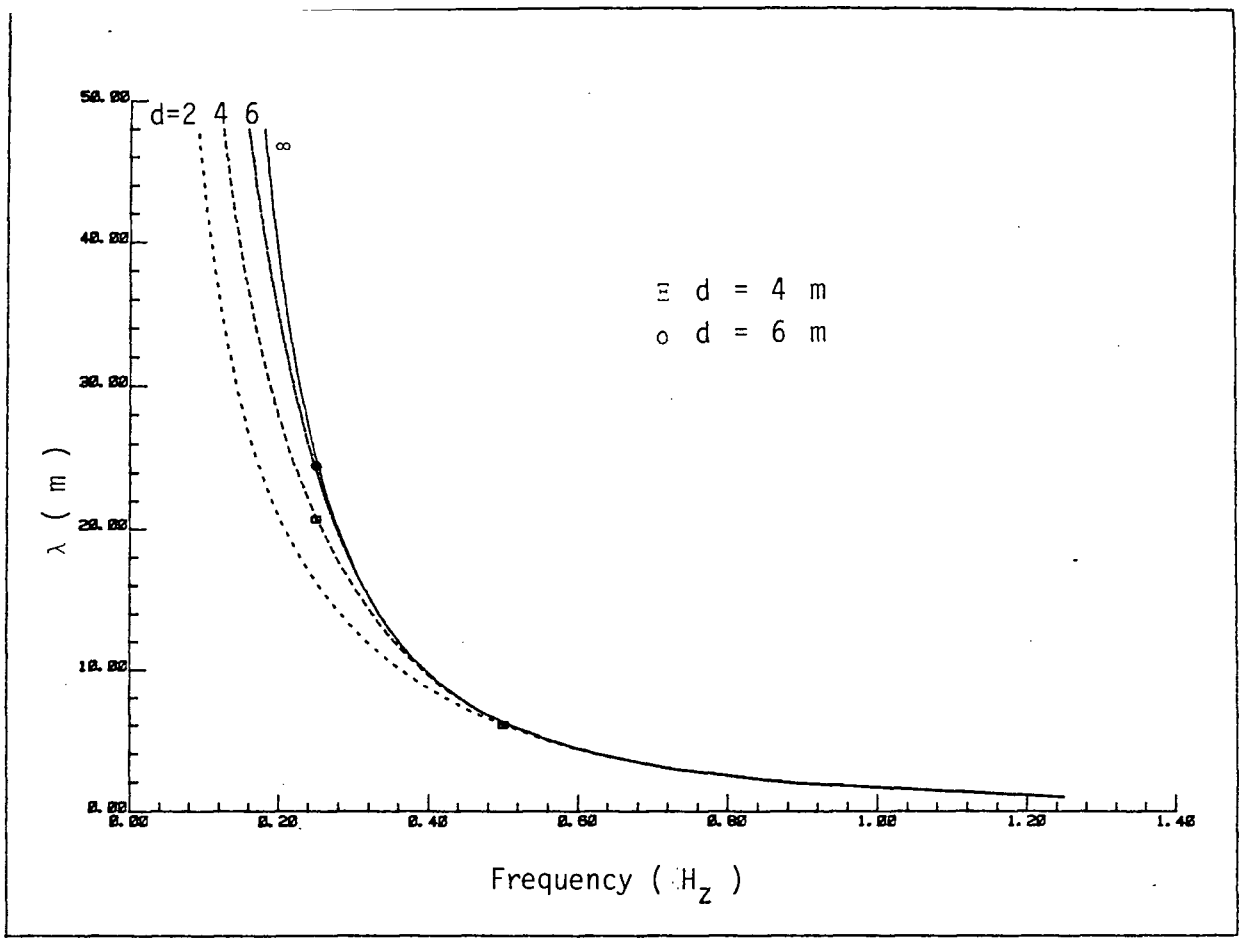

Figure 6. Prediction of Wave Length by Linear Numerical Model

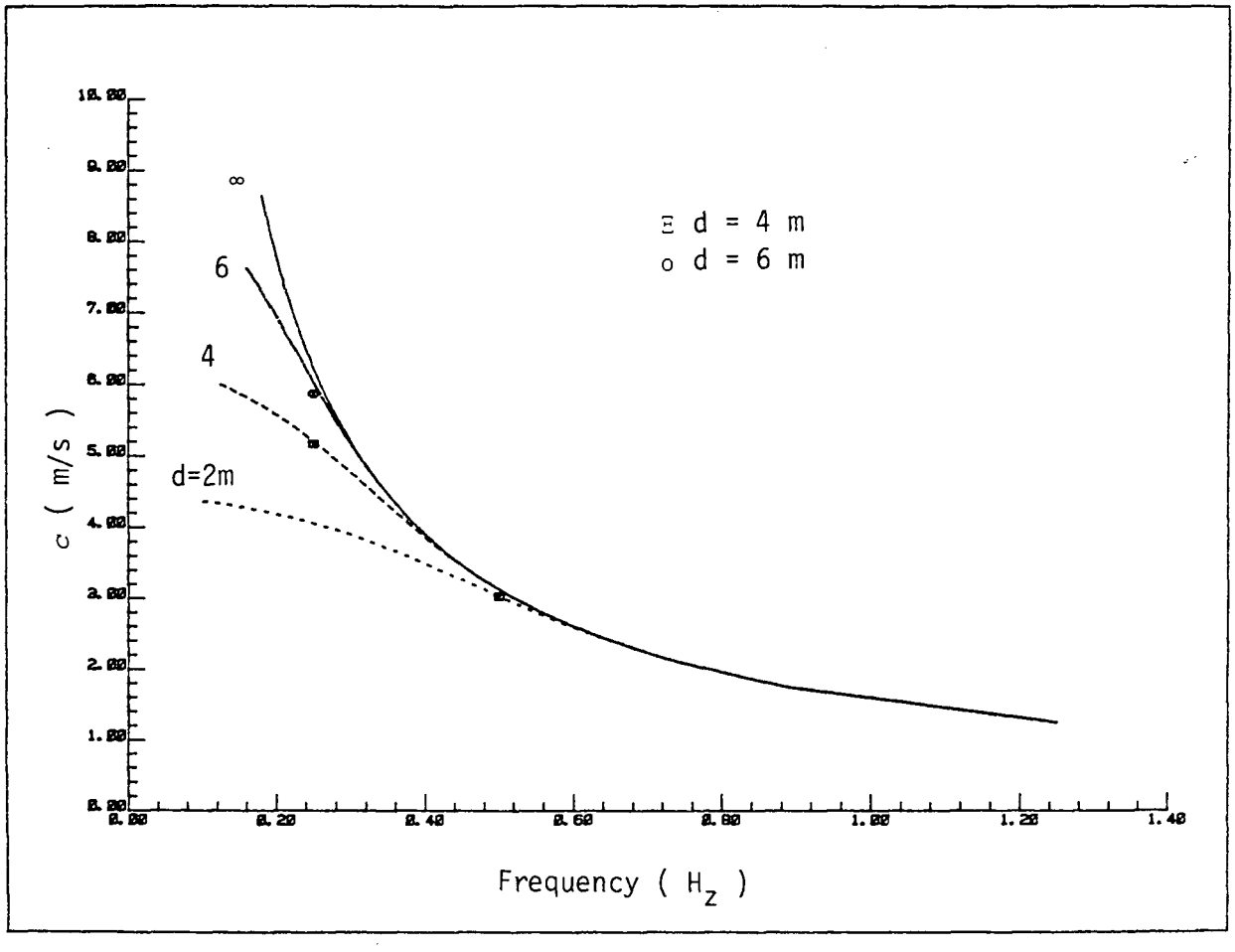

Figure 7. Comparison of Phase Velocity Between Solution and Wave Theory

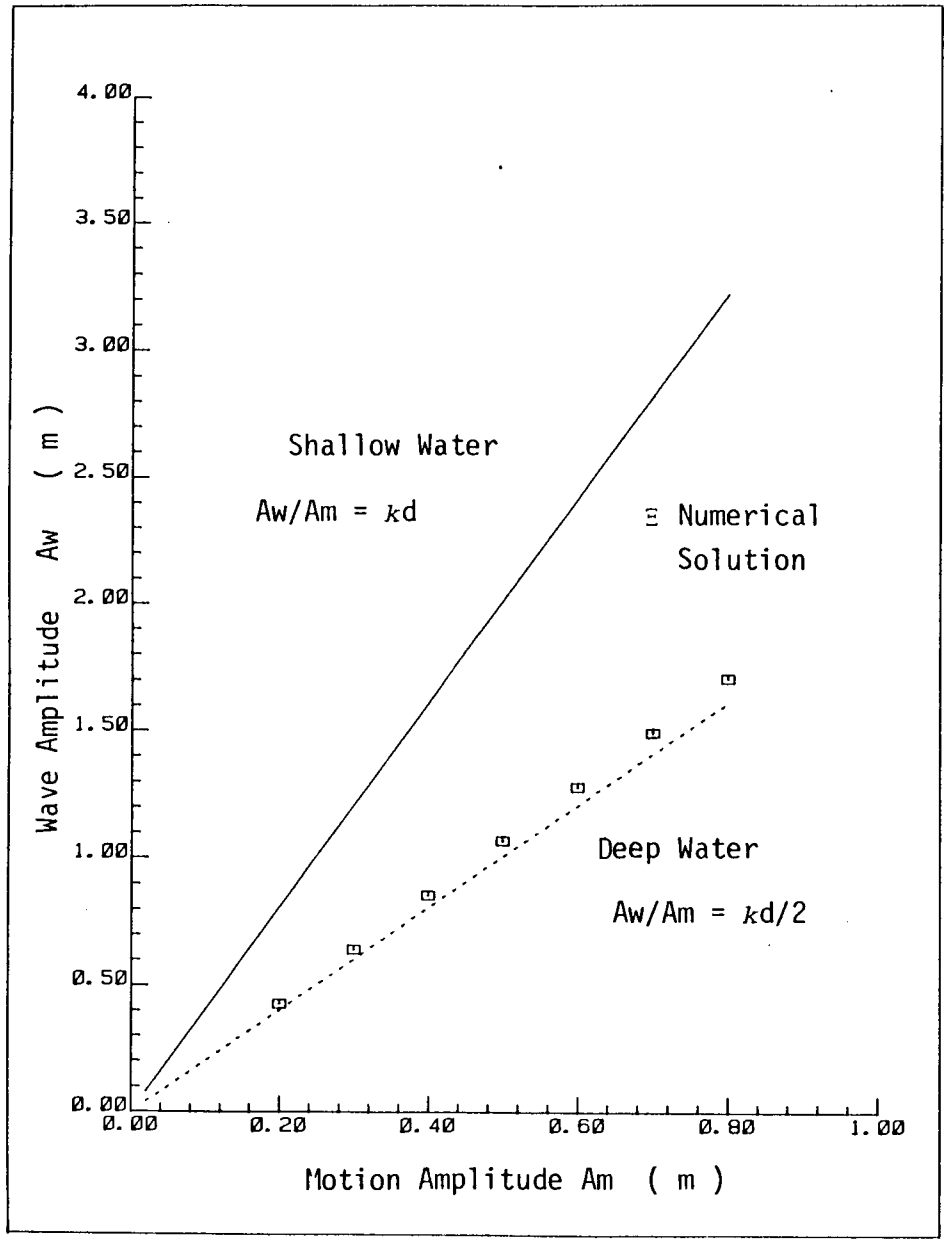

Figure 8. Wave Amplitude Predictions by Numerical Solution

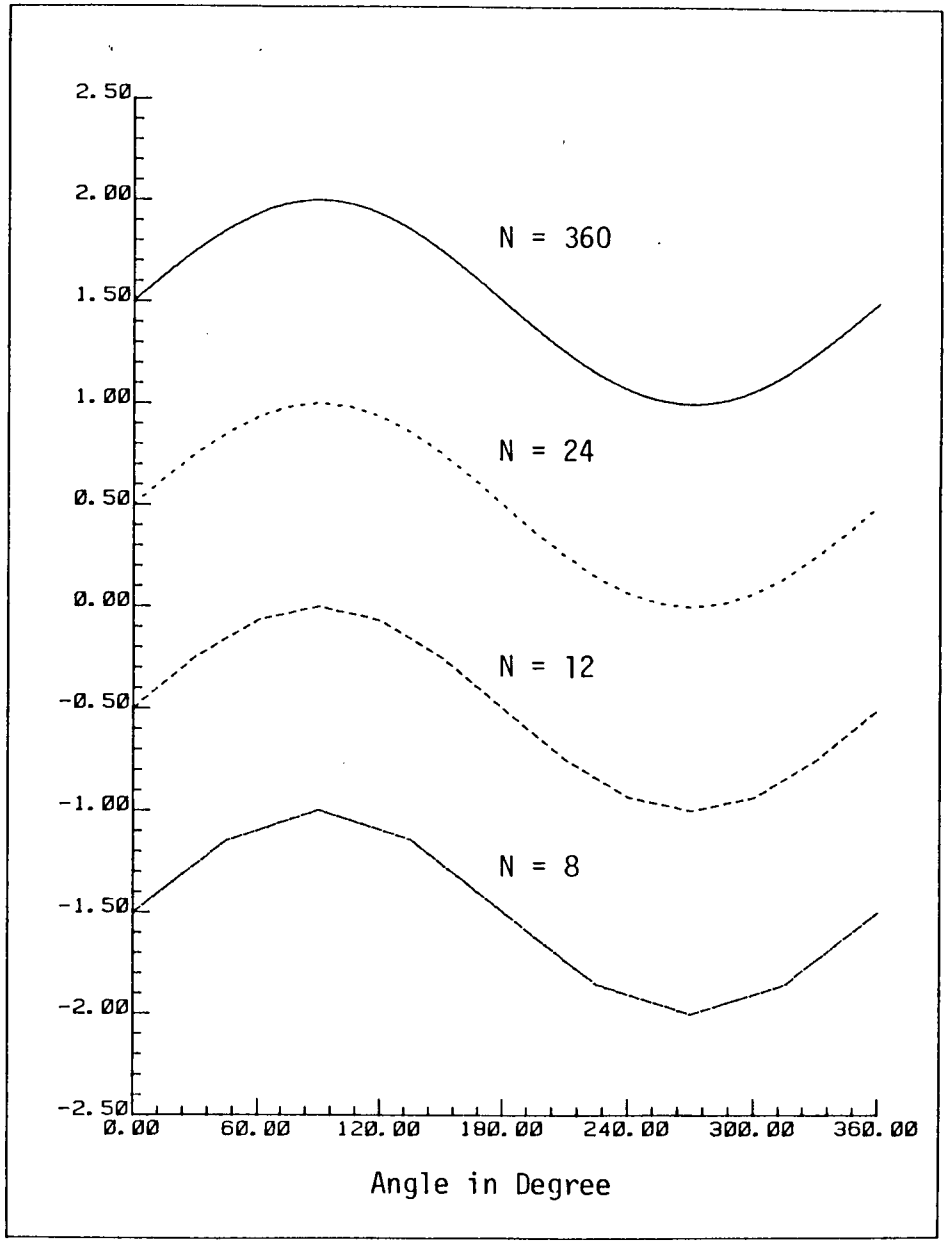

Figure 9. Wave Profile's Smoothness vs Element Number

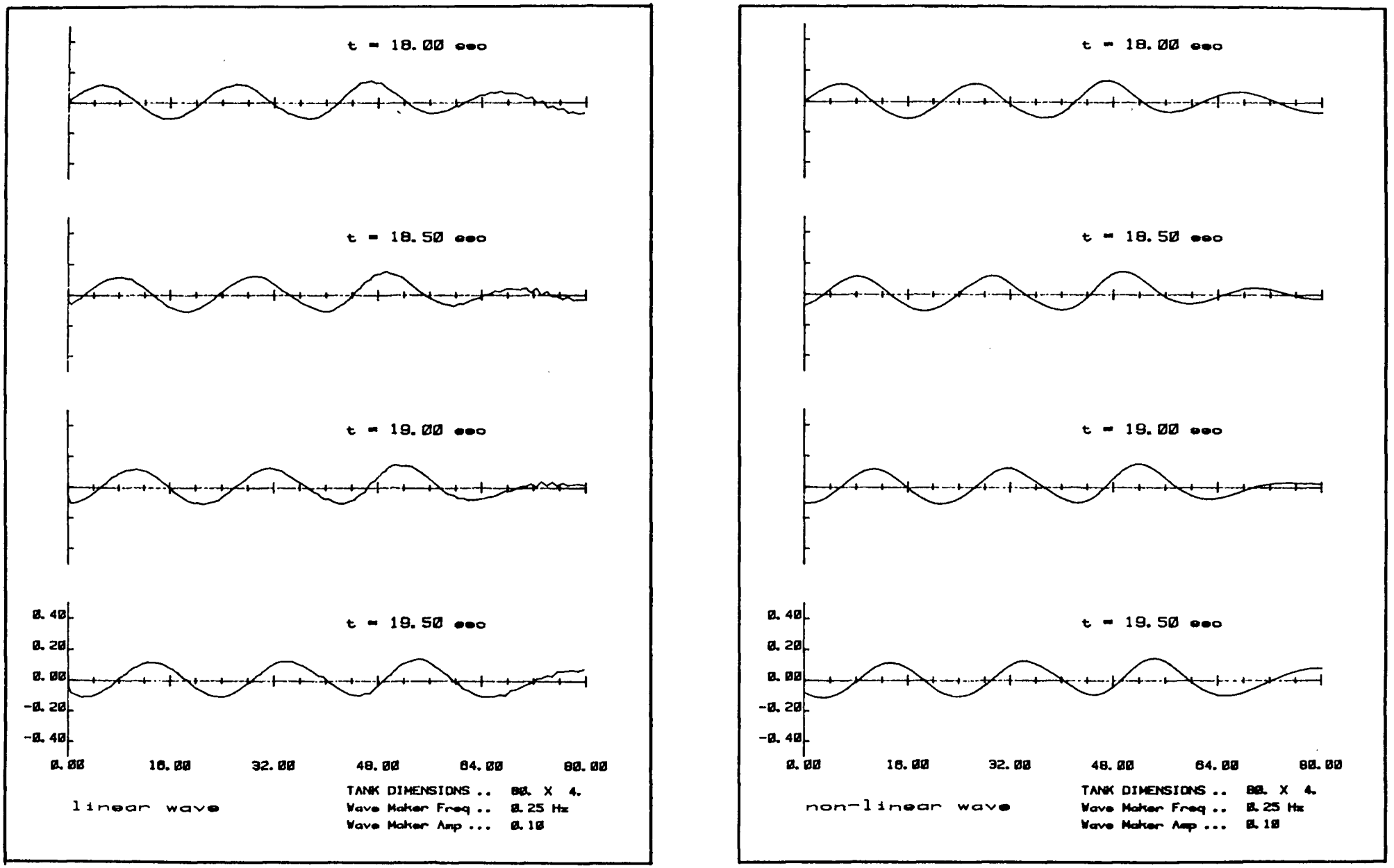

Figure 10. Comparison Between Linear and Non-linear Wave Tank Results (dt = 0.05 sec.)

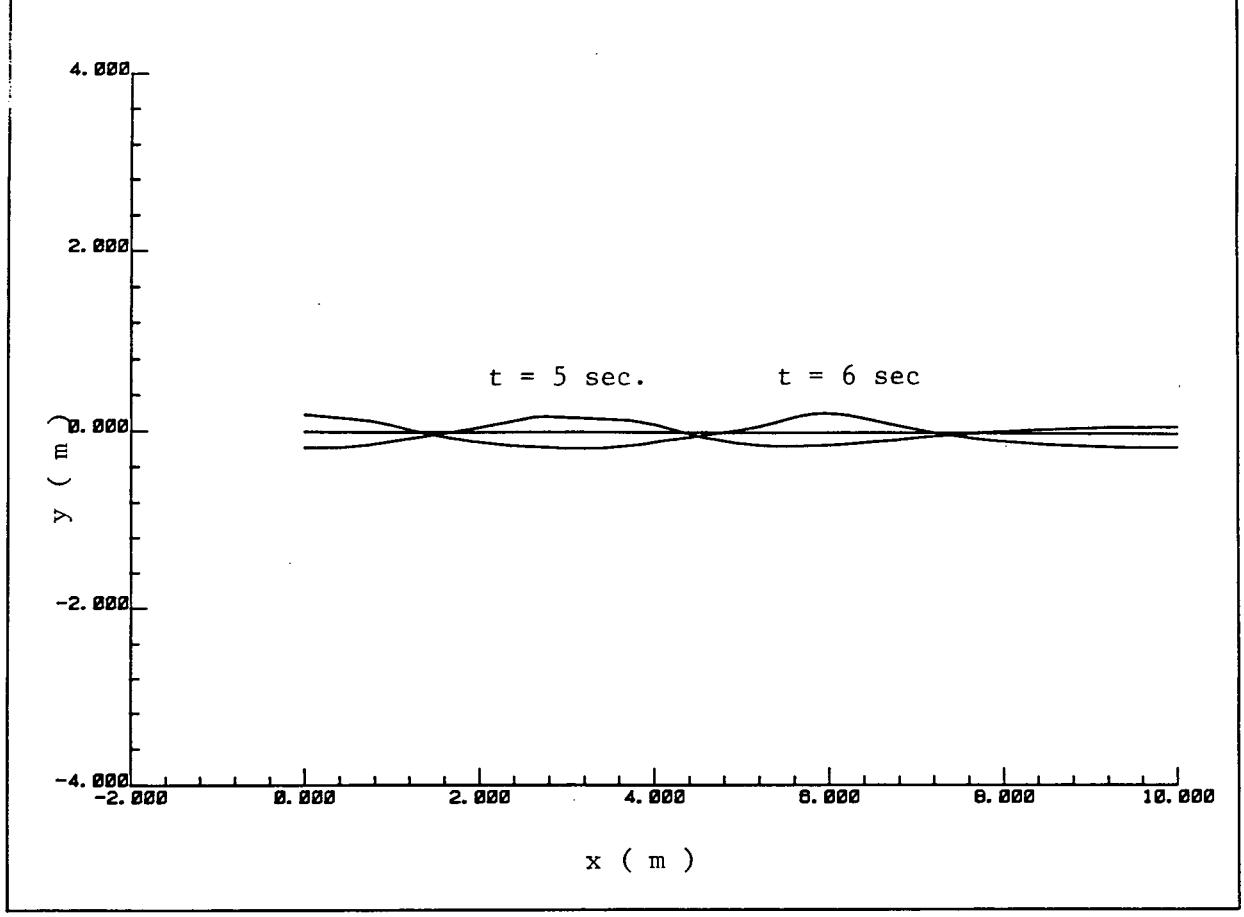

Figure 11. Non-linear Wave Modelling by Numerical Wave Tank

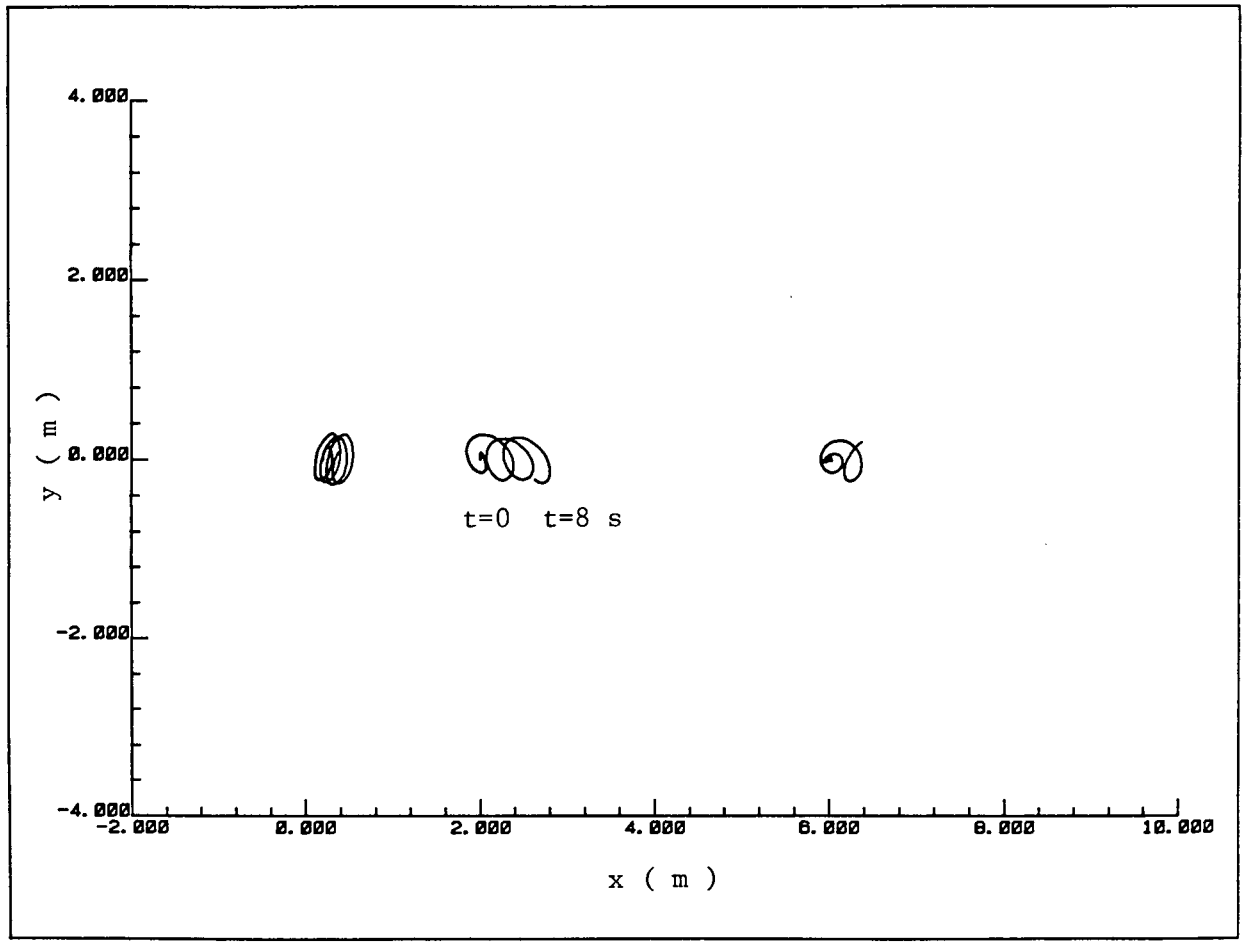

Figure 12. Motions of Free-Surface's Particles in Time (0 to 8 sec.)

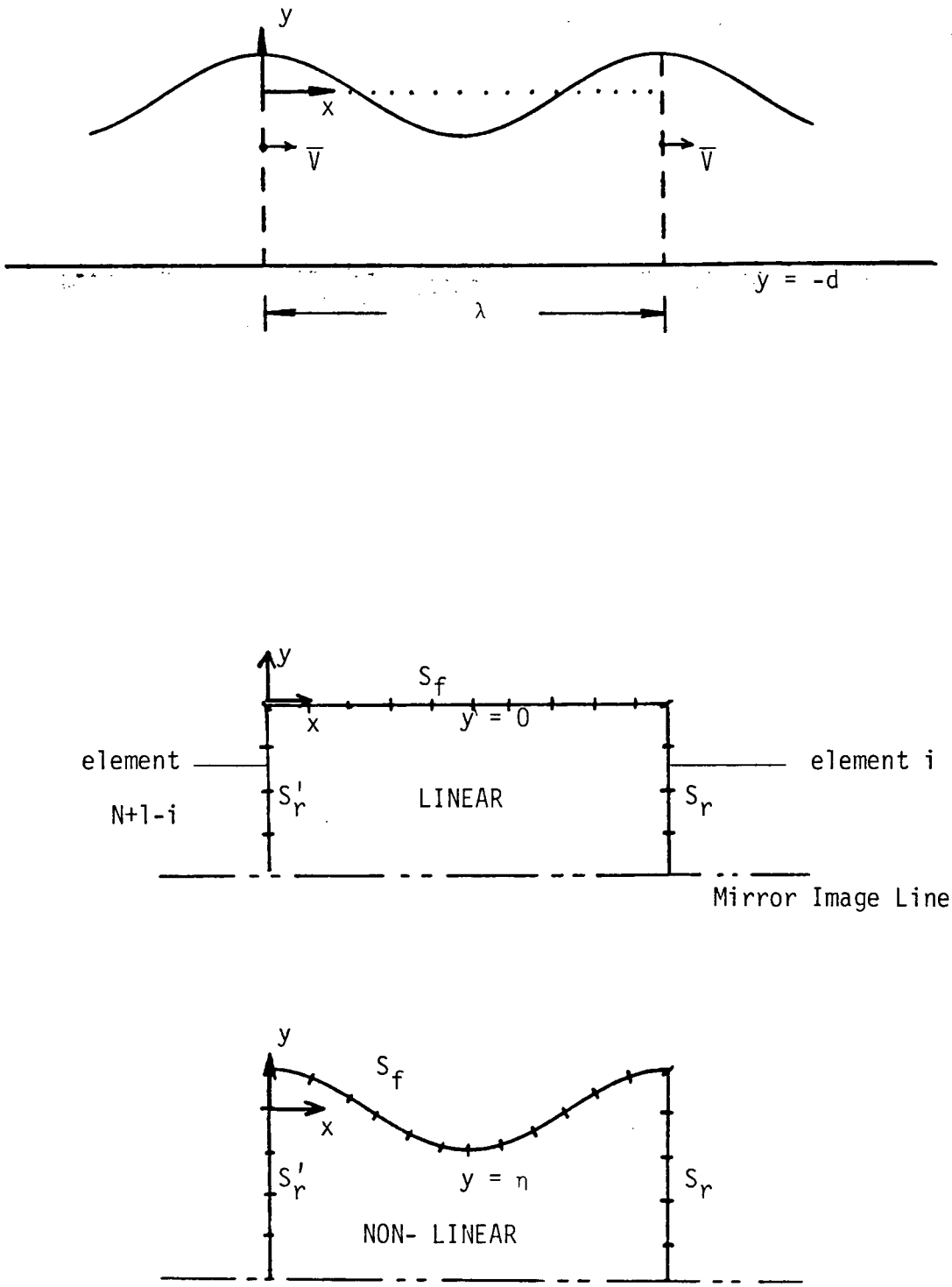

Figure 13. Single Wave Length Model for Spatially Periodic Wave

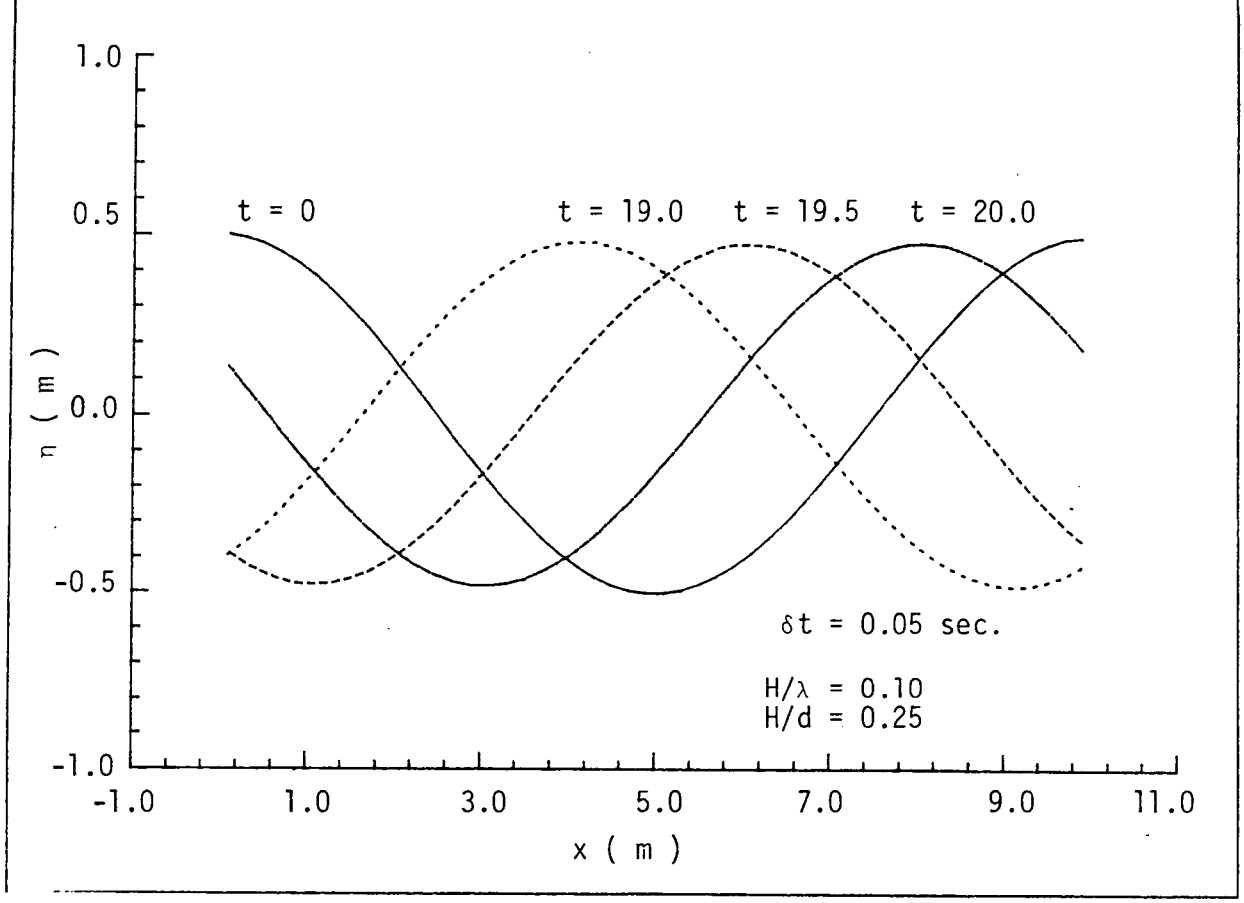

Figure 14. Simulation of Free-Surface Wave (Linear Modelling)

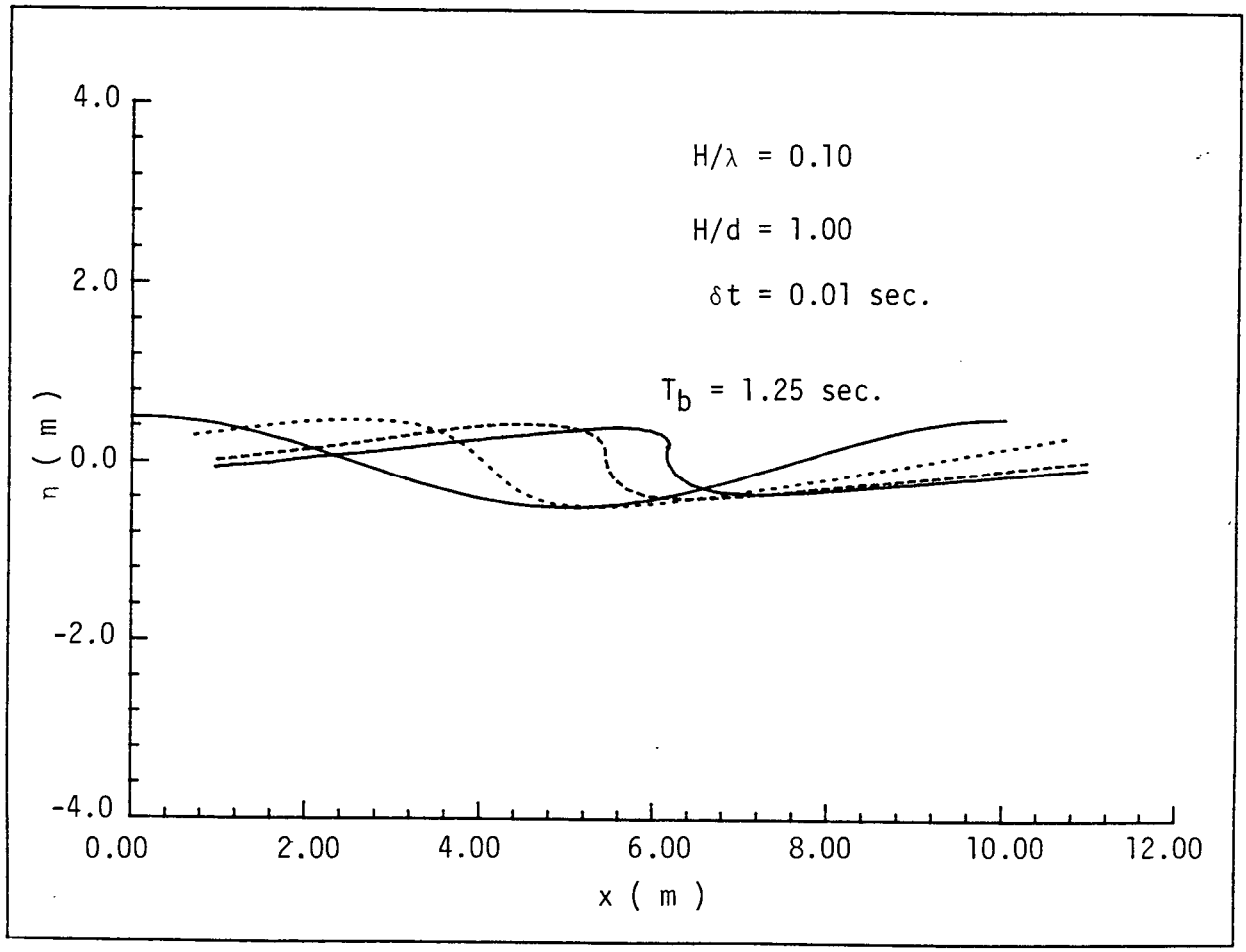

Figure 15. Deformation of High Amplitude Wave (Non-linear Modelling)

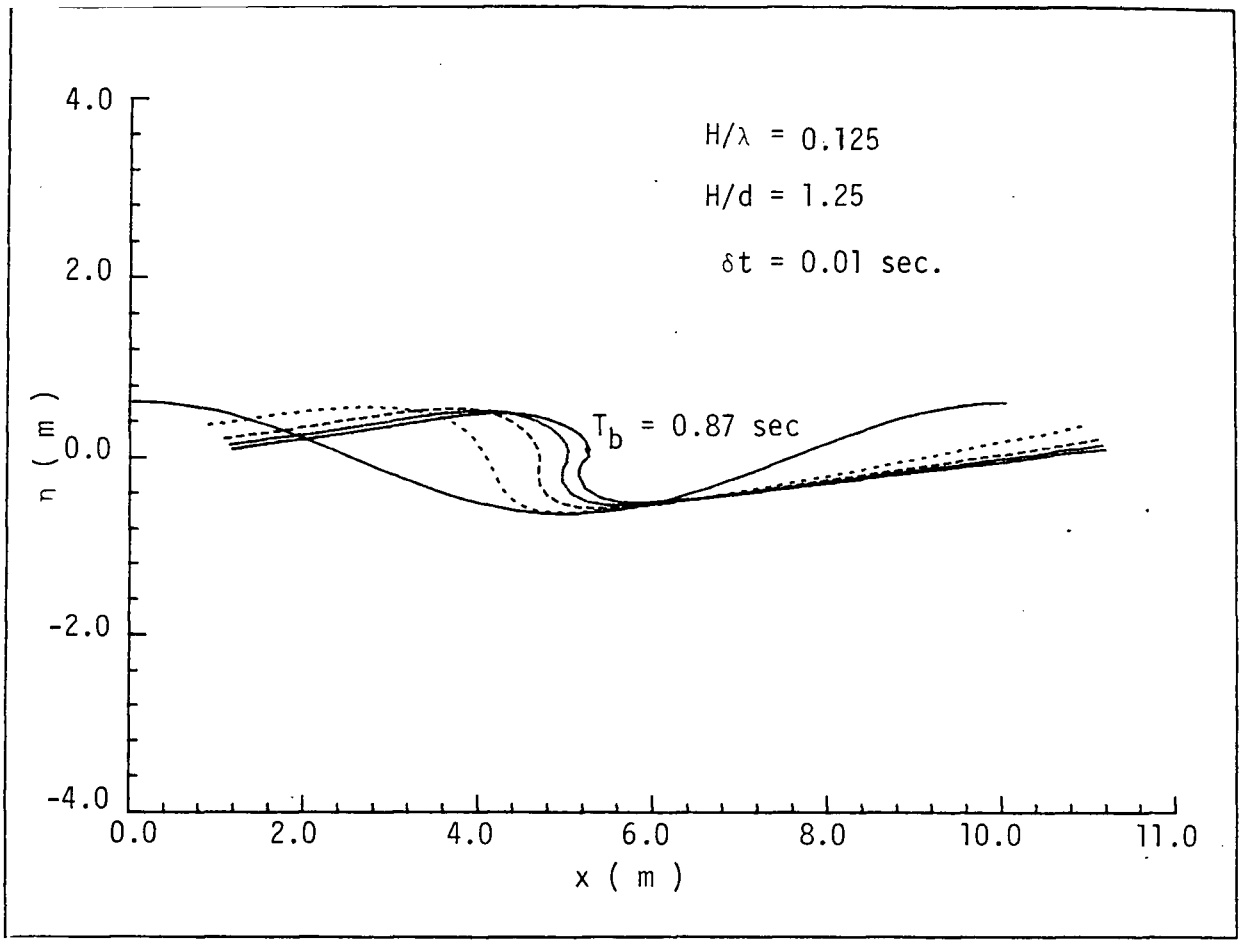

Figure 16. Deformation of High Amplitude Wave (Non-linear Modelling)

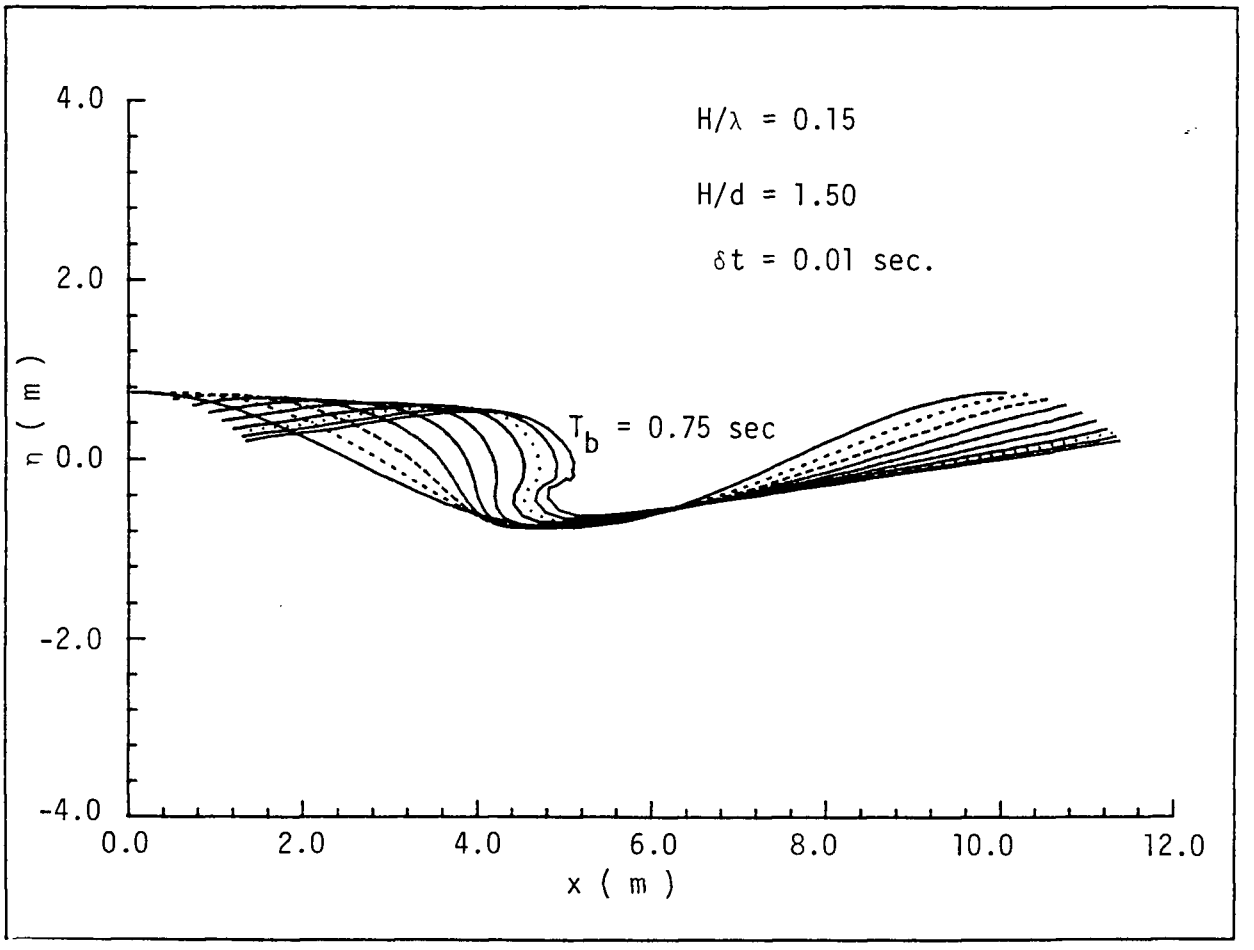

Figure 17. Deformation of High Amplitude Wave (Non-linear Modelling)

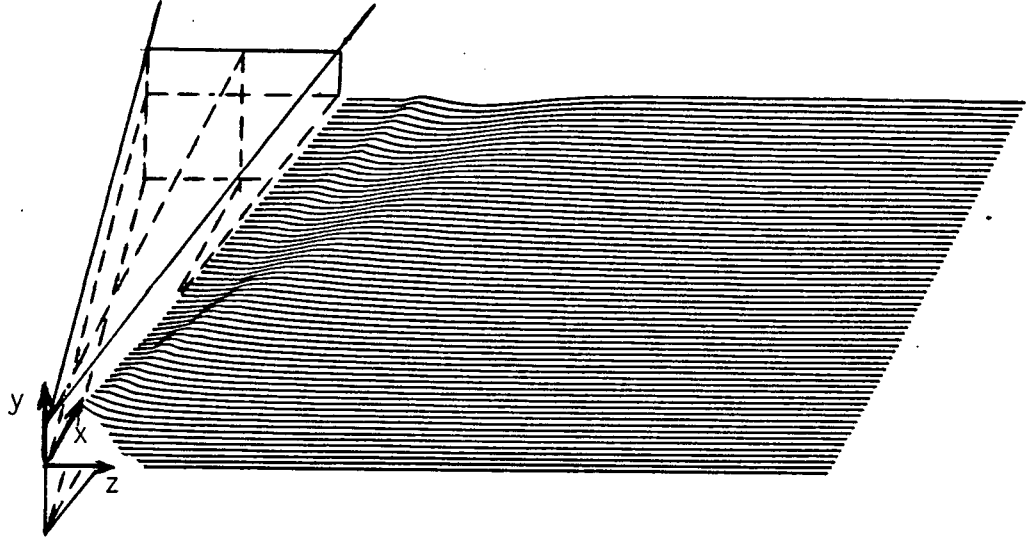

Figure 18. Waves Generated by a Wedge-shaped Model

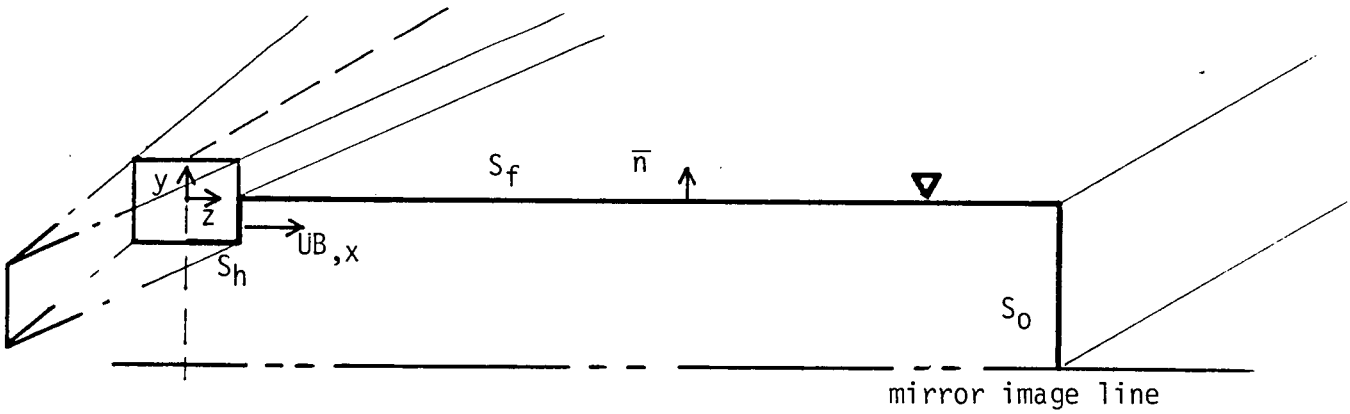

Figure 19. Sectional View of the Considered Domain

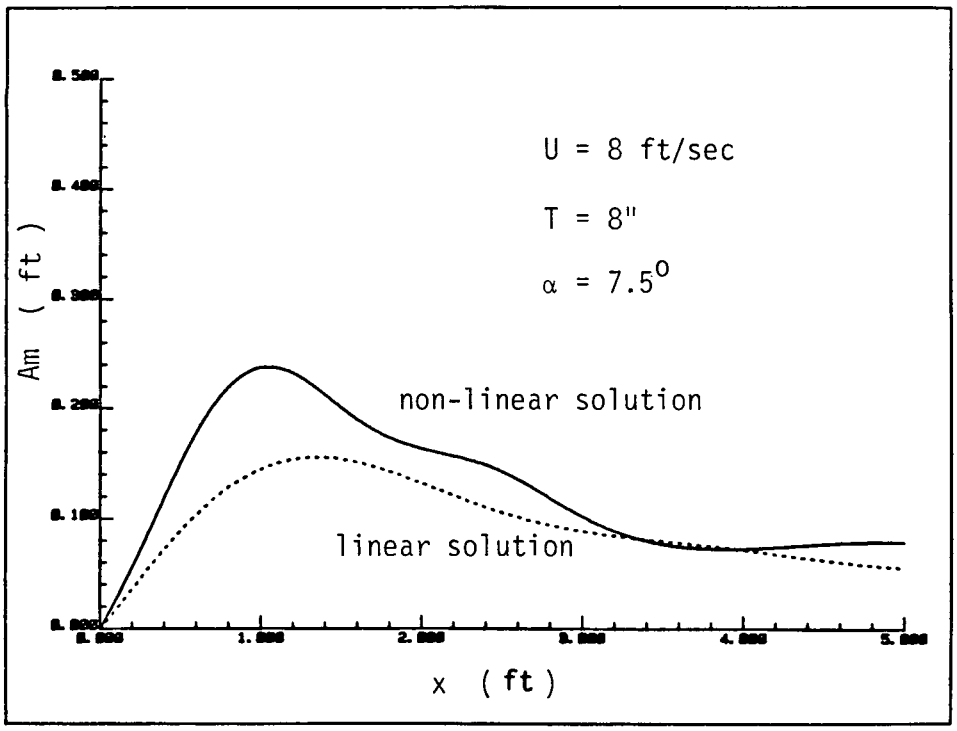

Figure 20. Bow Wave Prediction Calculated Along Wedge-shaped Model

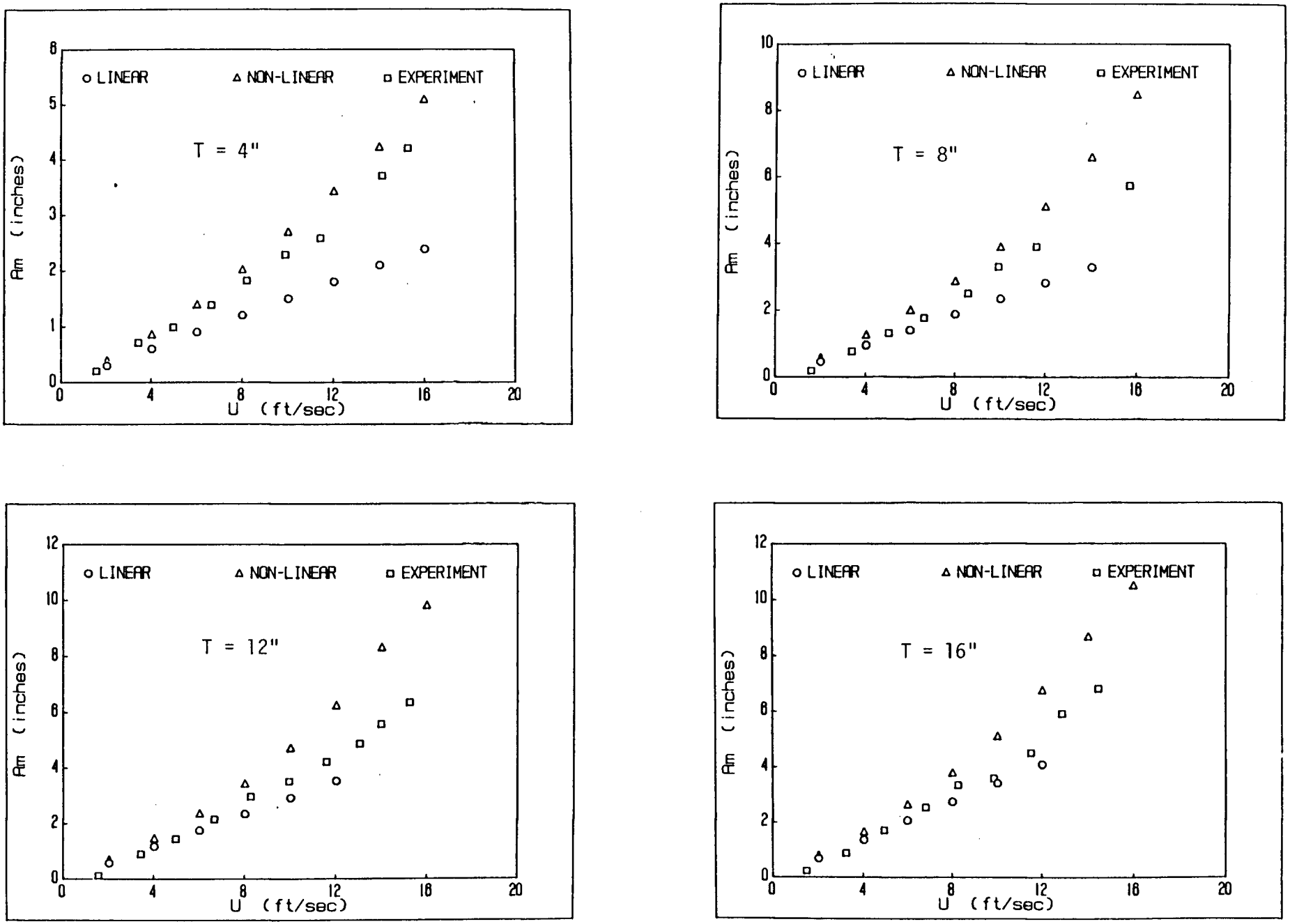

Figure 21. Bow Wave Predictions at Different Draft Calculated Along a 15° Wedge ($\alpha = 7.5^{o}$)

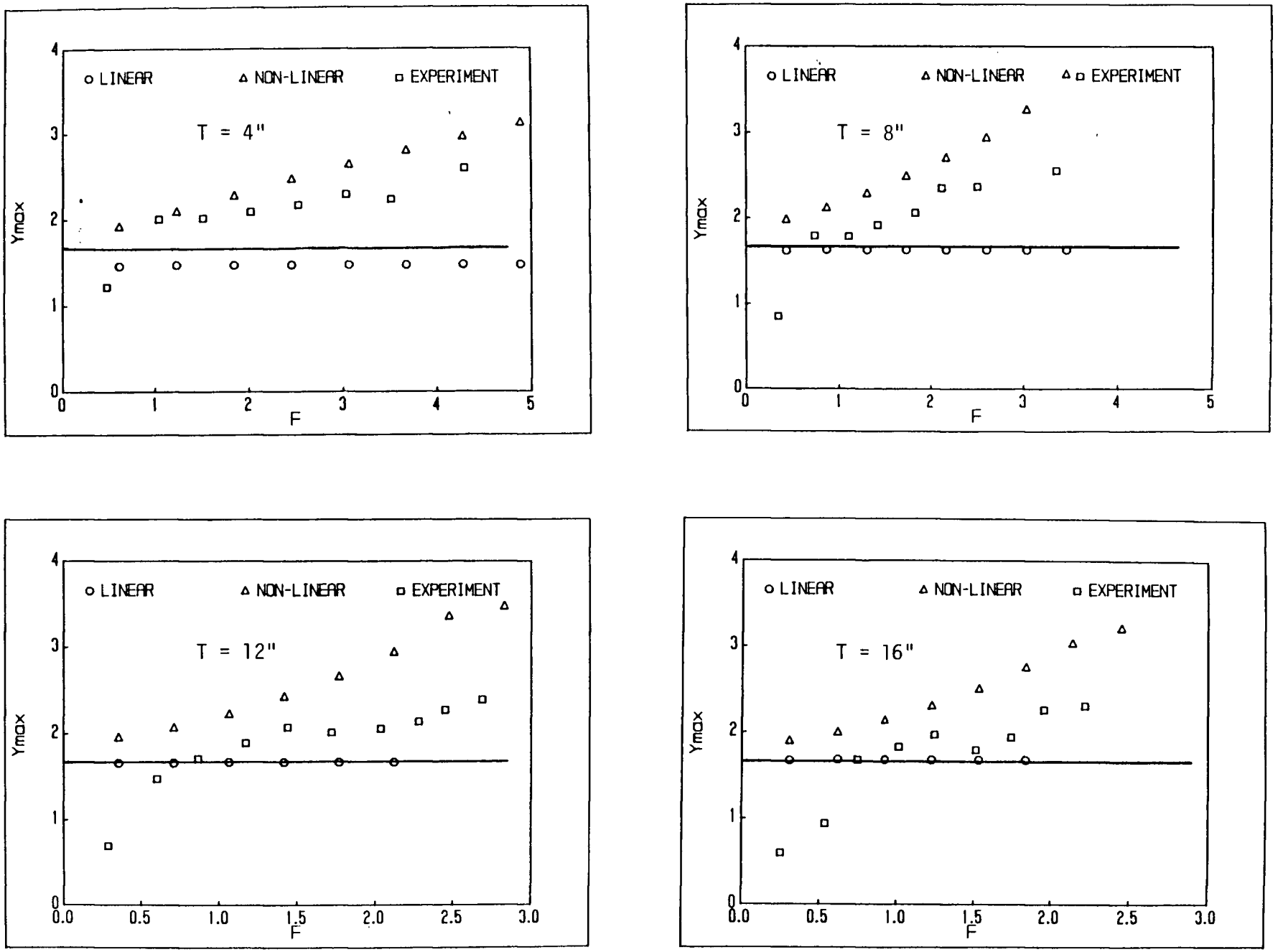

Figure 22. Non-dimensional Bow Wave Amplitude Comparisons at Different Drafts ($\alpha = 7.5^{o}$)

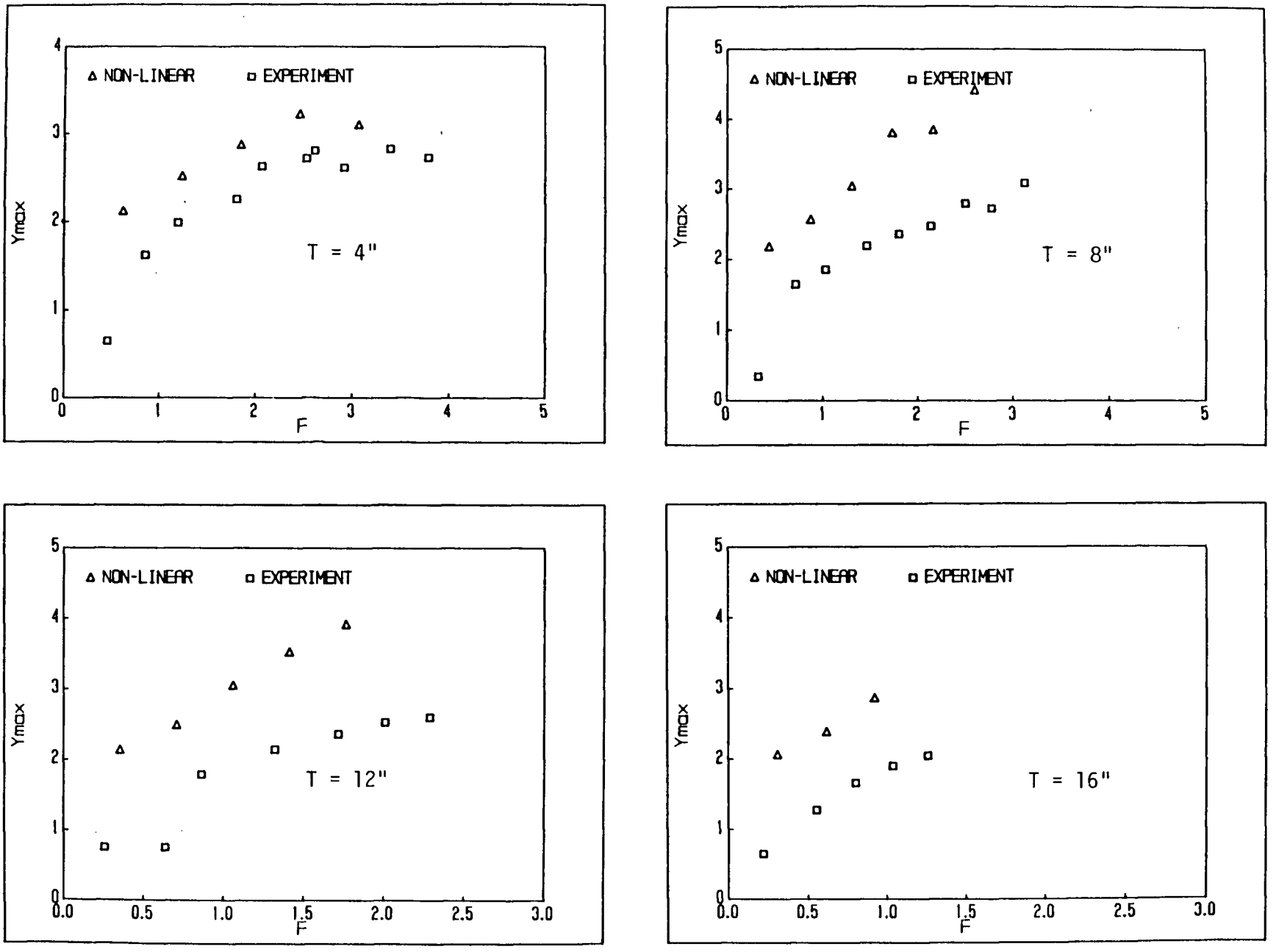

Figure 23. Non-dimensional Bow Wave Amplitude Comparisons at Different Drafts ($\alpha = 15^{o}$)

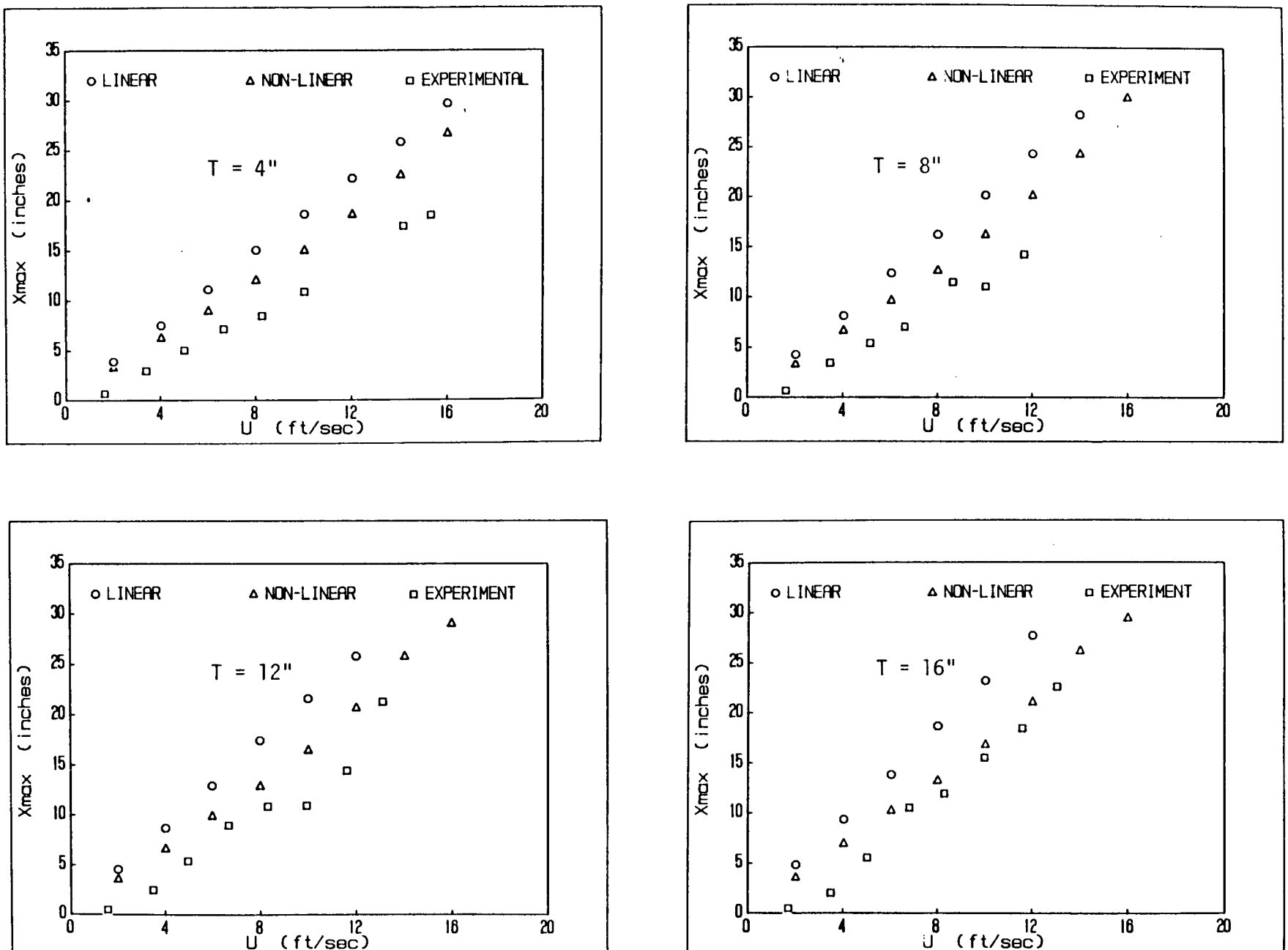

Figure 24. Longitudinal Position (Xmax) of Wave Peak ($\alpha = 15^{0}$)

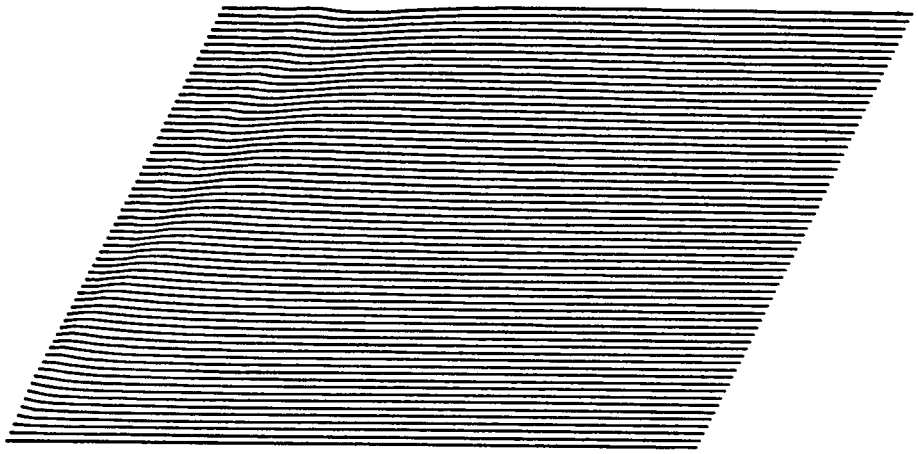

Linear Solution

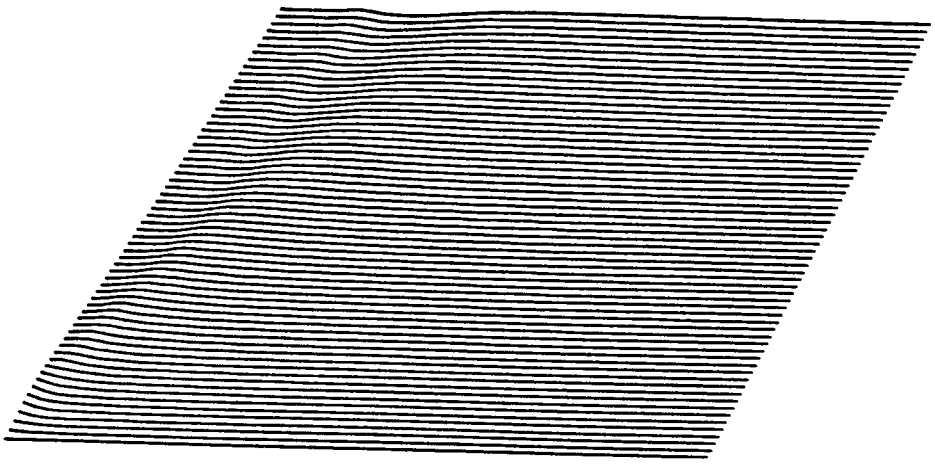

Non-linear Solution

Figure 25. Bow Wave Modelling at Low Model Speed (T = 12" , α = 7.5^{o}, U = 5 ft/sec.)

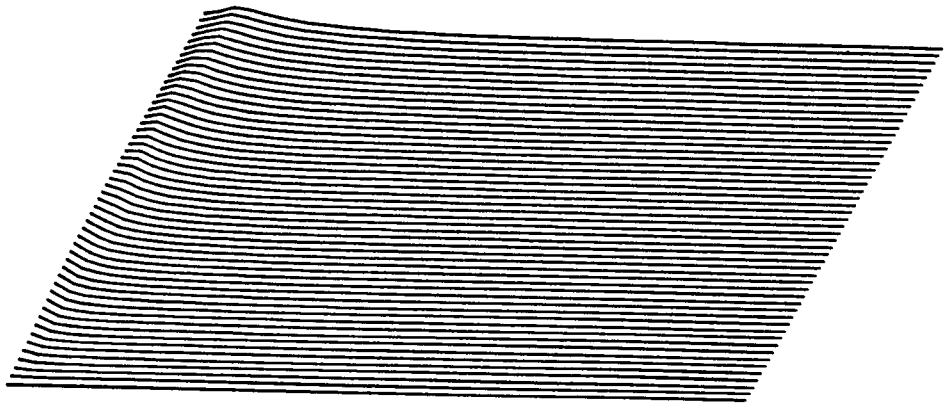

Linear Solution

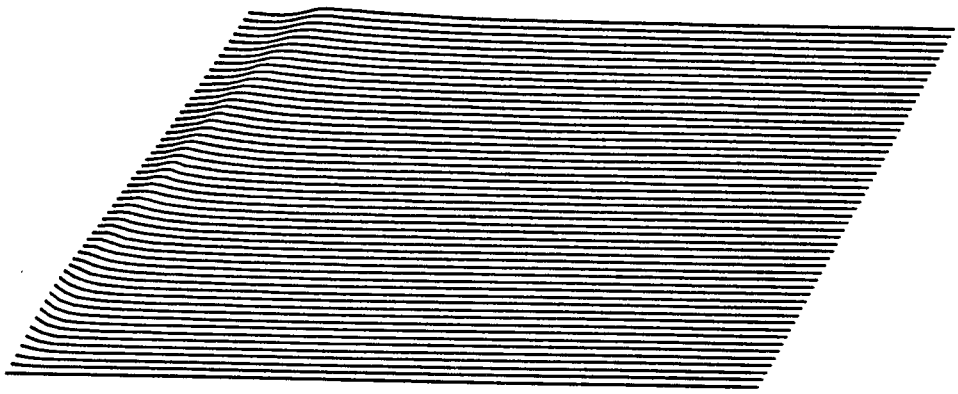

Non-linear Solution

Figure 26. Bow Wave Modelling at Intermediate Model Speed

(T = 8" , α = 7.5^{o} , U = 8 ft/sec.)

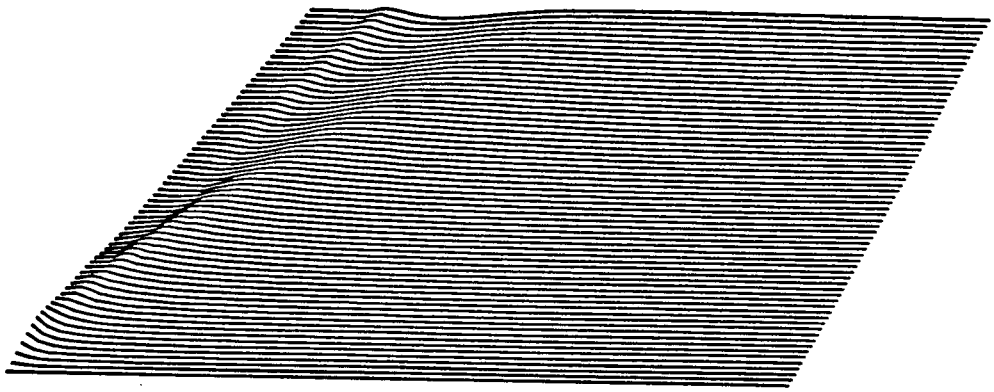

Non-linear Solution

Figure 27. Secondary Bow Wave Obtained at Low Model Speed

(T = 12" , α = 15° , U = 4 ft/sec.)

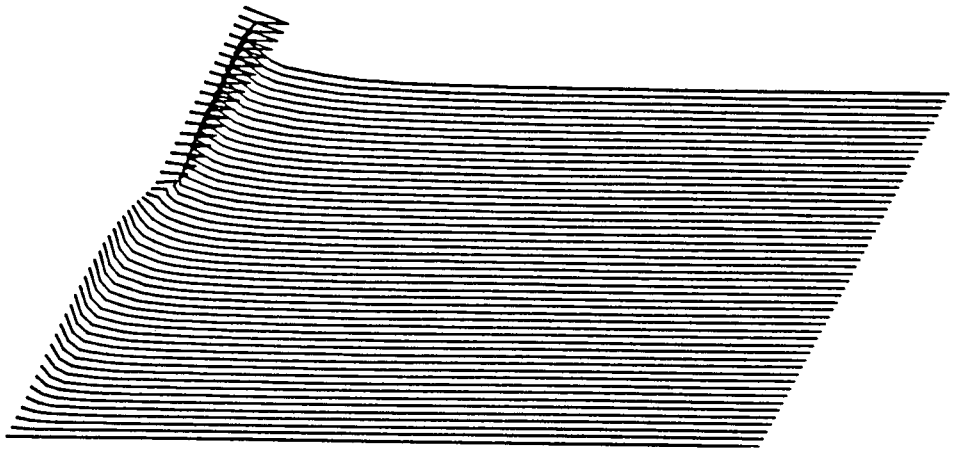

Non-linear Solution

Figure 28. Formation of Water Spray at High Model Speed

(T = 12" , α = 7.5^{o} , U = 14 ft/sec.)

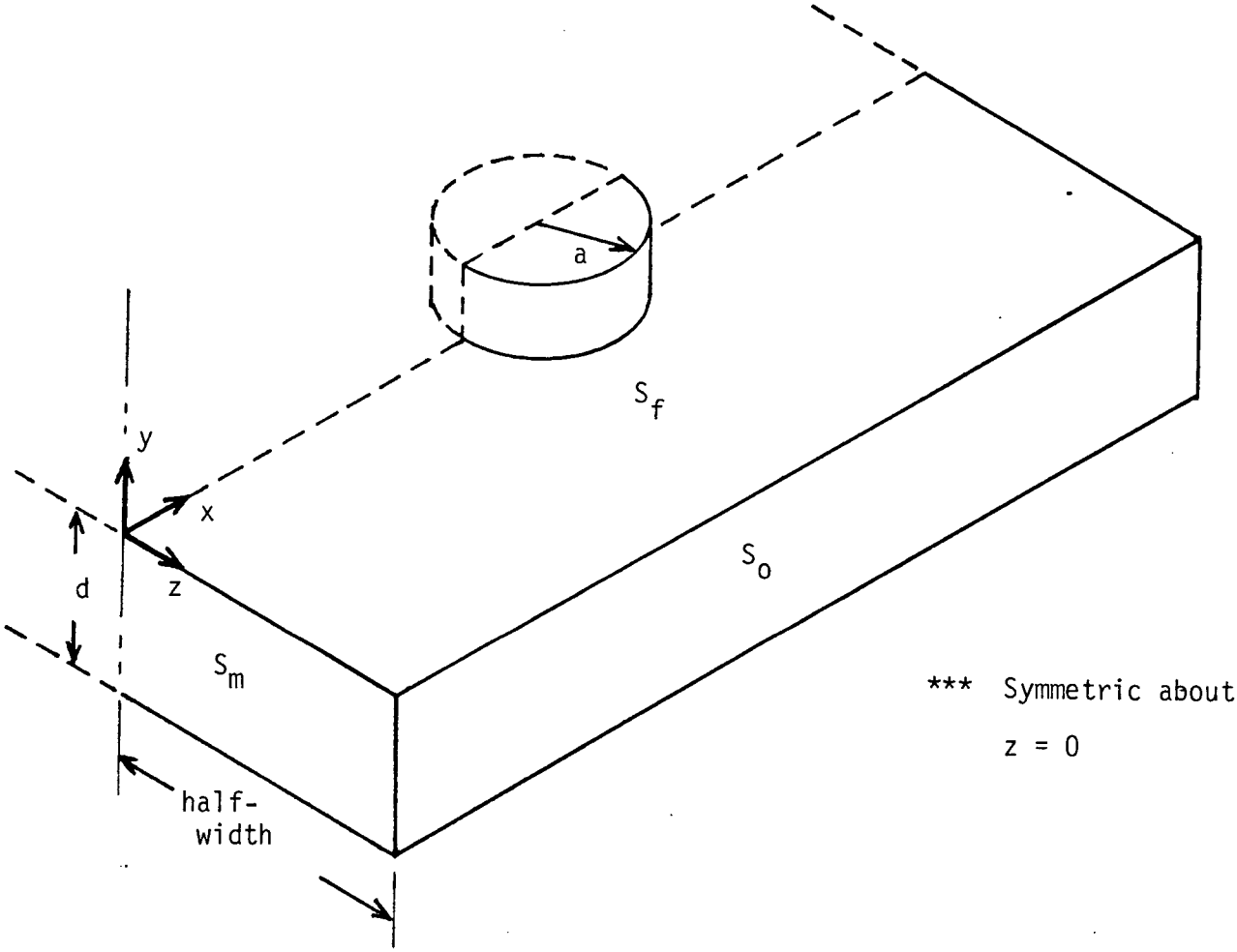

Figure 29. Numerical Modelling of Wave Tank with a Surface-Piercing Cylinder (3-D)

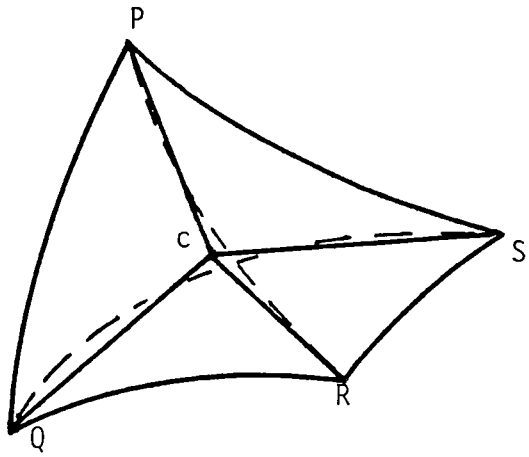

Figure 30. Quadrilateral Element

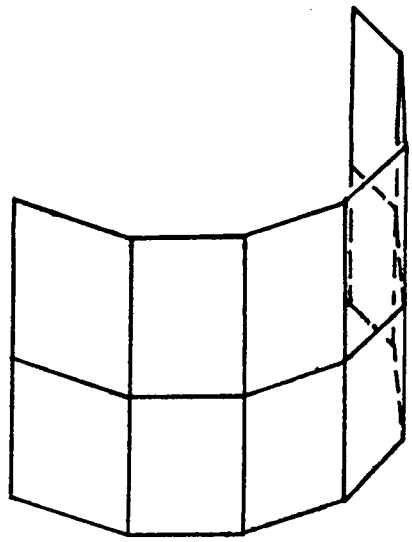

Figure 31. Half-cylinder Modelled by Quadrilateral Panels

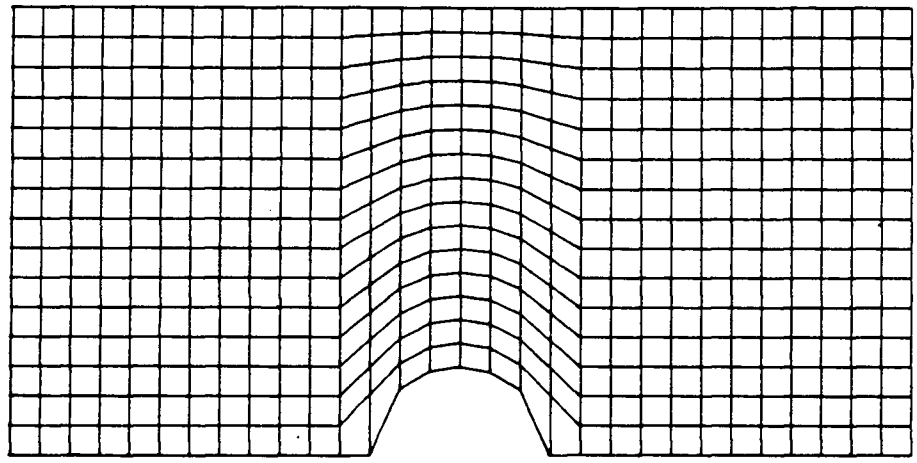

Figure 32. Free-Surface of Numerical Tank Represented by Quadrilateral Elements at Time t=0.

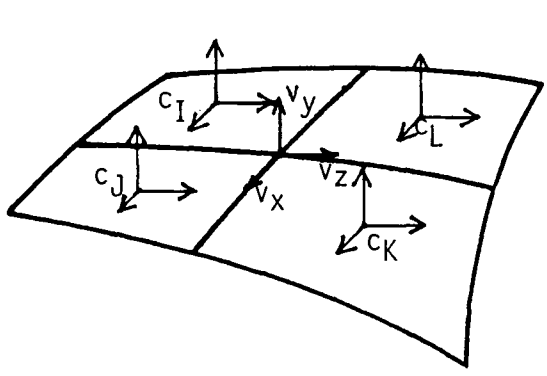

a) at Free-Surface

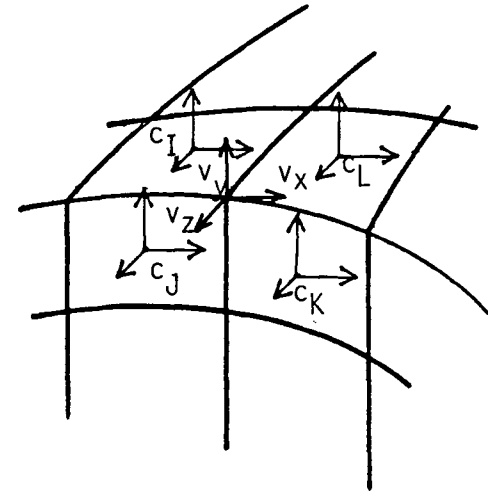

b) at Cylinder Wall and Free-Surface Intersection

Figure 33. Interpolation of Velocity Components Between Elements (3-D)

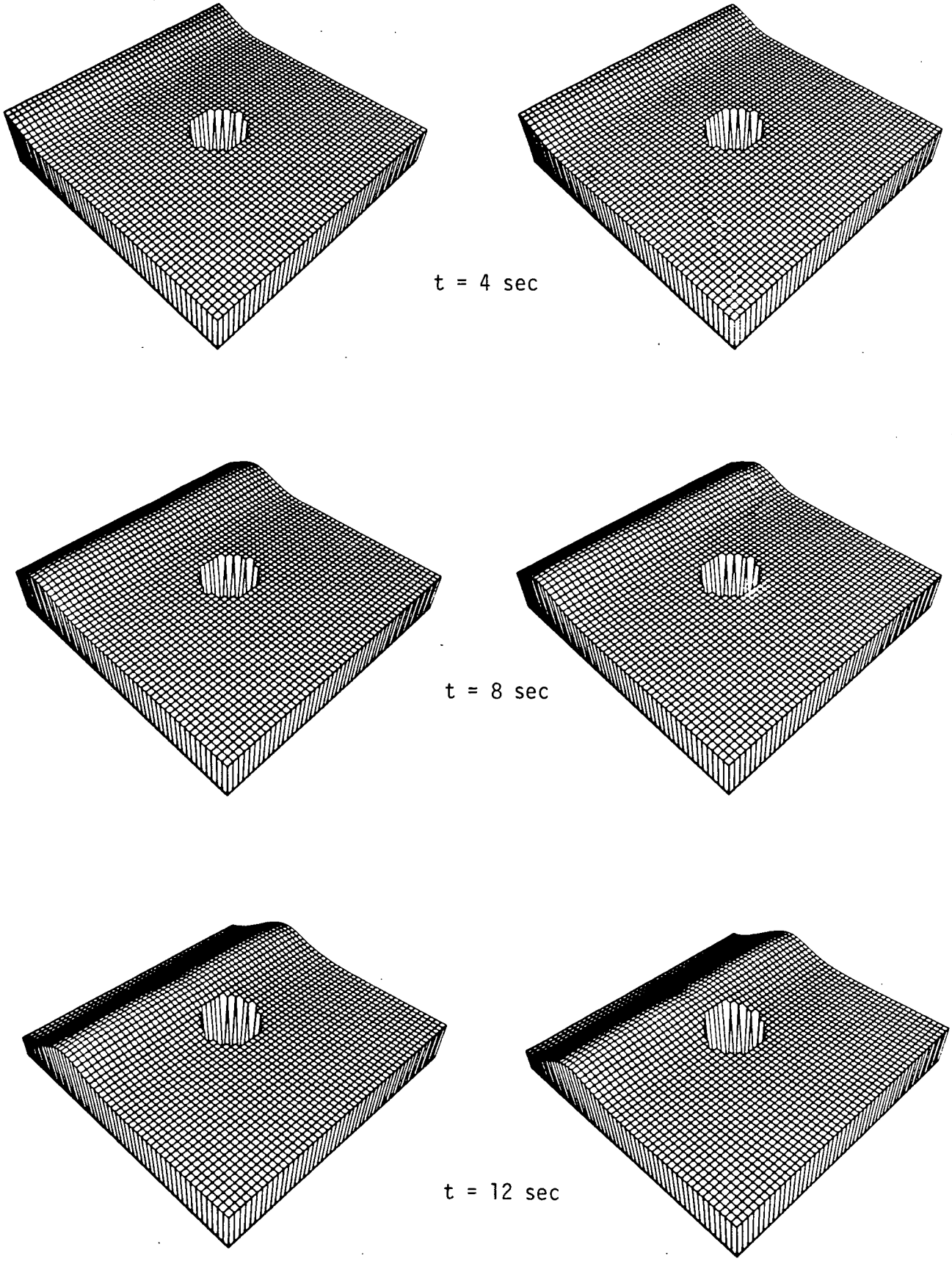

Figure 34.a Numerical Simulations of Diffracted Wave in a Tank at Frequency of 0.06105 Hz

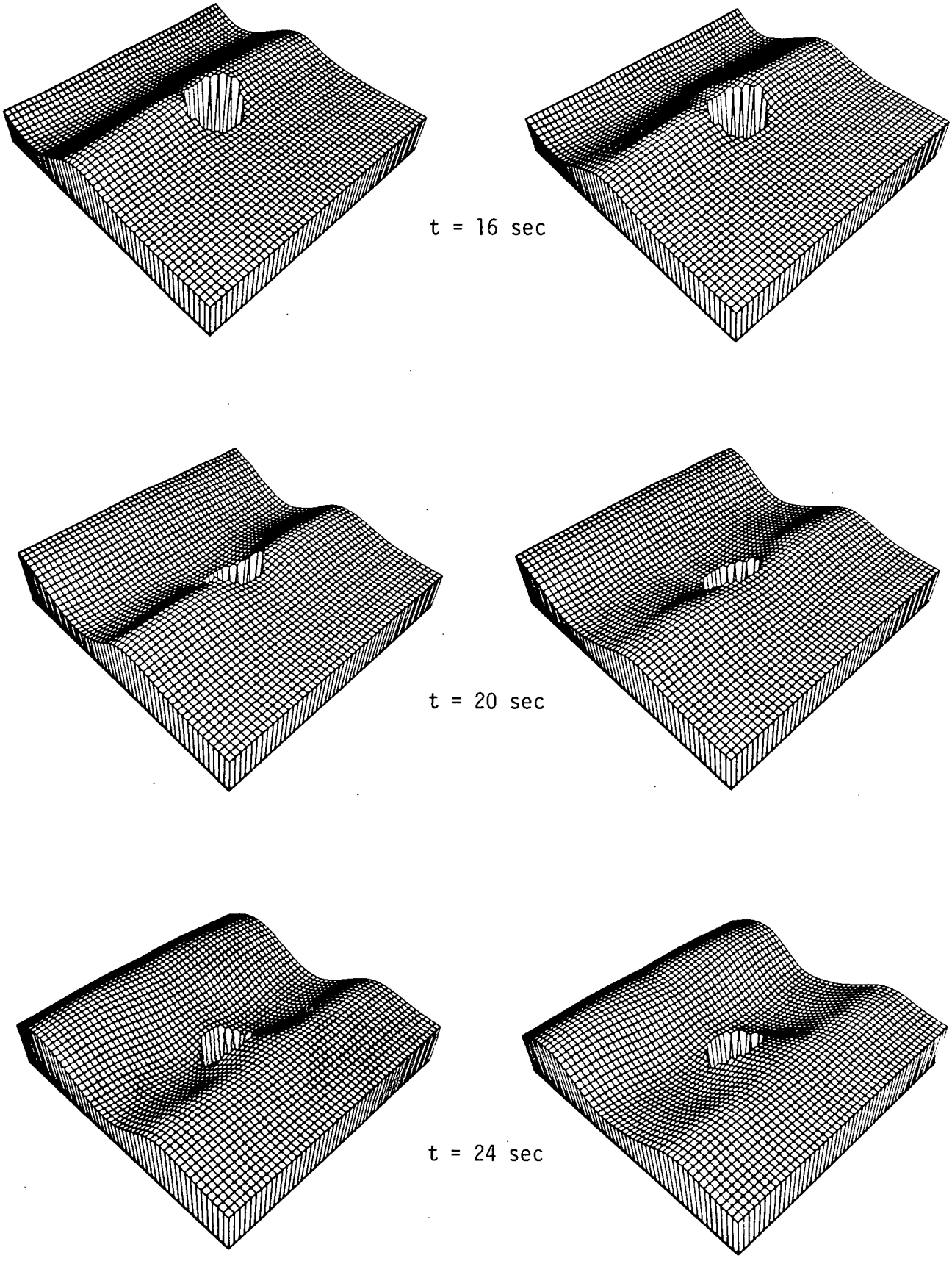

Figure 34.b Numerical Simulations of Diffracted Wave in a Tank at Frequency of 0.06105 Hz

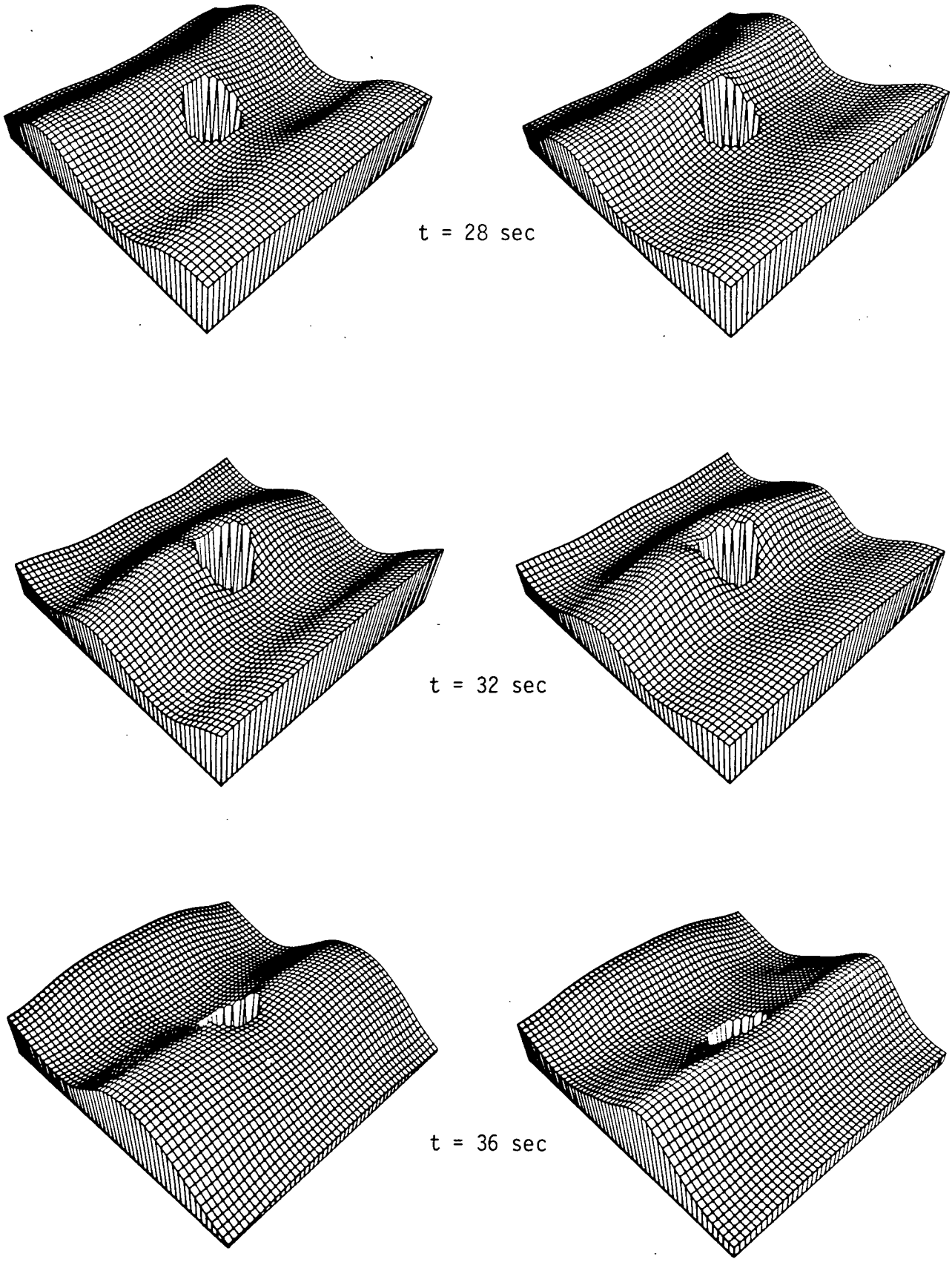

Figure 34.c Numerical Simulations of Diffracted Wave in a Tank at Frequency of 0.06105 Hz

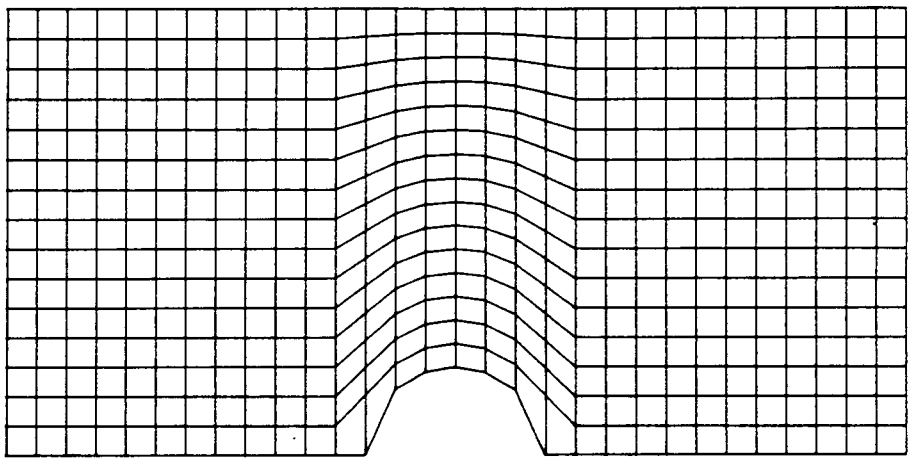

t = 0 sec

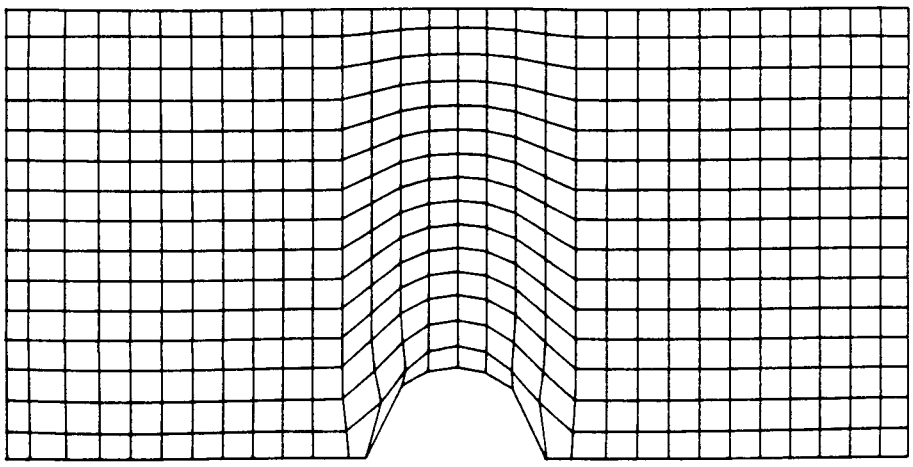

t = 36 sec

Figure 35. Deformation of Free-Surface Elements at t = 36 sec.

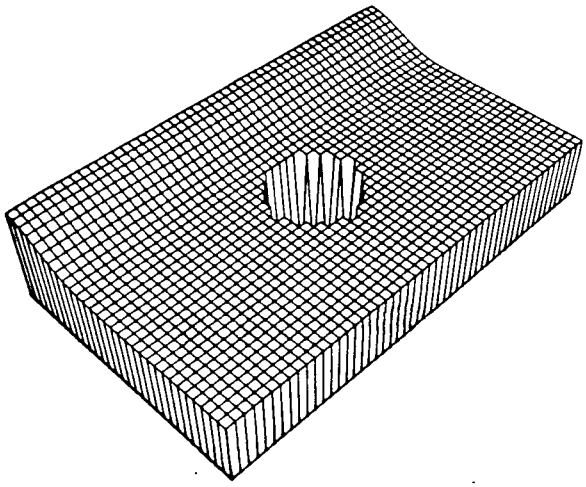

t = 4 sec

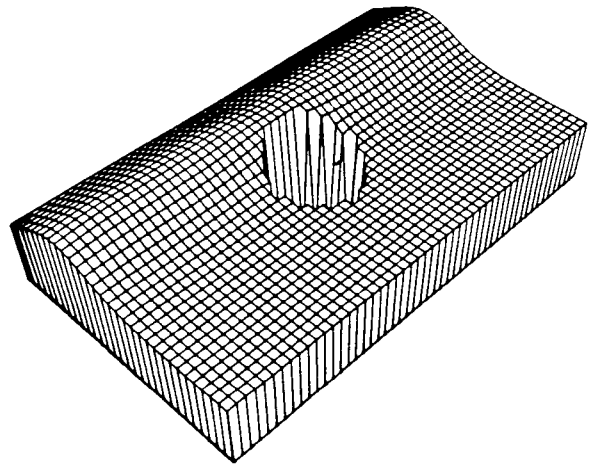

t = 8 sec

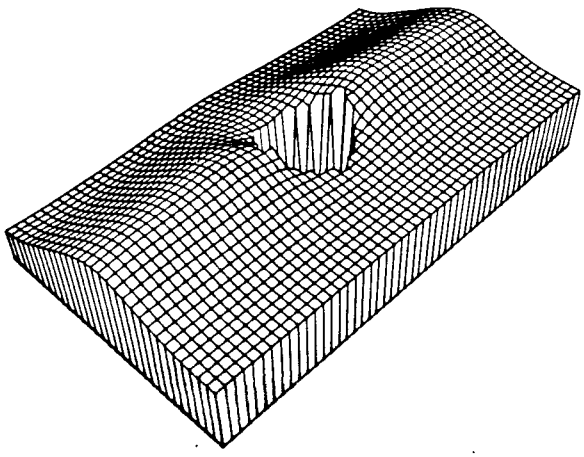

t = 12 sec

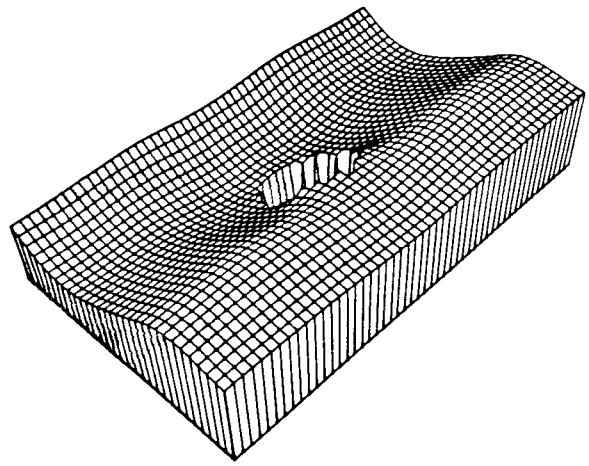

t = 16 sec

NON-LINEAR SOLUTION

Figure 36.a Diffracted Waves are Studied in a Short Tank (0.06105 Hz)

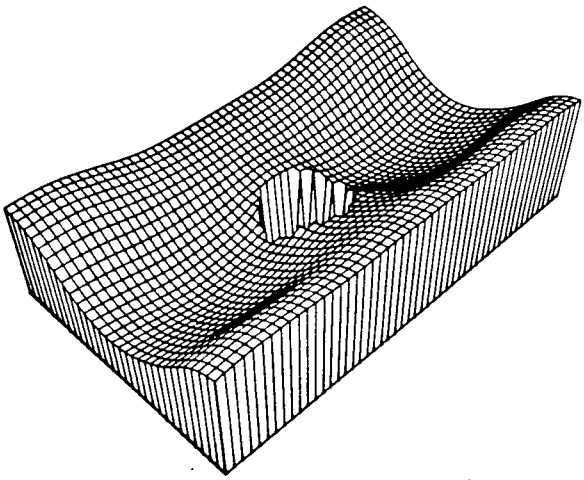

t = 20 sec

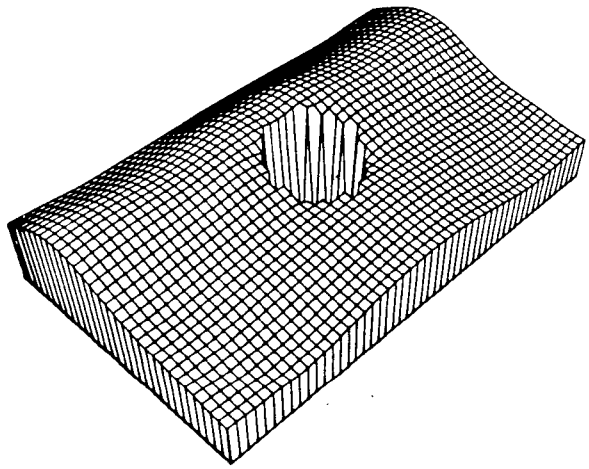

t = 24 sec

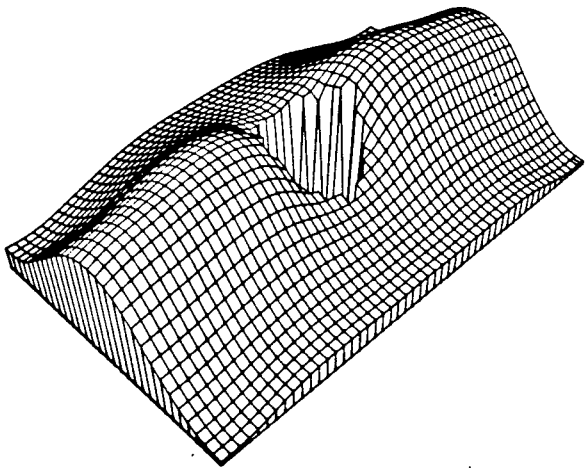

t = 28 sec

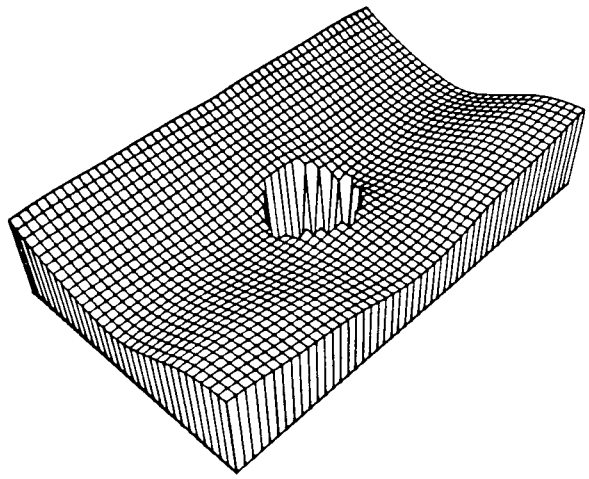

t = 32 sec

NON-LINEAR SOLUTION

Figure 36.b Diffracted Waves are Studied in a Short Tank (0.06105 Hz)

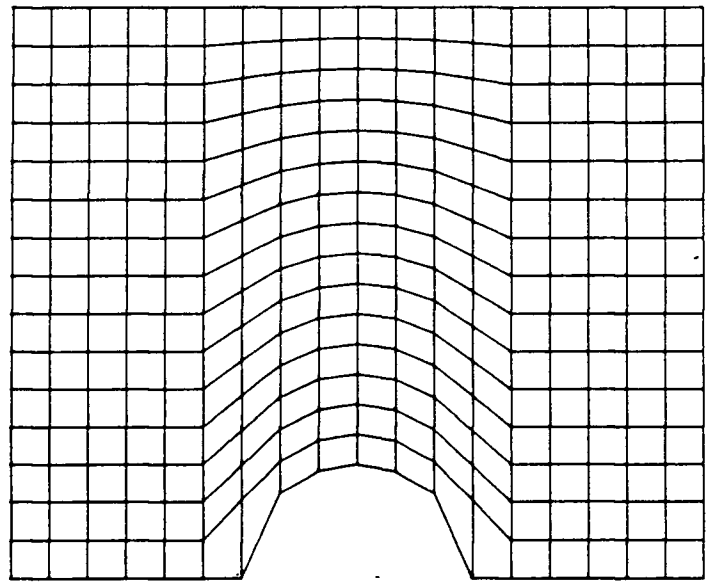

t = 0 sec

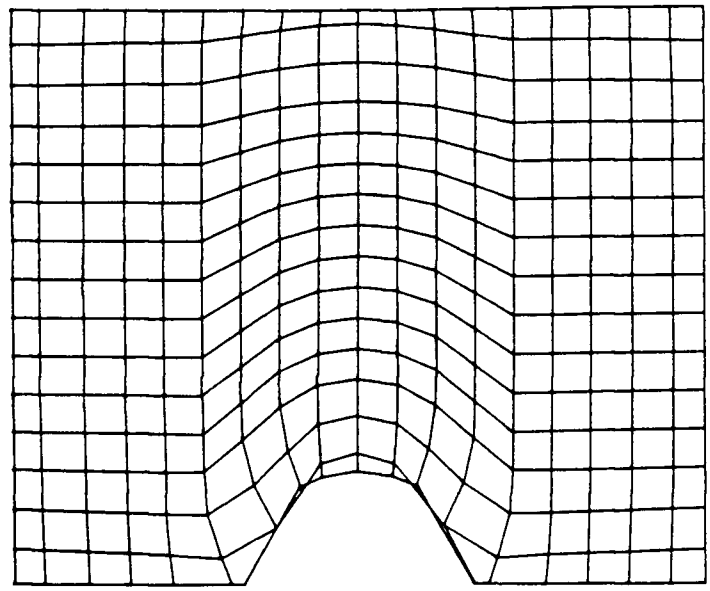

t = 32 sec

Figure 37. Deformation of Free-Surface Elements Affected by Shorter Tank Length at Time t = 32 sec.

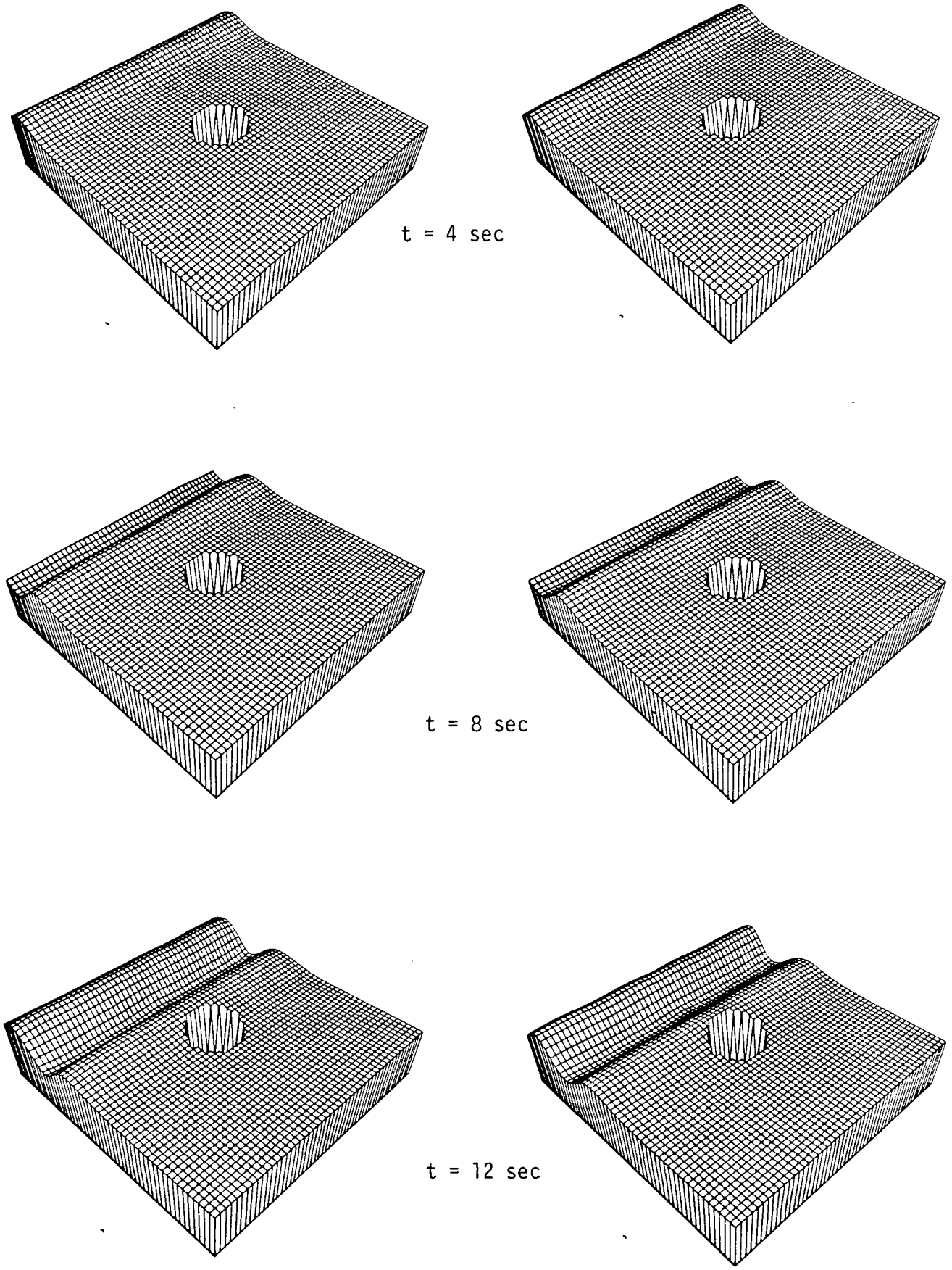

Figure 38.a Simulations of Diffracted Waves at Higher Frequency (0.1221 Hz)

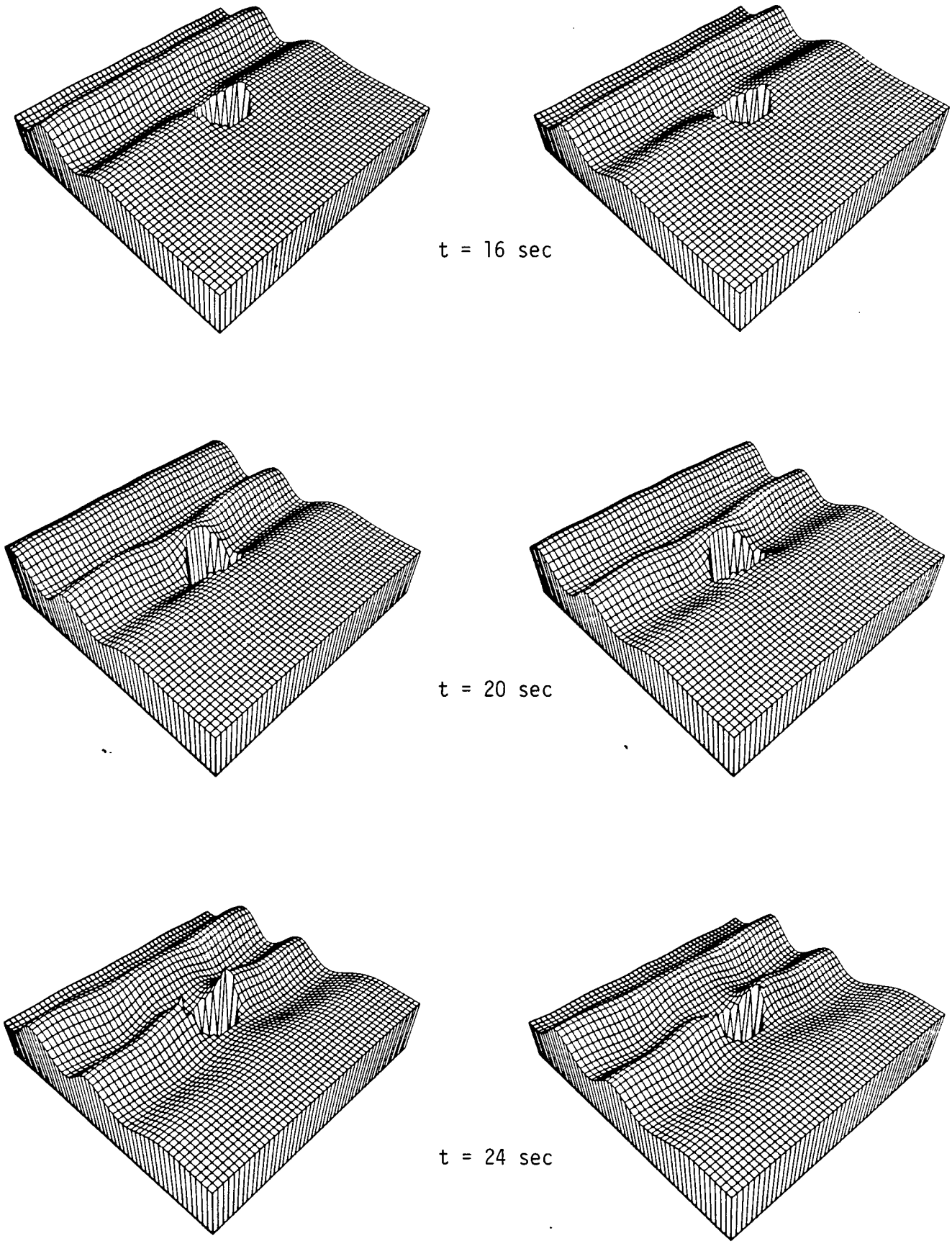

Figure 38.b Simulations of Diffracted Waves at Higher Frequency (0.1221 Hz)

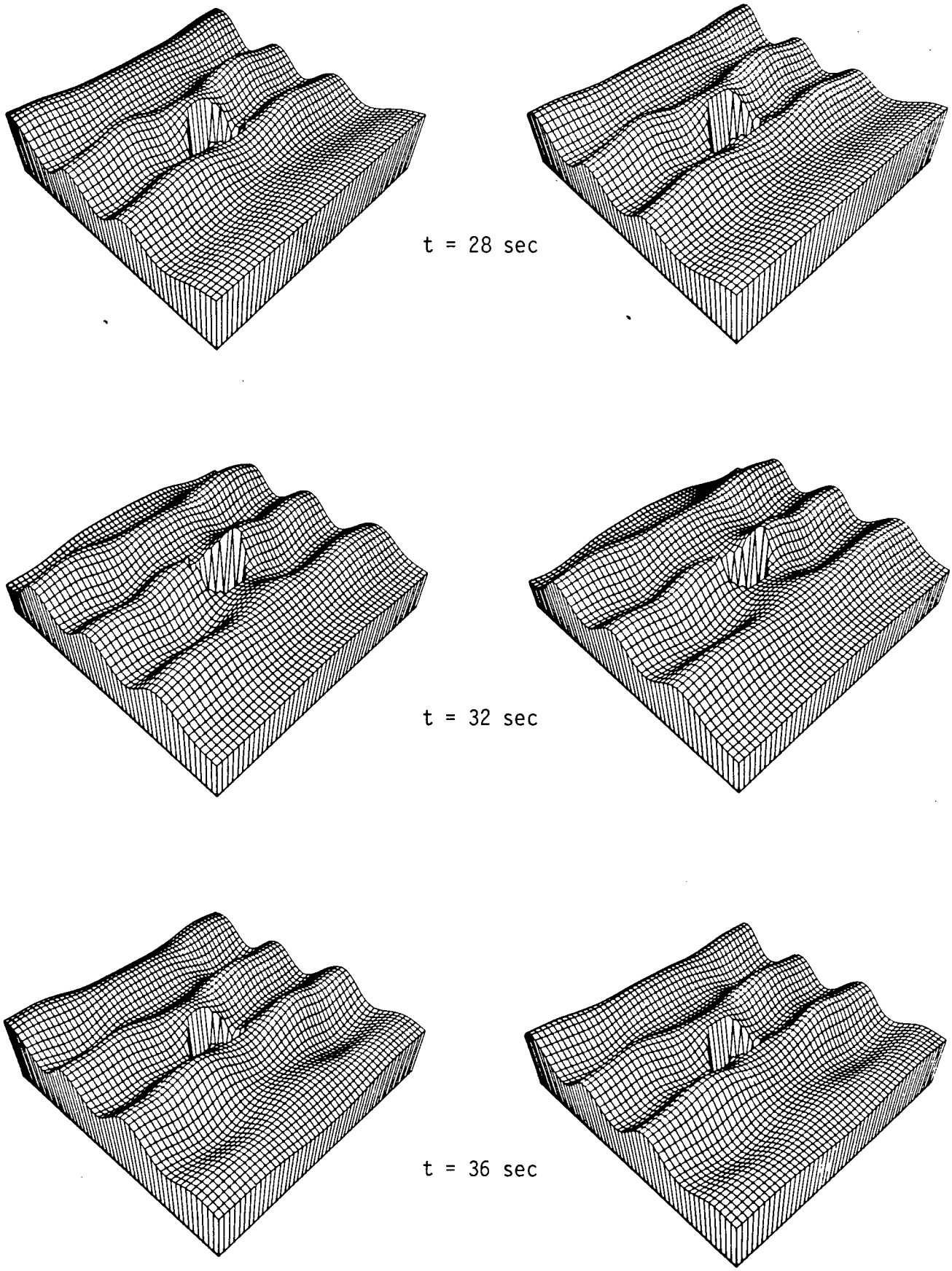

Figure 38.c Simulations of Diffracted Waves at Higher Frequency (0.1221 Hz)

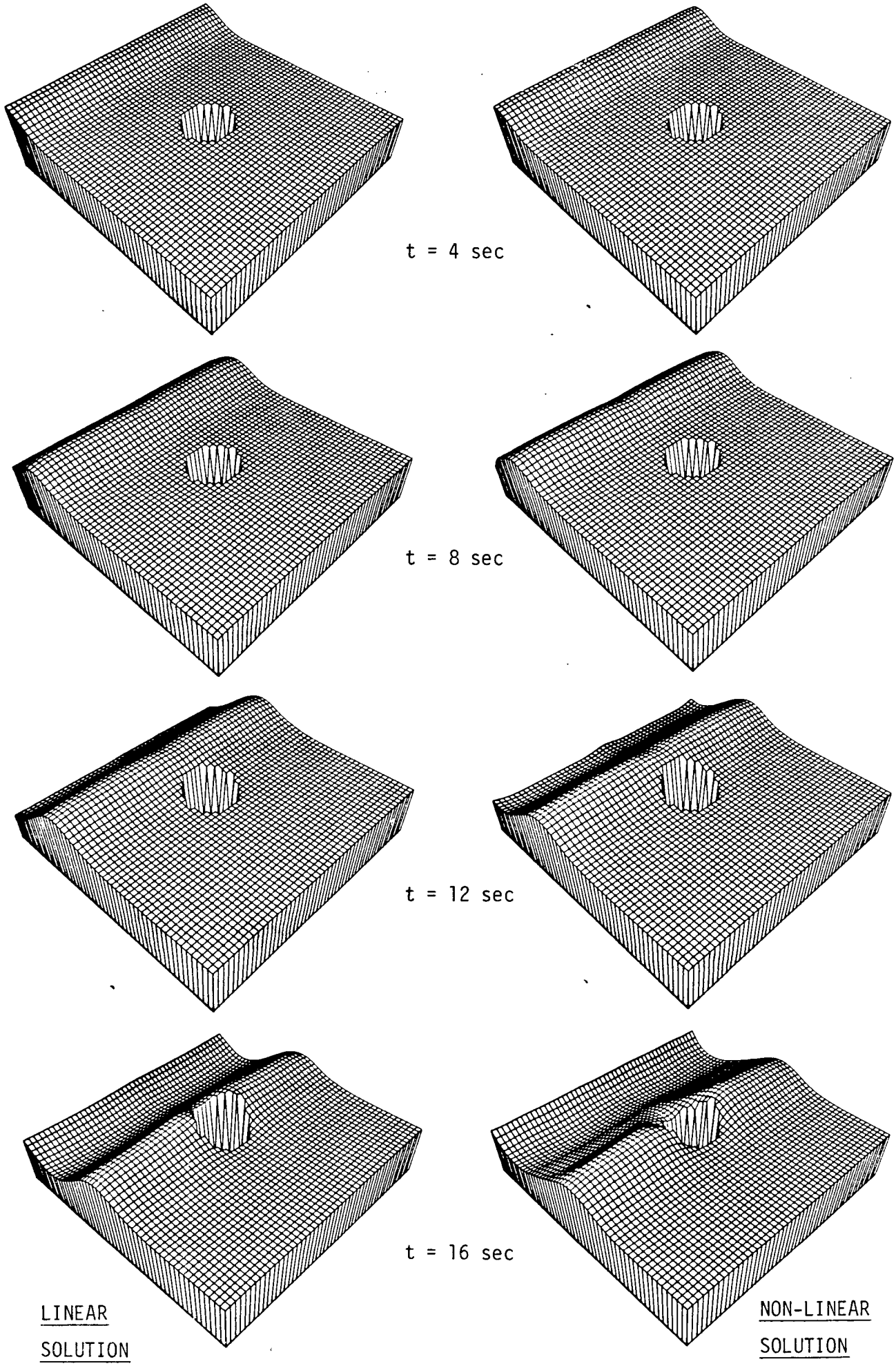

Figure 39. Failure of Non-linear Model at High Wave Amplitude

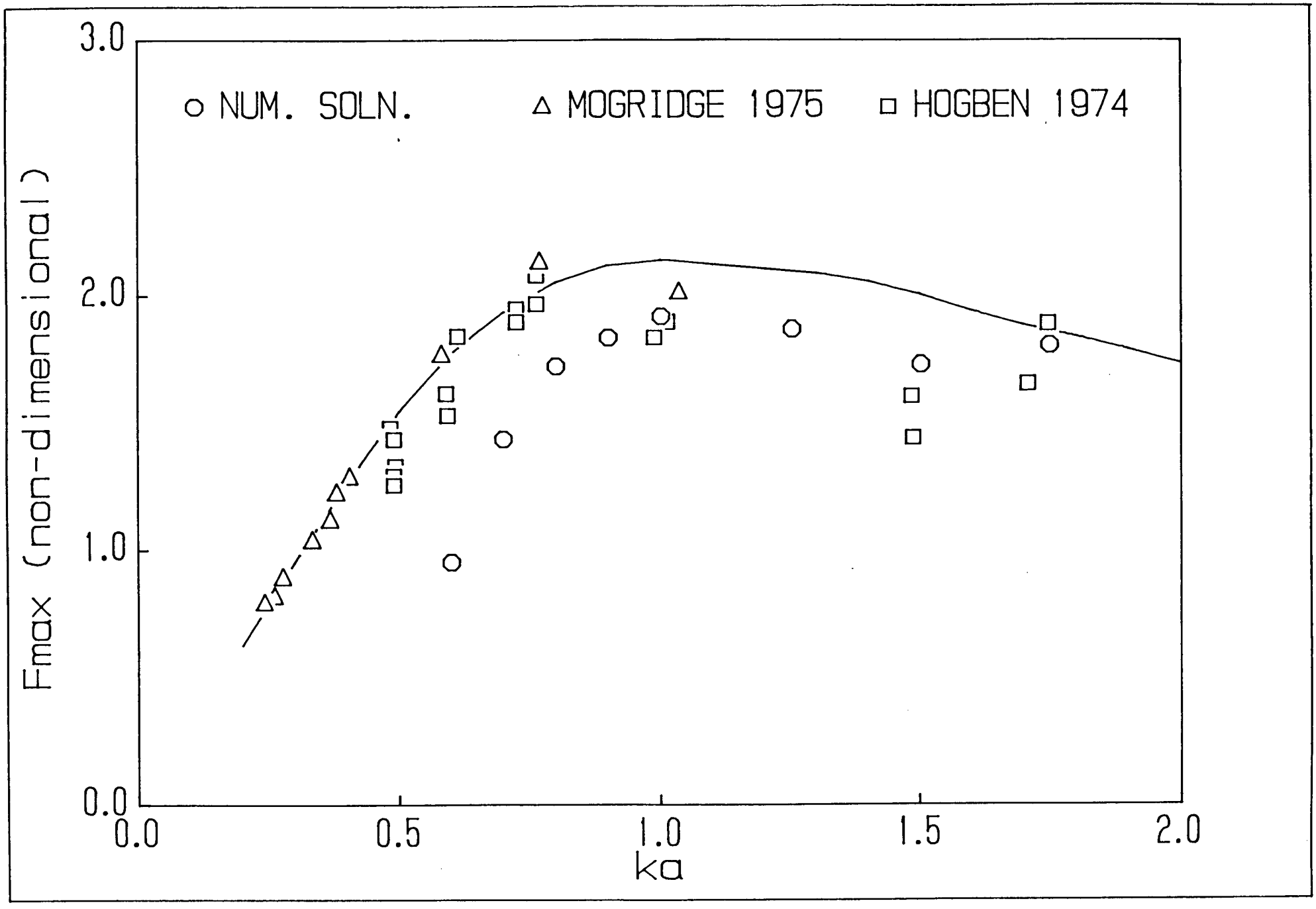

Figure 40. Non-linear Forces Calculated at the Cylinder at Various ka values

APPENDIX I

CONSTRUCTION OF A SYSTEM OF LINEAR EQUATIONS FROM THE BOUNDARY INTEGRAL EQUATION.

.....From equation (13) :

$$\phi(P) + \int_S \phi(Q)\, G_{,n}\, dS = \int_S \phi(Q)_{,n}\, G\, dS \qquad (13).$$

If the control boundary, S, is divided into N elements, and ϕ is assumed constant on each of these elements, equation (13) can be rewritten as :

$$\phi_i + \sum_{j=1}^{N} \phi_j\, G_{ij,n}\, \delta S_j = \sum_{j=1}^{N} \phi_{j,n}\, G_{ij}\, \delta S_j \quad ,$$

where

$$S = \sum_{j=1}^{N} \delta S_j \quad .$$

Subscript i and j are element numbers from 1 to N .

Since there are N elements, N equations of N unknowns

can be written. As a consequence, the following matrix can be obtained.

$$[\,A\,]\,\phi = [\,C\,]\,\phi_{,n} \qquad ,$$

where ϕ and $\phi_{,n}$ are column vectors. The associated entries of matrix A and C can be computed as :

$$A_{ij} = I_{ij} + \int_{-s_j}^{+s_j} G_{ij,n}\, dS$$

$$C_{ij} = \int_{-s_j}^{+s_j} G_{ij}\, dS \qquad ,$$

where

$$\delta S_j = 2s_j$$

and

$$I_{ij} = 1 \qquad \text{when } i=j$$

$$I_{ij} = 0 \qquad \text{when } i\neq j$$

I is the identity matrix.

The above integral terms for A_{ij} and C_{ij} can be calculated by any numerical integration technique. A Gaussian 5th order integration method is applied here. Details of

these integrals are found in Brebbia (1978) as well as Banerjee and Butterfield (1981). Although the involved integral equation for free-surface problems is usually more complicated than equation (13), the principle of writing down the matrix from the integral equation is very similar and straight forward.

Finally, it is mentioned in both Brebbia (1978) and Banerjee (1981) that, when carrying out the numerical integral for A_{ij} and C_{ij} , special consideration should be made to take care of the situation when i equals to j . These terms, A_{ii} and C_{ii} cannot be calculated directly as the other terms. Analytic solutions are provided by Brebbia and Banerjee, and should be used for the diagonal terms of both matrix A and C.

APPENDIX II

INTERPOLATION OF VELOCITY COMPONENTS BETWEEN ADJACENT ELEMENTS BY EQUATION (24).

From equation (24) :

$$v_y = dx + ey + f \qquad (24).$$

If three sucessive elements with number i-1 , i , i+1 are considered, and their v_y values are designated respectively by $v_y|_{i-1}$, $v_y|_i$, and $v_y|_{i+1}$, then, the following equations can be written :

$$\begin{aligned} d\,x_{i-1} + e\,y_{i-1} + f &= v_y\,|_{i-1} \\ d\,x_i + e\,y_i + f &= v_y\,|_i \\ d\,x_{i+1} + e\,y_{i+1} + f &= v_y\,|_{i+1} \end{aligned} .$$

$$\Rightarrow \begin{bmatrix} x_{i-1} & y_{i-1} & 1 \\ x_i & y_i & 1 \\ x_{i+1} & y_{i+1} & 1 \end{bmatrix} \begin{bmatrix} d \\ e \\ f \end{bmatrix} = \begin{bmatrix} v_{y\ i-1} \\ v_{y\ i} \\ v_{y\ i+1} \end{bmatrix} .$$

Upon solving this set of linear equations, equation (24) becomes a function of **x** and **y** only, and can be used to

interpolate the velocity value between these three elements. The same procedure is applied to interpolate v_x , in which the column vector on the right-hand-side of the above equation is replaced by v_x .